CHAPTER III

RESULTS & DISCUSSION

CHAPTER III

RESULTS AND DISCUSSION

PART (A)

STUDIES OF THE FREE LIGANDS

1 - D-C Polarographic Investigation:

(1) The polarograpic beaviour of acenapthenequinone monopenylhydrazone derivatives in ethanolic buffer solutions:

The principal aim of the present part is to consider the polarographic reduction of the acenaphthenequinone monophenylhydrazone derivatives. These compounds contain the electroactive C=O, C=N and N-N centers. The polarographic investigations were performed in the Britton-Robinson buffer solutions containing 40% (v/v) ethanol to ensure complete solubility of the compounds under investigation. The polarograms of these compounds are illustrated in Figs. (1-3).

a - The polarographic behaviour of acenaphthenequinone-(2-carboxyphenyl)-hydrazone:

The polarographic behaviour of this compound was followed over the pH range 2.5-11.4, Fig. (1). In solutions of pH <8 all the polarograms are composed of two reduction waves of almost equal heights. The limiting

current of the first wave decreases slightly with increasing the pH of the electrolysis solution. On the other hand, the limiting current of the second wave decreases gradually with increasing the pH of the solution until the wave vanished completely in solutions of pH > 11.5. The half wave potentials of the two reduction waves shifted to more negative values with rise of pH, denoting that hydrogen ions are consumed in the reduction process and the proton uptake proceeds the electron transfer[58].

b - The polarographic behaviour of acenaphthenequinone-(2-methoxyphenyl)-hydrazone:

The polarograms obtained for this compound are shown in Fig. (2). Within the pH range 3-11.2 two reduction waves of almost equal heights are obtained. The limiting current of the first one decreases slightly with increasing the pH and the limiting current of the second wave decreases gradually with increasing the pH of the solution until it vanished completely in solutions of pH > 11.2. The half wave potentials of the two reduction waves shifted to more negative values with rise of the pH of the medium indicating that hydrogen ions are consumed in the reduction process and the proton uptake proceeds the electron transfer.

c - **The polarographic behaviour of acenaphthenequinone-(2-chlorophenyl)-hydrazone:**

The polarograms of this compound are composed of two reduction waves of almost equal heights, Fig. (3). The pH values of the solutions was ranging from 2.6 to 11. The limiting current of the first wave decreases slightly with increasing the pH of the solution. On the other hand, the limiting current of the second one decreases gradually with increasing the pH of the solution until the wave vanished completely in solutions of pH > 10. The half wave potentials of the two reduction waves shifted to more negative values with rise of the pH denoting that hydrogen ions are consumed in the reduction process and the proton uptake proceeds the electron transfer.

(i) **The current-pH curves:**

The plots of the limiting current of the first wave, second wave and the total limiting current as a function of pH of the three compounds under consideration are shown in Figs. (1-3).

The i_l-pH curves of the first wave denote that the limiting current decreases gradually with increasing the pH until it reachs a constant value in strong alkaline

medium. This slight decrease may be due to the decrease of diffusion coefficient of the depolarizer species as a result of the viscocity change of the medium. On the other hand the i_l-pH curves of the second wave show that the limiting current decreases appreciably with increasing the pH until the wave completely vanishes in strong alkaline medium. The polarograms in such solutions comprise only the first wave.

(ii) Effect of pressure at mercury head:

The effect of mercury height on the polarographic limiting current can throw some light on the factors controlling the reduction process such as diffusion, rate of chemical reduction or adsorption. The relation between the limiting current (i_l) and the net pressure of mercury after correction for the back pressure ($h_{corr.}$), is given by [59]:

$$i_l = k\, h_{corr.}$$

or $$\log i_l = \log k + X \log h_{corr.}$$

The plots of $\log i_l$ vs. $\log h_{corr.}$ gives a straight line with a slope X. The value of X reveals the nature of the electrode reaction. For adsorption-controlled current X=1, for diffussion-controlled current X=0.5 and for kinetic-controlled process X=0.05. If the electrode

process is governed by contribution of two phenomena, then X may exhibit intermediate values between the above mentioned ones.

The plots of i_l vs. log $h_{corr.}$ for ligand I, II and III are shown in Figs. (4-6). The values of the slope X obtained for each ligand are cited in Tables (2-4). The results show that the reduction process of these compounds is mainly controlled by diffusion for ligands I and II and by diffusion with partial adsorption contribution for ligand III.

(iii) Analysis of the polarographic waves:

The analysis of the polarographic waves was carried out applying the fundamental equation characterising reversible polarographic waves[60]:

$$E_{de} = E_{\frac{1}{2}} - (0.0591/n).\log (i/i_d - i)$$

where: E_{de} is the potential of the dropping mercury electrode,

i_d is the diffusion current,

$E_{\frac{1}{2}}$ is the half-wave potential, and

n is the number of electrons consumed in the electrochemical reduction process.

The plots of E_{de} vs. log $(i/i_d - i)$ for the compounds under consideration are shown in Figs. (4-6). The plots

display linear correlations of slope values amounting to 135-54, Tables (5-7), which are in conflict with that predicted from the fundamental equation concerning the reversible electrode behaviour. For this reason, the polarographic wave would not be treated as a reversible one. On the contrary the treatment should involve the fundamental equation of the irreversible polarographic wave[60]:

$$E_{de} = E_{\frac{1}{2}} - (0.0591/\alpha n_a).\log (i/i_d - i)$$

were: α is the transfer coefficient[61],

n_a is the number of electrons involved in the potential-determining step.

Values of the transfer coefficient (α) can be evaluated for the probable values of (n_a) by considering the number of electrons involved in the rate determining step (n_a) to be one or two. As shown in Tables (5-7) the most probable values of the transfer coefficient (α) for all compounds along the first wave in solutions of pH's <8 and for the second wave along the entire pH range is obtained for n_a equals to one. On the other hand, in solutions of pH's >8 the most probable values of (α) for the first wave obtained for n_a equal to two. These results denote that the rate-limiting step of the electrode process may involve one and two electrons in acidic and alkaline solutions, respectively, whereas

for the second wave it involves one electron along the entire pH range in which the wave appears.

(iv) Half-wave potential-pH curves:

The $E_{\frac{1}{2}}$-pH curves for the compounds under investigation are shown in Figs. (4-6). Each curve exhibits linear correlation consisting of two segments indicating the presence of one pk_a value corresponding to an acid-base equilibrium[58].

From the slopes (S_2) of these segments and those of logarithmic analysis (S_1), the number of protons participating in the rate-limiting step can be determined using the following relationship[60]:

$$Z_{H^+} = (dE_{\frac{1}{2}}/dpH)/(0.0591/ n_a) = S_2/S_1$$

The number of protons along both waves in alkaline solutions (pH's >8) is found to be equal to one, Tables (5-7). In acidic solutions the rate-limiting step does not involve the consumption of proton due to the fast proton uptake in these media.

(2) Effect of concentration of the ligands:

The polarographic reduction of ligands I, II and III in a solution of pH 7.0 in presence of 30% (by volume) ethanol at different concentrations ranging

from $2x10^{-4}$M to $1.2x10^{-3}$M is shown in Fig. (7). The $E_{\frac{1}{2}}$ values of the first and second waves shift to more negative potentials with increasing the concentration of the depolarisers which confirms the irreversible nature of the waves, obtained from their analysis.

The polarograms obtained for different concentrations of ligand are tested to achieve the validity of Ilkovic equation. The plots of the diffusion current values of the first and second waves vs. the concentration, Fig. (7), gives straight lines passing through the origin, which indicates the validity of Ilkovic equation in the form of i_l=KC and hence the possible analytical determination of these ligands within this range of concentrations tested.

The electrode reaction:

The polarographic reduction of the three hydrazones under study denotes almost a common behaviour. In acid solutions the reaction involves four electrons along two waves whereas in strong alkaline media one wave corresponding to the uptake of two electrons is observed. The waves obtained correspond most probably to the reduction of the -HN-N=C centres of the hydrazone part. This is based on the premise that the behaviour observed

is quite similar to that of other hydrazones. Based on this the reduction can be formulated as follows:

1. In acid solutions:

1st wave $\rangle C=N-\overset{H}{\underset{|}{N}}-\emptyset X+2e^{-}+2H^{+} \longrightarrow \rangle C=NH+X\emptyset-NH_2$

The reaction corresponds the fission of the N-N bond

2nd wave $\rangle C=NH+2e^{-}+2H^{+} \longrightarrow \rangle CH-NH_2$

The reaction involves the saturation of the C=N of the kitimine structure.

2. In alkaline solutions:

In this case, the first reaction is inhibited and only the second one can proceed at the electrode surface.

$\rangle C=N-NH-\emptyset X+2e^{-}+2H^{+} \longrightarrow \rangle CH-NH-NH-\emptyset X$

The reaction product is the hydrazino derivative. The three steps show that each reduction process would comprise two electrons and two protons.

The sequence of the electrode reaction can be obviated by considering the result of the investigation of the waves, the most probable α-parameter and corresponding n_a values and also the number of protons involved in the rate determining step and the mechanism of the

electrode reaction can be represented as follows:

In acidic solutions:

1st step $\rangle C=N-NH- \overset{H^+}{\rightleftharpoons} \rangle C=^+NH-NH-$

$$\rangle C=^+NH-NH- + 2e^- + H^+ \xrightarrow{E^1_{\frac{1}{2}}} \rangle C=NH + H_2N-$$

2nd step $\rangle C=NH \overset{H^+}{\rightleftharpoons} \rangle C=N^+H_2$

$$\rangle C=^+NH_2 + 2e^- + H^+ \xrightarrow{E^2_{\frac{1}{2}}} \rangle CH-NH_2$$

In strong alkaline solutions:

$$\rangle C=N-NH + 2e^- + 2H^+ \xrightarrow{E_{\frac{1}{2}}} \rangle CH-NH-NH-$$

Table (2): Data obtained for 2×10^{-4} M of acenaphthenequinone-(2-carboxyphenyl)-hydrazone in buffer solutions in different pH's containing 40% (by volume) ethanol.

pH	i_d (UA)	$-E_{\frac{1}{2}}$ (volt)	d (log i_1/log h)
4.35	0.78	0.38	0.4 (1st wave)
			0.34 (2nd wave)
8.33	0.61	0.48	0.48 (1st wave)
			0.57 (2nd wave)

Table (3): Data obtained for $2x10^{-4}$M of acenaphthenequinone-(2-methoxyphenyl)-hydrazone in buffer solutions in different pH's containing 40% (by volume) ethanol.

pH	i_d (UA)	$-E_{\frac{1}{2}}$ (volt)	d (log i_l/log h)
3.5	0.78	0.35	0.58 (1st wave)
			0.52 (2nd wave)
9.05	0.43	0.55	0.57 (1st wave)
			0.62 (2nd wave)

Table (4): Data obtained for $2x10^{-4}$M of acenaphthenequinone-(2-chlorophenyl)-hydrazone in buffer solutions in different pH's containing 40% (by volume) ethanol.

pH	i_d (UA)	$-E_{\frac{1}{2}}$ (volt)	d (log i_l/log h)
2.95	0.81	0.35	0.72 (1st wave)
			0.41 (2nd wave)
9.75	0.51	0.56	0.45 (1st wave)
			0.75 (2nd wave)

Polarogram of Ligand I in different pH values

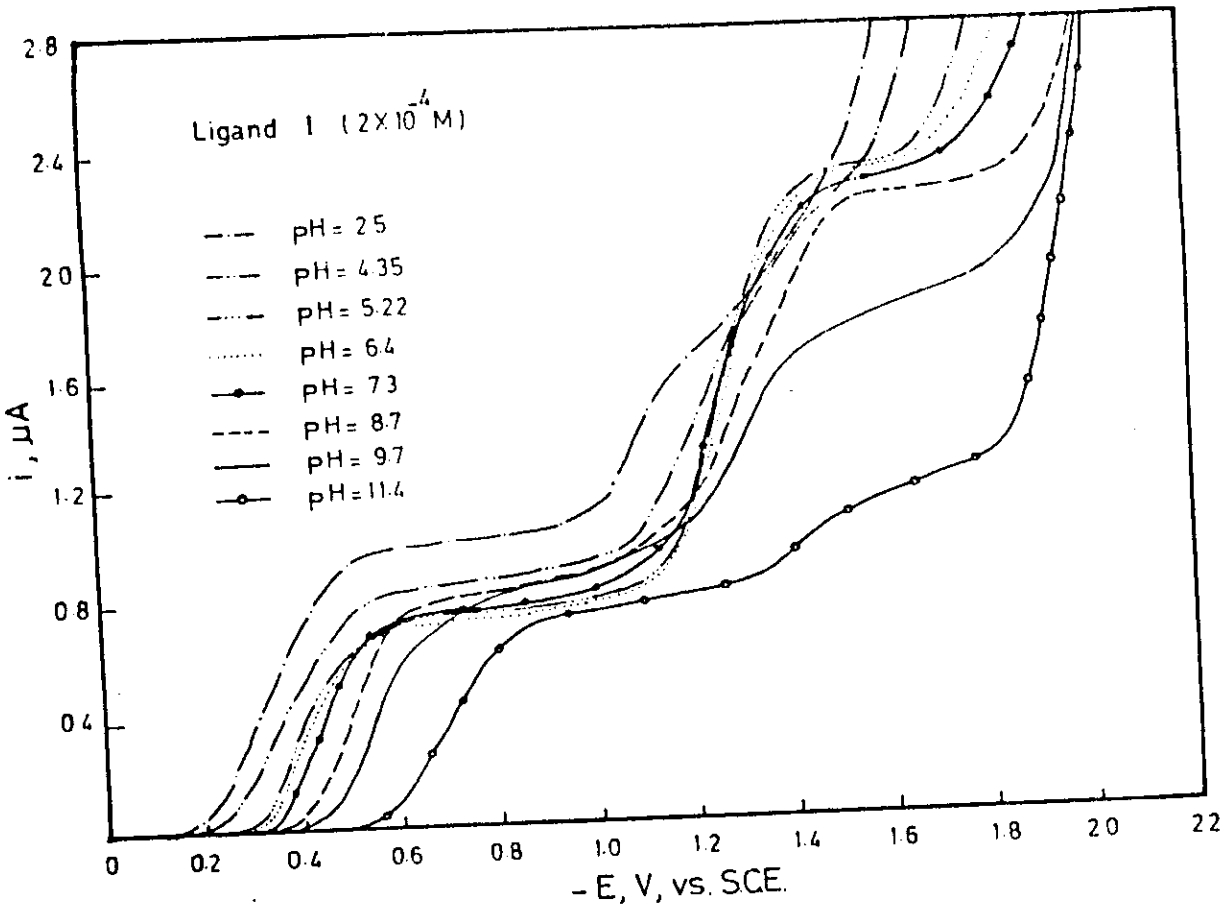

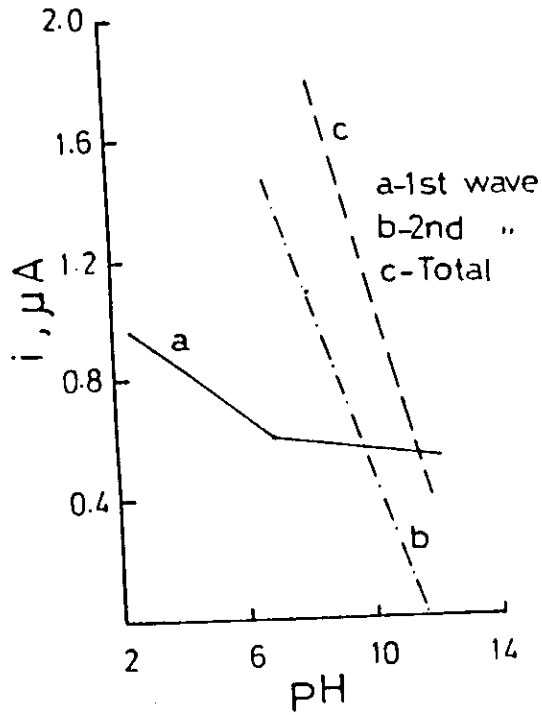

Fig. (1)

Polarogram of Ligand II in different pH values

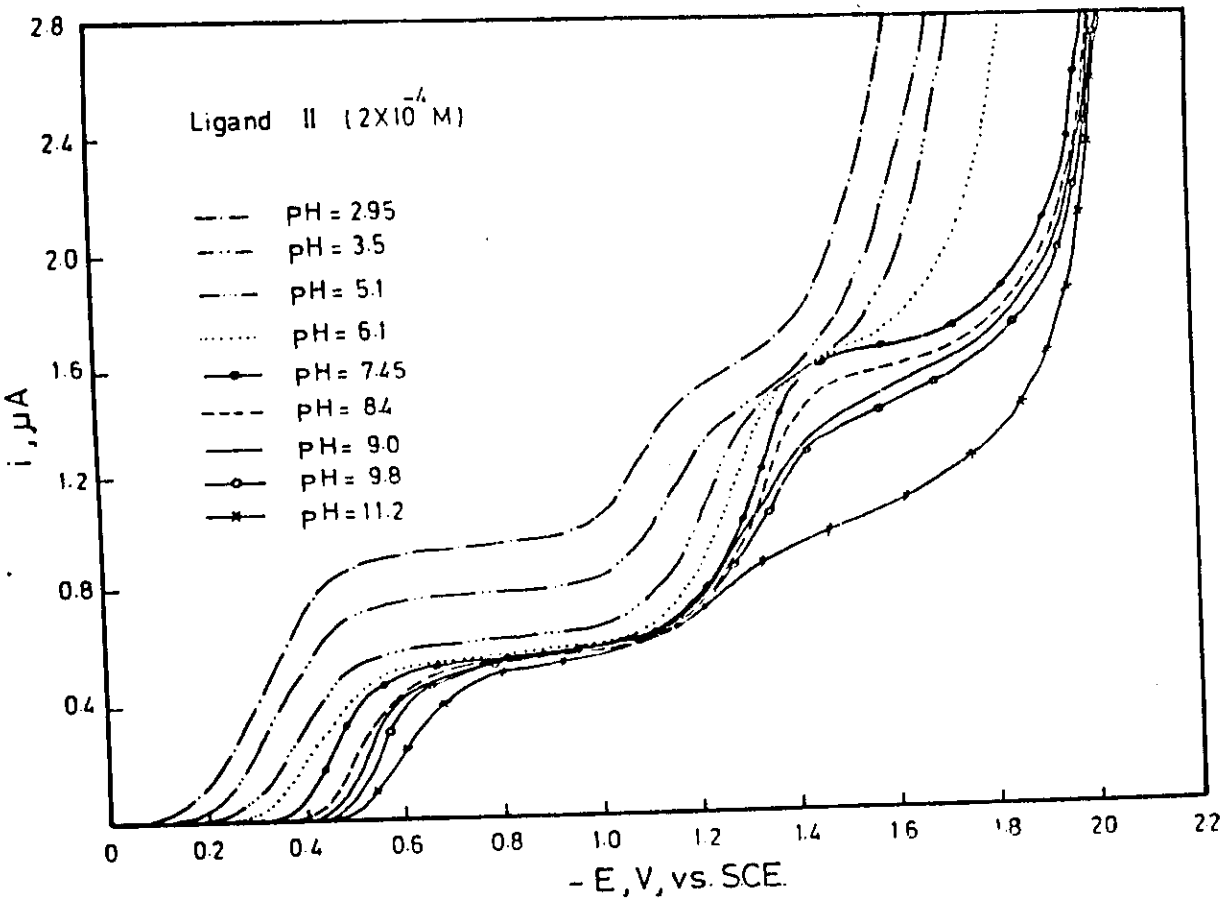

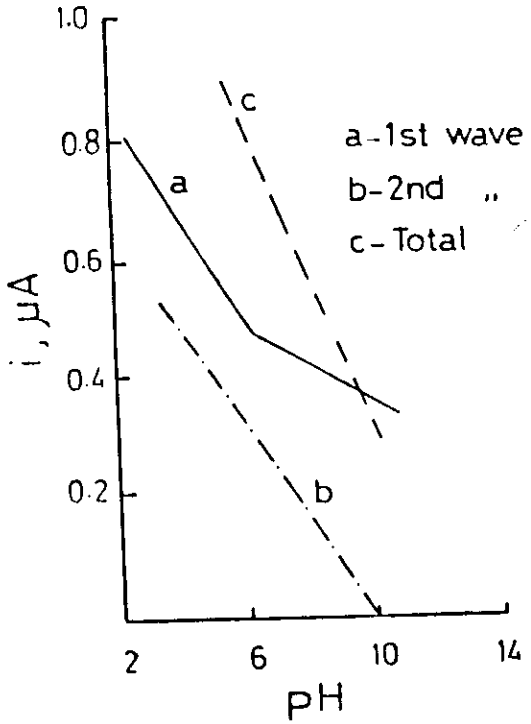

Fig. (2)

Polarogram of Ligand III in different pH values

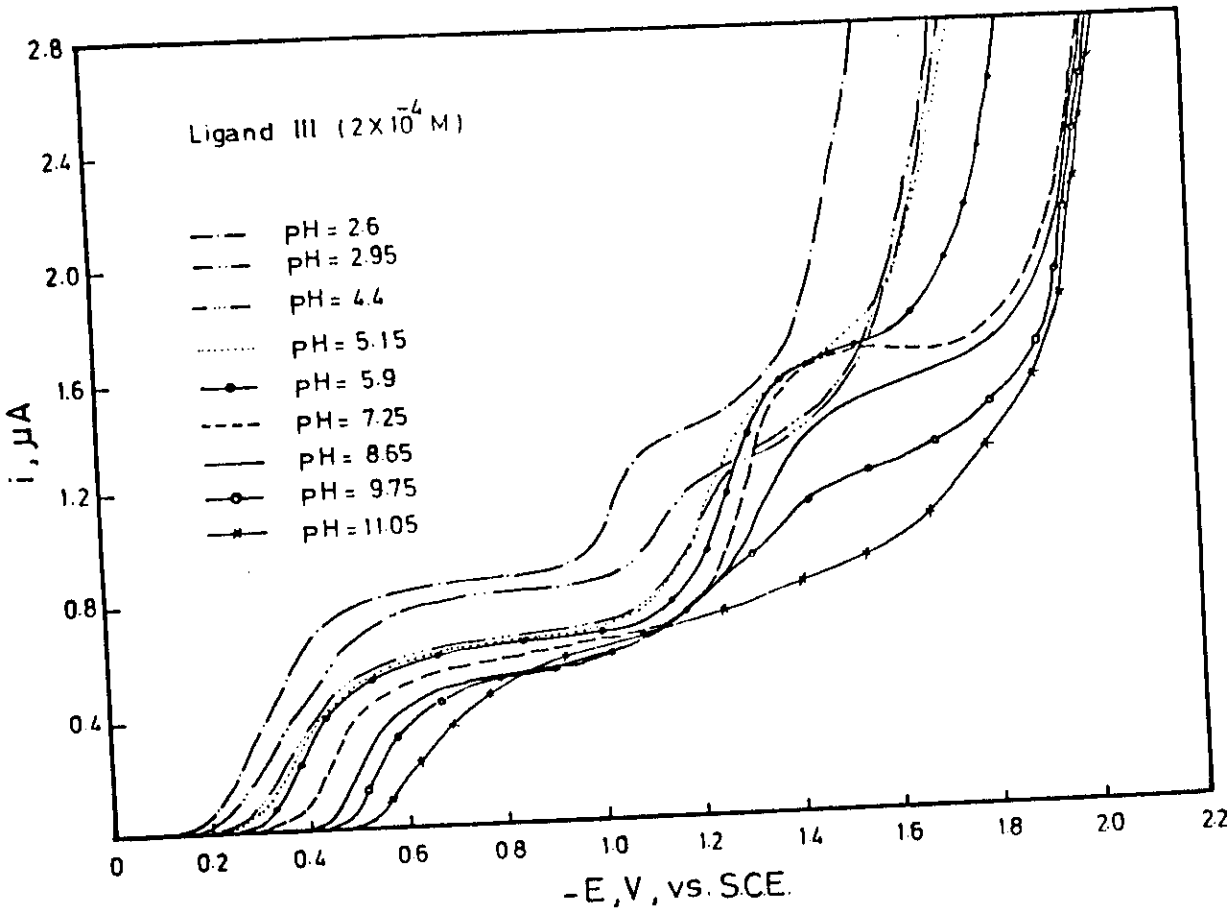

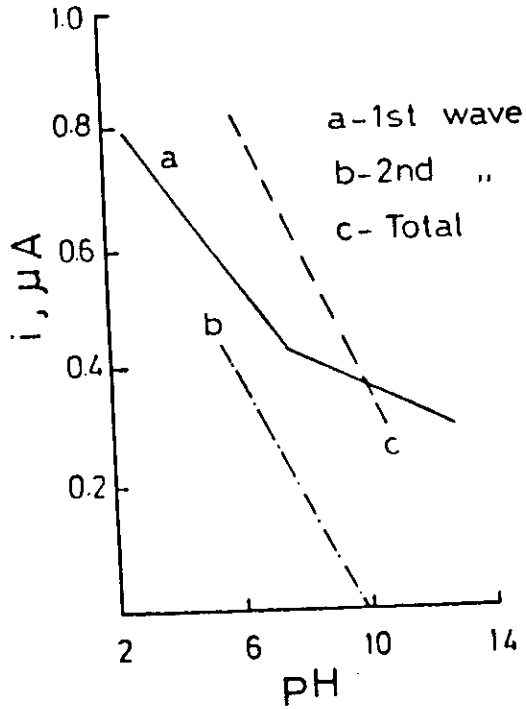

Fig. (3)

Ligand I

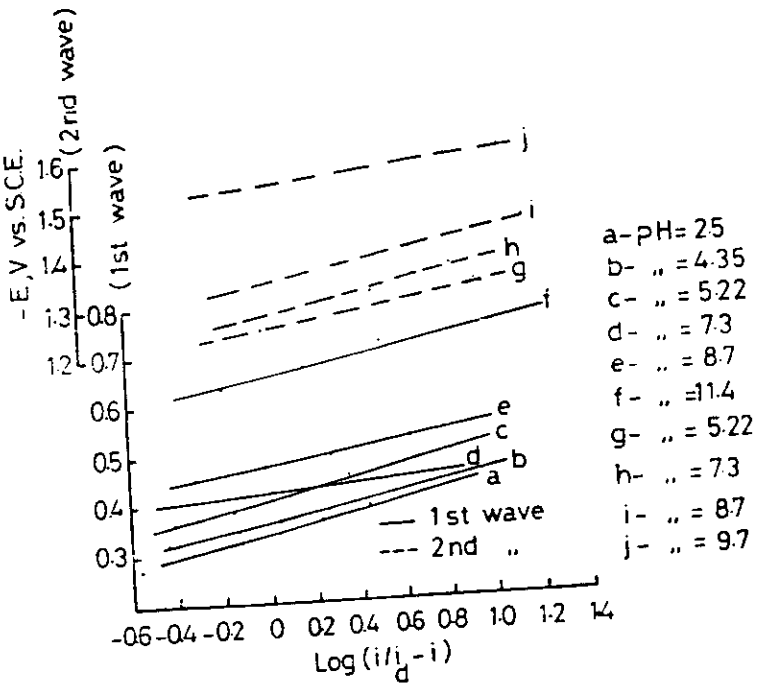

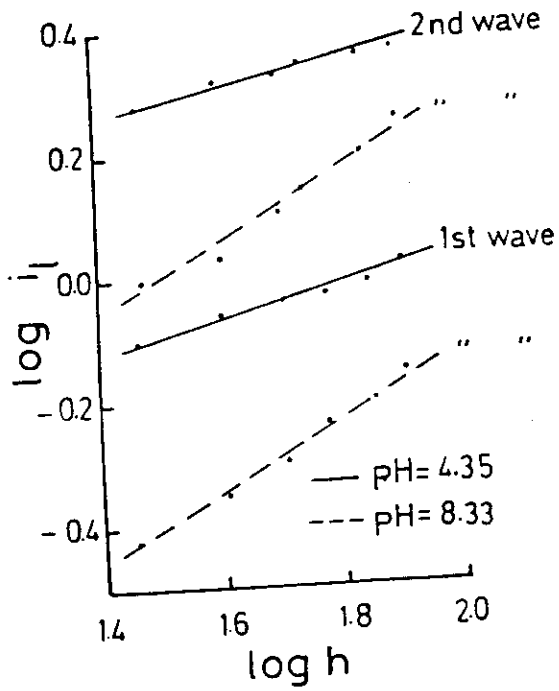

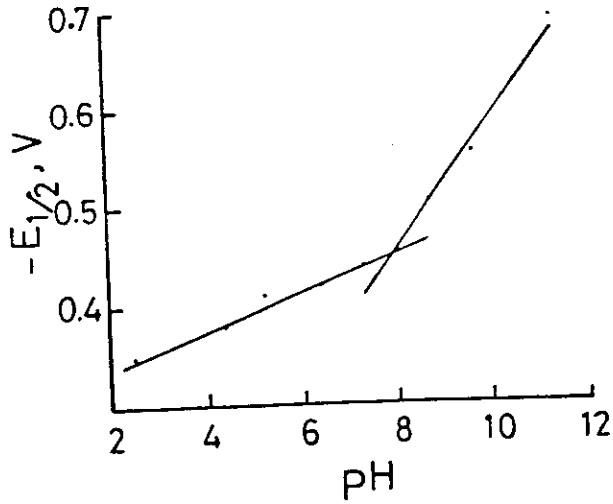

Fig.(4)

Ligand II

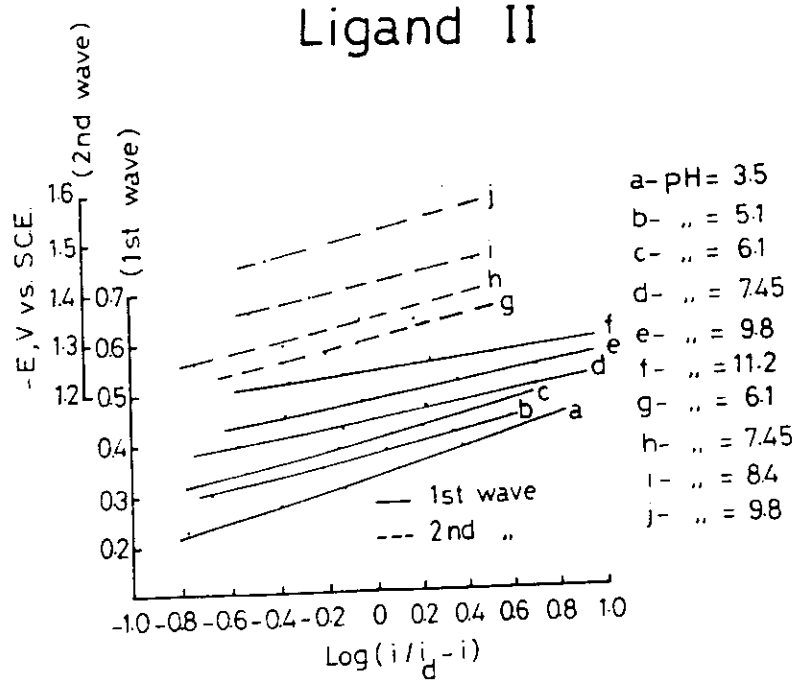

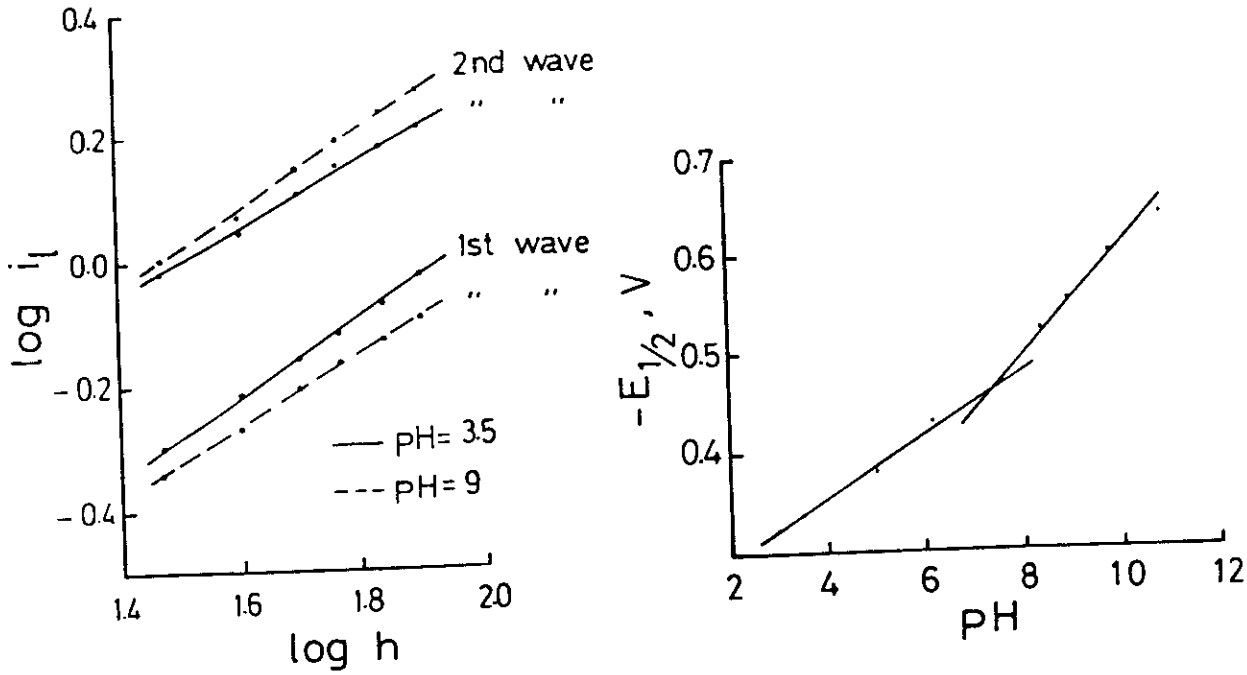

Fig.(5)

Ligand III

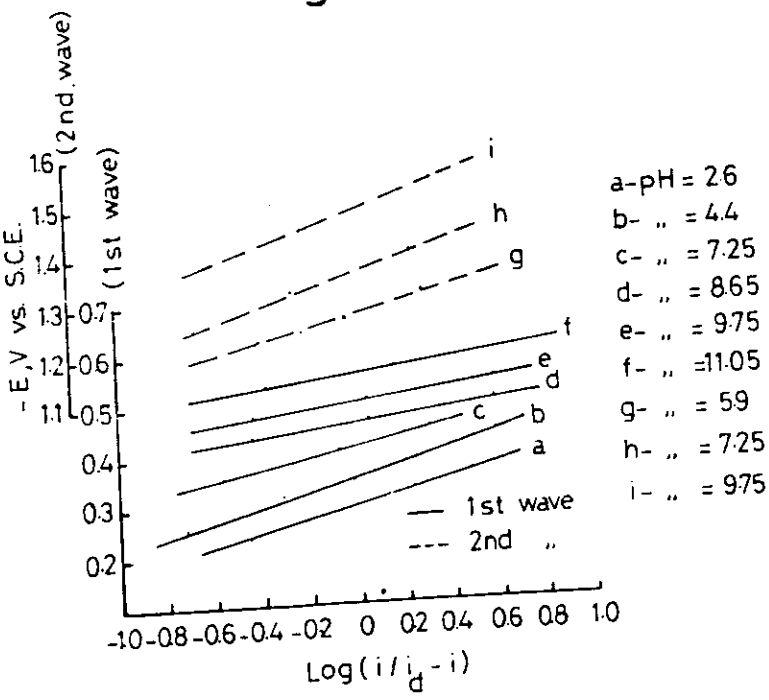

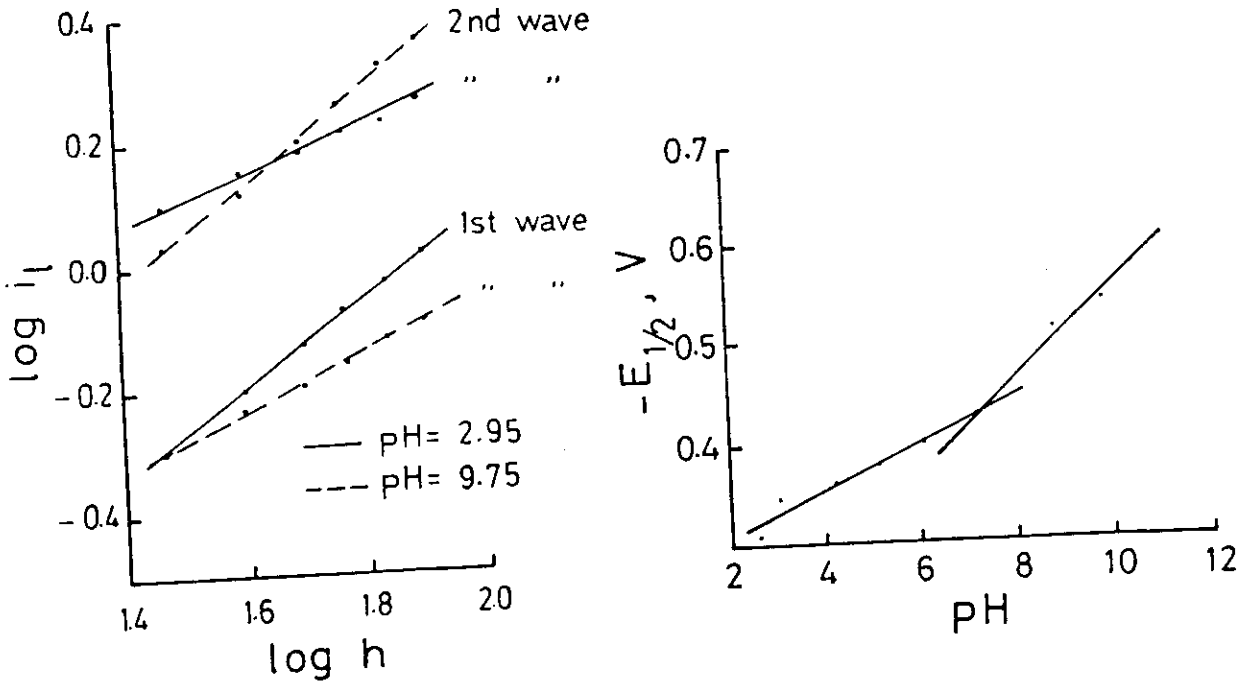

Fig. (6)

Polarograms of Different Concentrations of Ligands I, II and III

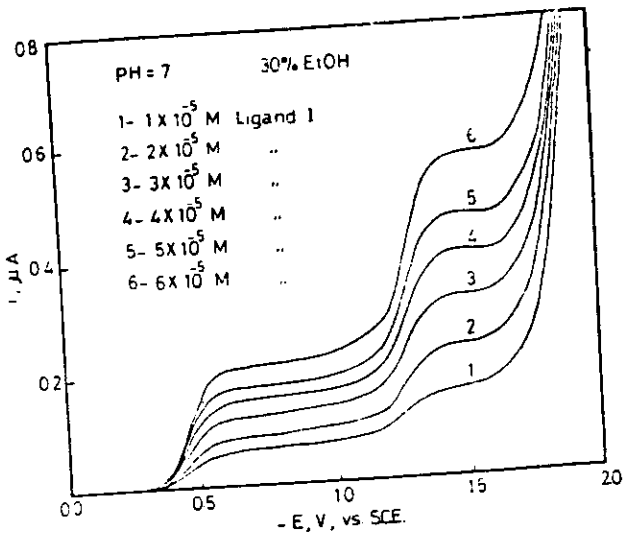

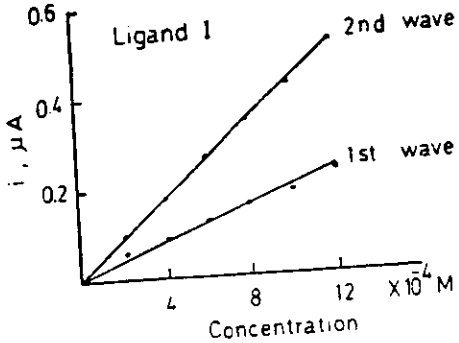

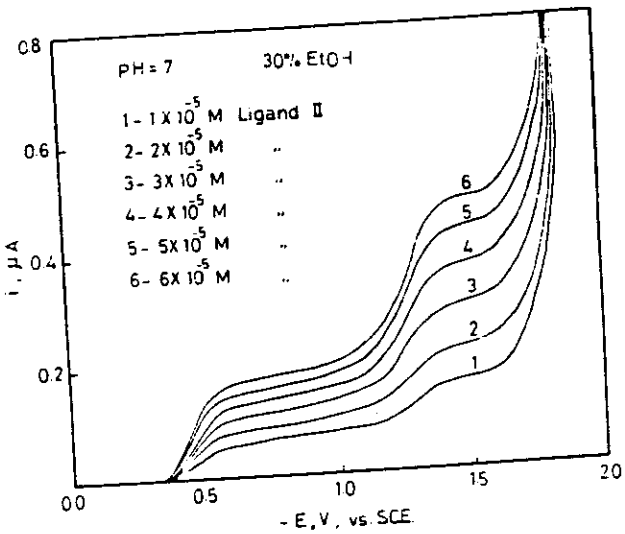

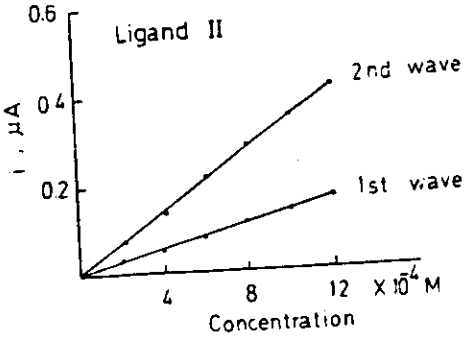

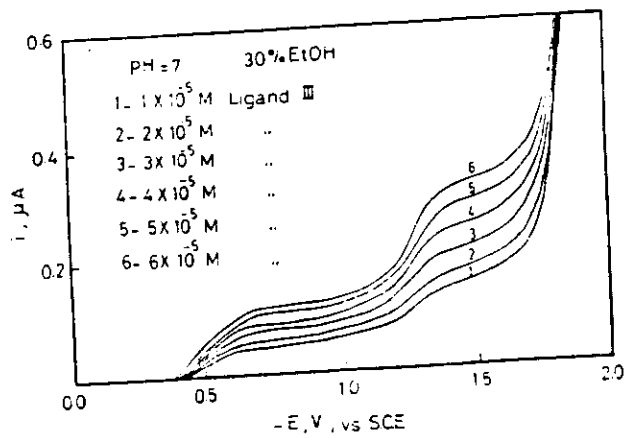

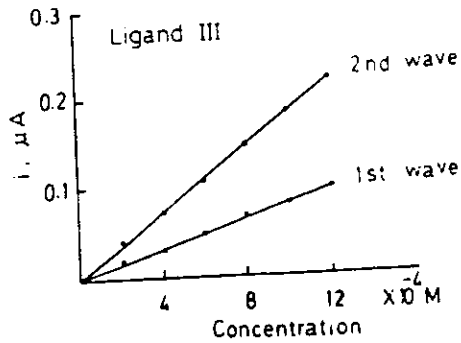

Fig.(7)

Table (5): Values of i_d, $E_{\frac{1}{2}}$, Z_{H^+}, αn_a and α for $2x10^{-4}$M of ligand (I) in aqueous buffer solutions of various pH values containing 40% (v/v) ethanol.

pH	i_d,UA	$E_{\frac{1}{2}}$,V	S_1,mV	S_2,mV	Z_{H^+}	αn_a	α n_a=1	α n_a=2
2.5	0.96	0.35(a)	109	20.2	0.18	0.54	0.54	0.27
4.35	0.78	0.38(a)	99	20.2	0.20	0.59	0.59	0.30
5.22	0.73	0.41(a)	96	20.2	0.21	0.61	0.61	0.31
	1.48	1.27(b)	82			0.72	0.72	0.36
6.4	0.65	0.42(a)	92	20.2	0.22	0.64	0.64	0.32
	1.46	1.27(b)	69			0.85	0.85	0.43
7.3	0.6	0.44(a)	59	20.2	0.34	1.00	1.00	0.50
	1.4	1.28(b)	66			0.89	0.89	0.45
8.7	0.62	0.5 (a)	75	62.5	0.83	0.79	0.79	0.40
	1.3	1.31(b)	65			0.91	0.91	0.46
9.7	0.62	0.56(a)	78	62.5	0.80	0.76	0.76	0.38
	0.98	1.33(b)	63			0.93	0.93	0.47
11.4	0.53	0.69(a)	84	62.5	0.74	0.70	0.70	0.35

(a) first wave, (b) second wave

$S_1 = dE_{de}/\log (i/i_d-i)$

$S_2 = dE_{\frac{1}{2}}/pH$

Table (7): Values of i_d, $E_{\frac{1}{2}}$, Z_{H^+}, αn_a and α for 2×10^{-4} M of ligand (III) in aqueous buffer solutions of various pH values containing 40% (v/v) ethanol.

pH	i_d, UA	$E_{\frac{1}{2}}$, V	S_1, mV	S_2, mV	Z_{H^+}	αn_a	α n_a=1	α n_a=2
2.6	0.86	0.31(a)	125	27.5	0.22	0.47	0.47	0.24
2.95	0.81	0.35(a)	136	27.5	0.20	0.44	0.44	0.22
4.4	0.66	0.37(a)	132	27.5	0.21	0.45	0.45	0.23
5.15	0.65	0.4 (a)	125	27.5	0.22	0.47	0.47	0.24
	0.92	1.25(b)	132			0.45	0.45	0.23
5.9	0.64	0.4 (a)	137	27.5	0.20	0.43	0.43	0.22
	0.92	1.29(b)	118			0.50	0.50	0.25
7.25	0.56	0.43(a)	100	27.5	0.27	0.59	0.59	0.30
	0.90	1.34(b)	94			0.63	0.63	0.32
8.65	0.51	0.5 (a)	59	56.5	0.96	1.00	1.00	0.50
	0.76	1.36(b)	65			0.91	0.91	0.46
9.75	0.51	0.56(a)	57	56.5	0.99	1.03	1.03	0.52
	0.59	1.38(b)	62			0.95	0.95	0.48
11.05	0.55	0.63(a)	65	56.5	0.87	0.91	0.91	0.46

(a) first wave, (b) second wave

$S_1 = dE_{de}/\log (i/i_d - i)$

$S_2 = dE_{\frac{1}{2}}/pH$

2 - Spectrophotometric Studies:

(i) Spectral behaviour of acenaphthenequinone monophenylhydrazone derivatives in buffer solutions and the determination of their acid ionisation constants:

The spectra of $5x10^{-5}$M of ligands I, II and III in universal buffer solutions containing 30% by volume ethanol of pH 2-12 are shown in Figs. (8-10).

The spectra of the three ligands show one band at $\lambda_{max.}$= 288, 278 and 280 nm together with a shoulder at longer wavelength, for ligands I, II and III respectively. The longest developed band appeared at $\lambda_{max.}$= 320, 310 and 314 nm for ligands I, II and III. A clear isosbestic point appeared at 295, 288 and 285 nm for ligands I, II and III. This indicates that the first band is due to the nonionised form whereas the second is due to the ionised form of the compound. The isosbestic pcint indicates that an acid-base equilibrium cccured between the nonionised and ionised species.

The ionisation constants (pk_a) of ligands I, II and III were determined by applying four different methods:

(1) Half-Height method[62]:

The pk_a equals to the pH at half-height of the absorbance-pH curves, Figs. (8-10). The values of pk_a for ligands I, II and III are given in Table (8).

(2) The modified limiting absorbance method[63-65]:

The pk_a is calculated by using the equation:

$$pH = pK + \log \bar{\gamma} + \log \frac{A-A_{min.}}{A_{max}-A}$$

where A is the absorbance at a given pH value. $\bar{\gamma}$ is the activity coefficient of the ions present at equilibrium.

A_{min}, A_{max} are the absorbances corresponding to the total concentration of neutral and ionised species existing in solution.

The pk_a value can be evaluated by plotting log $\frac{A-A_{min.}}{A_{max}-A}$ vs. pH, Figs. (8-10). The pk_a value thus corresponds to the pH value at zero log $\frac{A-A_{min.}}{A_{max}-A}$. The values of pk_a are collected in Table (8).

(3) The Colleter method[66]:

The value of K can be calculated from the equation:

$$K = \frac{C_{H_2^+} - MC_{H_3^+}}{M - 1}$$

in which $$M = \left(\frac{A_3 - A_1}{A_2 - A_1}\right).\left(\frac{C_{H_1^+} - C_{H_2^+}}{C_{H_1^+} - C_{H_3^+}}\right)$$

where A_1, A_2 and A_3 are the absorbances at three different H^+ ion concentrations $C_{H_1^+}$, $C_{H_2^+}$ and $C_{H_3^+}$ respectively. The values calculated for ligands I, II and III are collected in Table (8).

(4) Modified isobestic point[67]:

for acid-base equilibria

$$R\text{-}OH \rightleftharpoons R\text{-}O^- + H^+$$

The following relation can be applied:

$$pH = pk_a + \log \bar{\gamma} + \log \left(\frac{\epsilon_{R\,O^-}}{\epsilon_{ROH}}\right) + \log \frac{(A-A_{min})_{RO^-}}{(A-A_{min})_{ROH}}$$

where $\epsilon_{R\text{-}OH}$ and ϵ_{RO^-} are the extinction coefficients of nonionised and ionised forms at λ_1 and λ_2 respectively. The correlation of $\frac{(A-A_{min})_{RO^-}}{(A-A_{min})_{ROH}}$ with pH yields linear relationship. The intersept of this line at log $\frac{(A-A_{min})_{RO^-}}{(A-A_{min})_{ROH}}$ equals zero gives a value equivalent to the following term:

$$pk_a + \log \bar{\gamma} + \log \frac{\epsilon_2}{\epsilon_1}$$

from which pk_a can be calculated. The pk_a values determined by the different methods are given in Table (8).

Spectra of Ligand I in buffer solutions

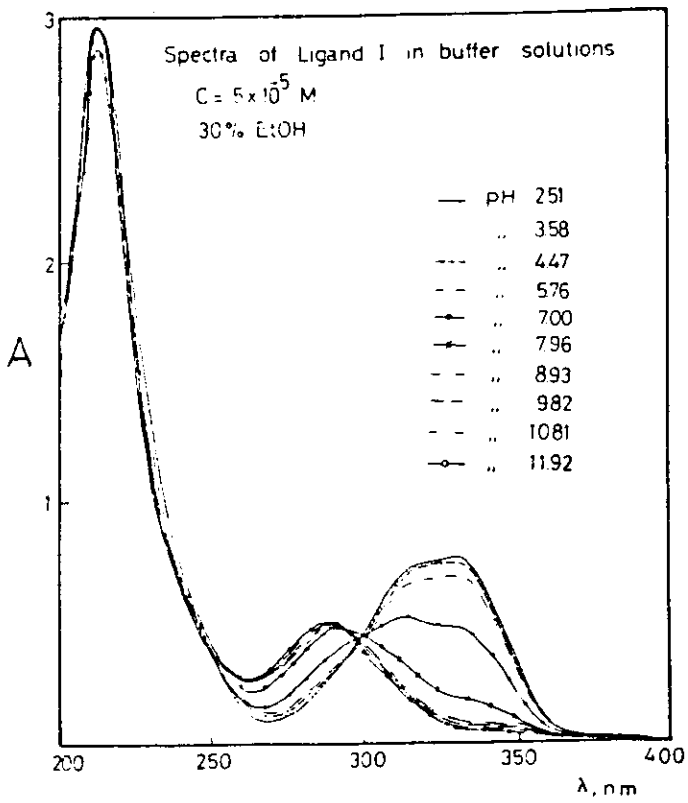

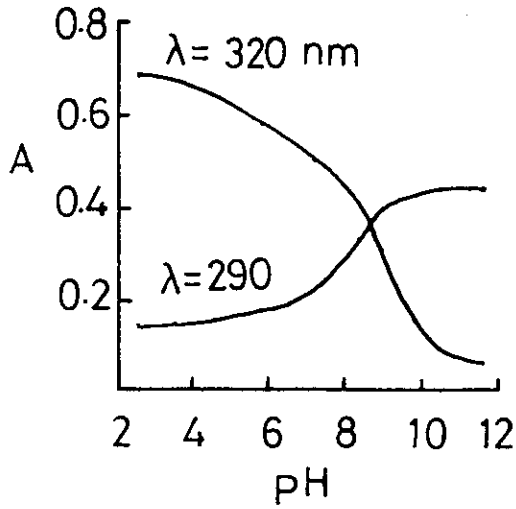

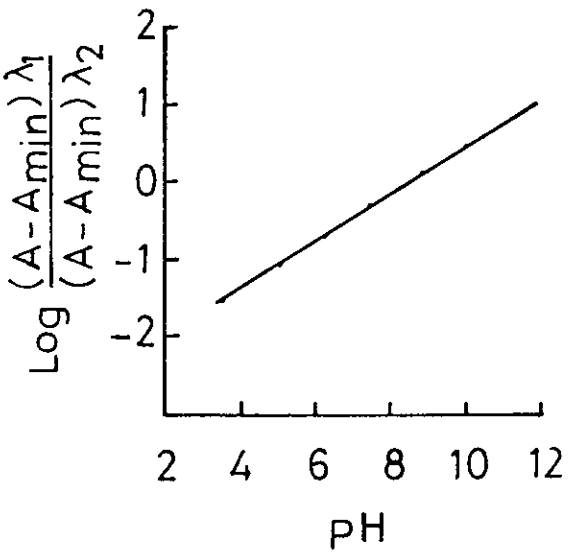

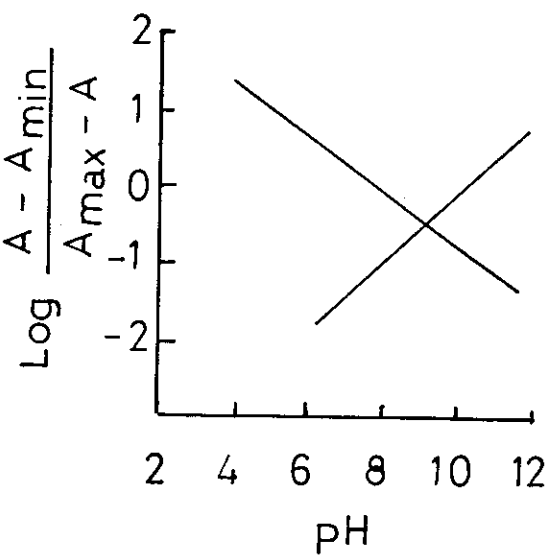

Fig.(8)

Spectra of Ligand II in buffer solutions

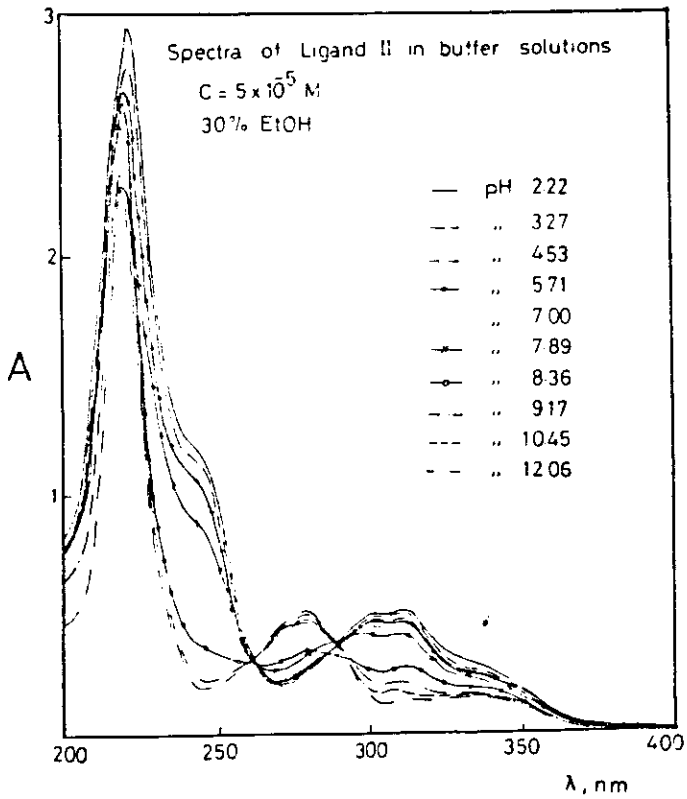

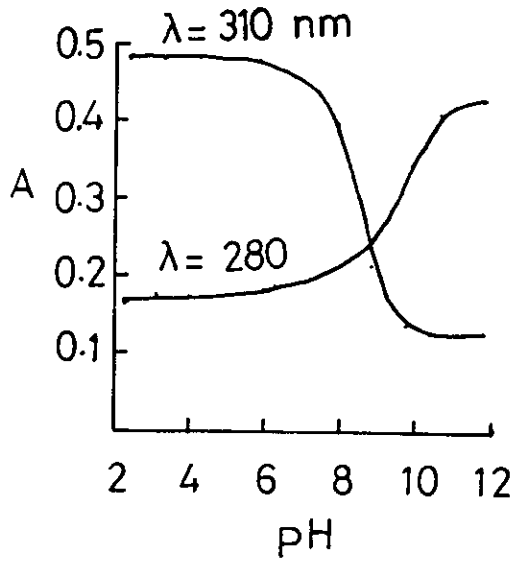

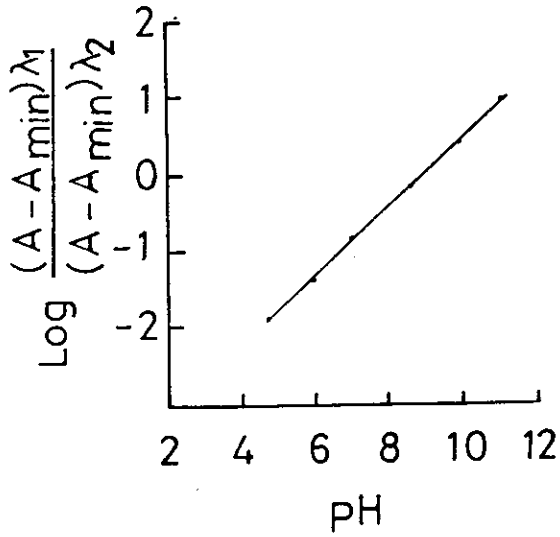

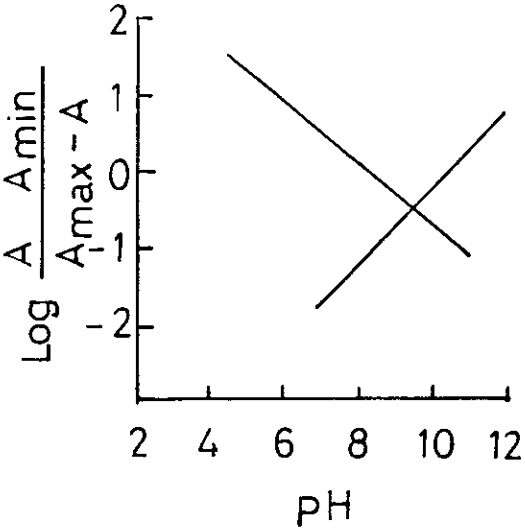

Fig. (9)

Spectra of Ligand III in buffer solutions

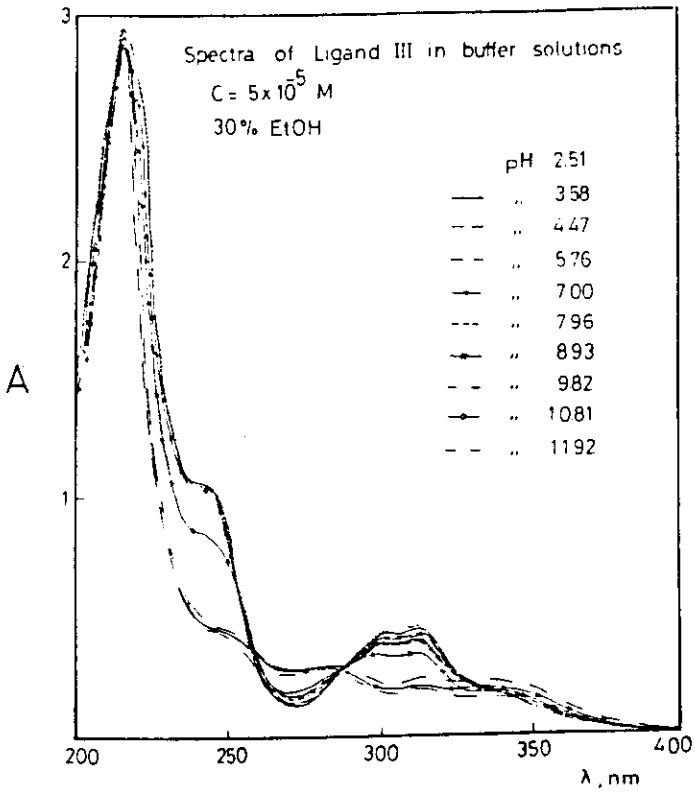

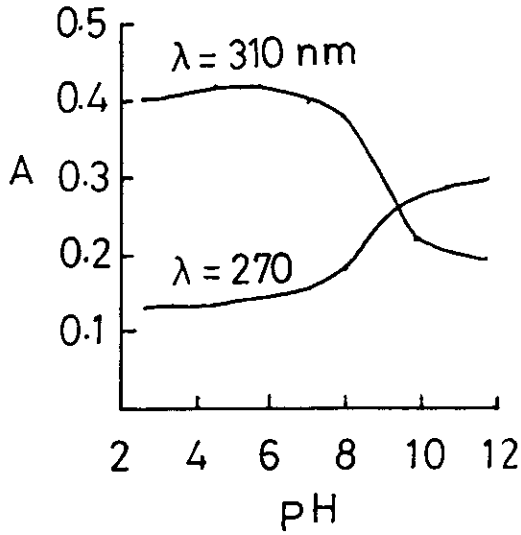

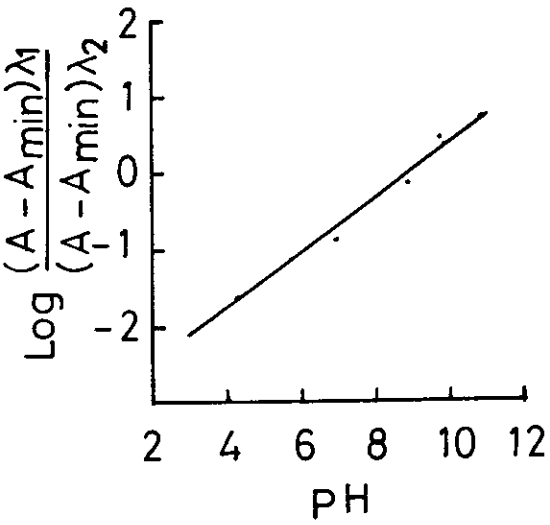

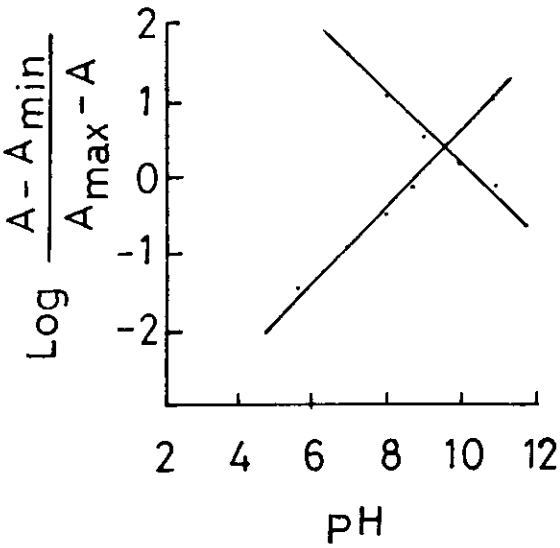

Fig (10)

(I) The Electronic Absorption Spectra in Ethanol:

The uv-visible absorption spectra of the compounds under investigation are scanned in ethanol within the wavelength range 200-500 nm Fig. (11) , and the spectral data are given in Table (9).

The spectra display three absorption bands; the first one (A) in the (200-210 nm) region is due to the moderate energy ($\pi - \pi^*$) transition corresponding to ($^1L_a \longleftarrow {}^1A$) state, while the second band (B) at ($\simeq$225 nm) is due to the low energy ($\pi-\pi^*$) transition ($^1L_b \longleftarrow {}^1A$) state in the phenyl moities. On the other hand, the third band (C) at longer wavelength side (at >270 nm) being sensitive to the nature of substituent (X) is assigned to an electronic transition involving CT interaction within the whole molecule taking place either in the hydrazone form (a) or in the azo form (b):

(a)

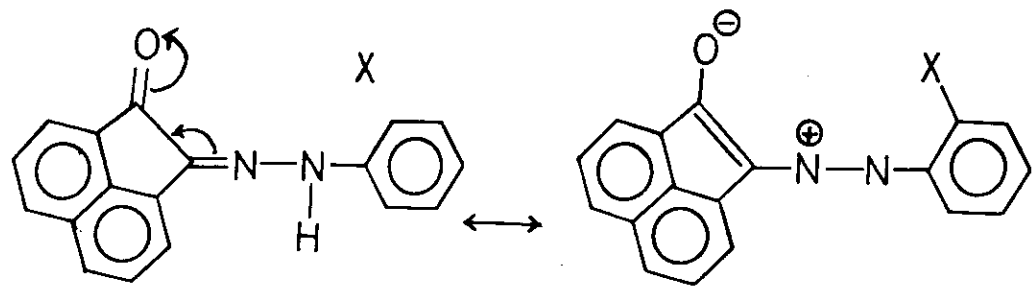

(b)

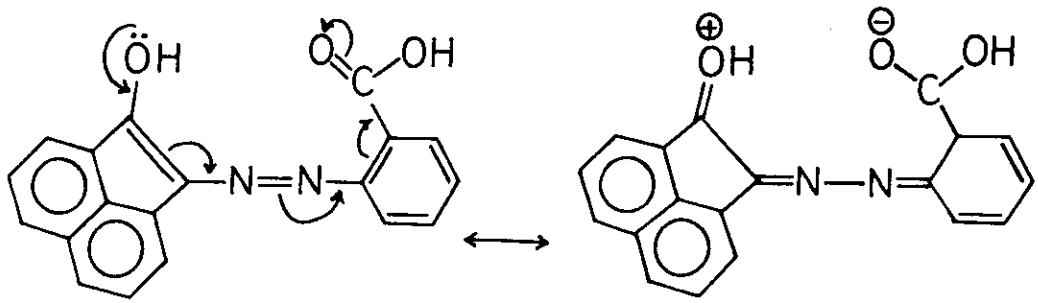

(ii) Electronic absorption spectra of acenaphthenequinone mono-phenylhydrazone derivatives in different organic solvents:

The uv-visible spectra of the compounds under investigation are scanned in some organic solvents of different polarities namely; ethanol, DMF, n-propanol, chloroform, dioxane, benzene and cyclohexane. These compounds have low solubilities in nonpolar solvents, but their spectra from the saturated solutions can be recorded. The representative spectra are shown in Fig. (11) and the spectral data are summarized in Table (9).

It is well known that, the absorption spectrum of organic molecule is, essentially, the summation of the absorption bands of the different molecular fragments. So, the absorption spectra of such compounds should have bands due to electronic transitions within the aromatic moities, as well as bands due to electronic transitions within the whole molecule, one should consider the interaction between the different parts of the molecule leading to the phenomenon of intramolecular charge transfer which will lead to either the appearance of new bands, or a shift in the position of the absorption bands due to transitions within the molecular parts influenced by charge migration.

The CT character of this band can be supported by calculating the E_{CT} values using the following equation[68]:

$$E_{CT} = I_p - (E_A + C) \quad (1)$$

considering the ionization potential (I_p) of OH group as a donor part (8.51 ev), the electron affinity (E_A) of the C=O group as an acceptor part (-1.5 ev) and the coulombic force (C) between the electron transfered and the positive hole left behined (5.2-5.6 ev). The E_{CT} values obtained using equation (1) amount to 4.41-4.81 ev whereas those obtained practically using the relation

$$E_{CT} = \frac{1241.728}{\lambda_{(nm)(CT)}} \text{ ev} \quad (2)$$

amount to 4.05-4.43 ev the fact which show that these compounds are present in solution in their hydrazone form.

(II) Electronic Absorption Spectra in Different Organic Solvents:

The uv-visible spectra of the acenaphthenquinone-(2-X phenyl)-hydrazone, X=COOH (I), OCH_3 (II) and Cl(III) in ethanol, dimethylformamide (DMF), dioxane, n-propanol, benzene, chloroform and cyclohexane within the wavelength range 200-500 nm are given in Fig. (11) while their pectral data are listed in Table (9).

The electronic spectra can be devided into two regions; the first one extended up to 280 nm contains mainly the two bands (A) and (B) which are almost solvent and substituent independent and are assigned to the local excitation within the phenyl moeities due to ($^1L_a \longleftarrow {}^1A$) and ($^1L_b \longleftarrow {}^1A$) respectively. These two bands are not observed in the spectra of some solvents such as benzene due to the opacity of it in the uv region.

The second region extends from 280 to 380 nm containing mainly a broad, less intense and solvent dependent band (C) which is due to the charge transfer interaction. This band displays a red shift of the order I > II > III which is attributed to the higher acceptor character of the COOH > Cl and the donation character of OCH_3 group which will facilate the intramolecular charge transfer.

Attempts have been made to assess the influence of solvents using variety of experimental conditions and thus give some empirical values to different solvents, this is the so called microscopic and macroscopic solvent polarity parameters.

(i) <u>Microscopic Solvent Polarity Parameters</u>:

The first empirical parameter is the so called Z-value introduced by **Kosower**[69,70] who was the first to

set up comprehensive scale for solvent polarity. He found that the charge transfer absorption of 1-alkyl-pyridinium iodides exhibited a pronounced negative solvatochromism and used 1-ethyl-4-methoxycarbonylpyridinium as a test dye

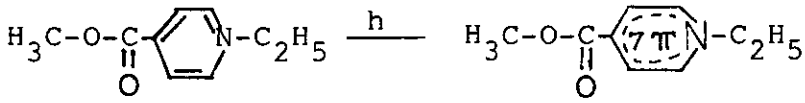

ground state excited state

Kosower termed the molar transition energies, calculated from the position of the absorption maximum, Z-values

$$Z = \frac{2.8259}{\lambda_{nm}} \text{ K.Cal.mole}^{-1} \qquad (3)$$

Reichardt et al.[71,72] applied Kosower's technique to a series of pyridinium-N-phenol betaines; (a and b) which are perhaps the most solvent dependent spectra known. The molar transition energies of these betaines termed E_T value and can be calculated by the following relation:

$$E_{T\ (\text{K.Cal.mole}^{-1})} = 2.859\text{x}10^{-3} \text{ x } \nu_{(\text{cm}^{-1})}$$

E_T is another empirical solvent polarity.

Taft and Kamlet[73-75] considered the solvent effect to be composed of three independent contributions; polarity (π), acidity (α) and basicity (β). α and β scales of solvents are a type of solvent pparameters which reflect the hydrogen bonding strength of:

(i) hydrogen bond donor solvent HBD (α) and

(ii) hydrogen bond acceptor solvent HBA (β).

It is noticed that the bands due to the local excitation are not affected by the change of the polarity of the medium, hence our forth-coming discussion will be restricted to the CT band.

The microscopic solvent polarity parameters E_T or Z-values as well as the recent solvent polarity parameters π, α and β-values are plotted vs the λ_{max} of the CT band [representative example is given in Fig. (12)], the plots give linear relation with some deviations in each case. This linearity indicates that the hydrogen bond donor solvent (α) or the hydrogen bond acceptor solvent (β) support the occurence of the specific association through protondonor acceptor system.

(ii) <u>The Macroscopic Solvent Polarity Parameters</u>:

The properties of the solvent which show a reasonable

degree of correlation with the transition energy is the dielectric constant and refractive index. The relation govering this behaviour was given by **Gati and Szalay**[76] in the form of:

$$\Delta \bar{\nu} = (a-b)\ \left(\frac{n^2 - 1}{2n^2-1}\right) + b\ \left(\frac{D-1}{D+1}\right)$$

in which a,b are constants depending on the nature of the solute, n is the refractive index and D is the dielectric constant of the medium. According to this relation the plot of $\Delta \bar{\nu}$ as a function of the term $\frac{D-1}{D+1}$ would be a linear relation if the dielectric forces are the predominant factor influencing the shift of the band position. The plot shown in Fig. (13) indicates that this is not the case for the compounds under investigation.

A more precise relation are the functions of dielectric constant given by **Suppan**[77] of the type:

$$F(D) = \frac{2(D-1)}{2(D+1)} \text{ and } \phi\ (D) = \frac{D-1}{D+2}$$

relating the shift in band position with dielectric constant of the medium. The plot of λ_{max} of the CT band in different organic solvent used, against the functions F(D) or ϕ(D) gave no linear relation indicating that dielectric properties of the medium are not the main factors affecting the excitation energy.

On the other hand, **Bayliss[78] and McRae[79]** derived a multiparameter equation containing the function of F(n) and $F_2(n)$:

$$F(n) = \frac{n^2-1}{2n^2+1} \quad , \quad F_2(n) = \frac{n^2-1}{n^2+1}$$

relating the shift in the CT band position with the refractive index of the medium. The plots of λ_{max} of the CT band against these two functions gave also non-linear relation. Furthermore, thhe plots of λ_{max} as a function of F(D,n)[80] and $F^-(D,n)$[79]:

$$F(D,n) = [\frac{D-1}{2D+1} - \frac{n^2-1}{2n^2+1}] \quad , \quad F^-(D,n) = [\frac{D-1}{D+2} - \frac{n^2-1}{n^2+2}]$$

show the same deviation from linearity.

This behaviour reveals that these parameters are not the only factors affecting the position of the CT band but a specific solute solvent interaction (solvation or more effectivelly hydrogen bonding between solute and solvent molecules) is also contributing to the solvent shift. So, the shift of the CT band is actually the resultant effect of the (i) changed solvent polarity (ii) the shift due to intermolecular hydrogen bond formed between the solvent molecules and organic ligand, and (iii) the shift due to intramolecular hydrogen bond.

Absorption Spectra of Solutions of Ligands I, II and III in Different Organic Solvents

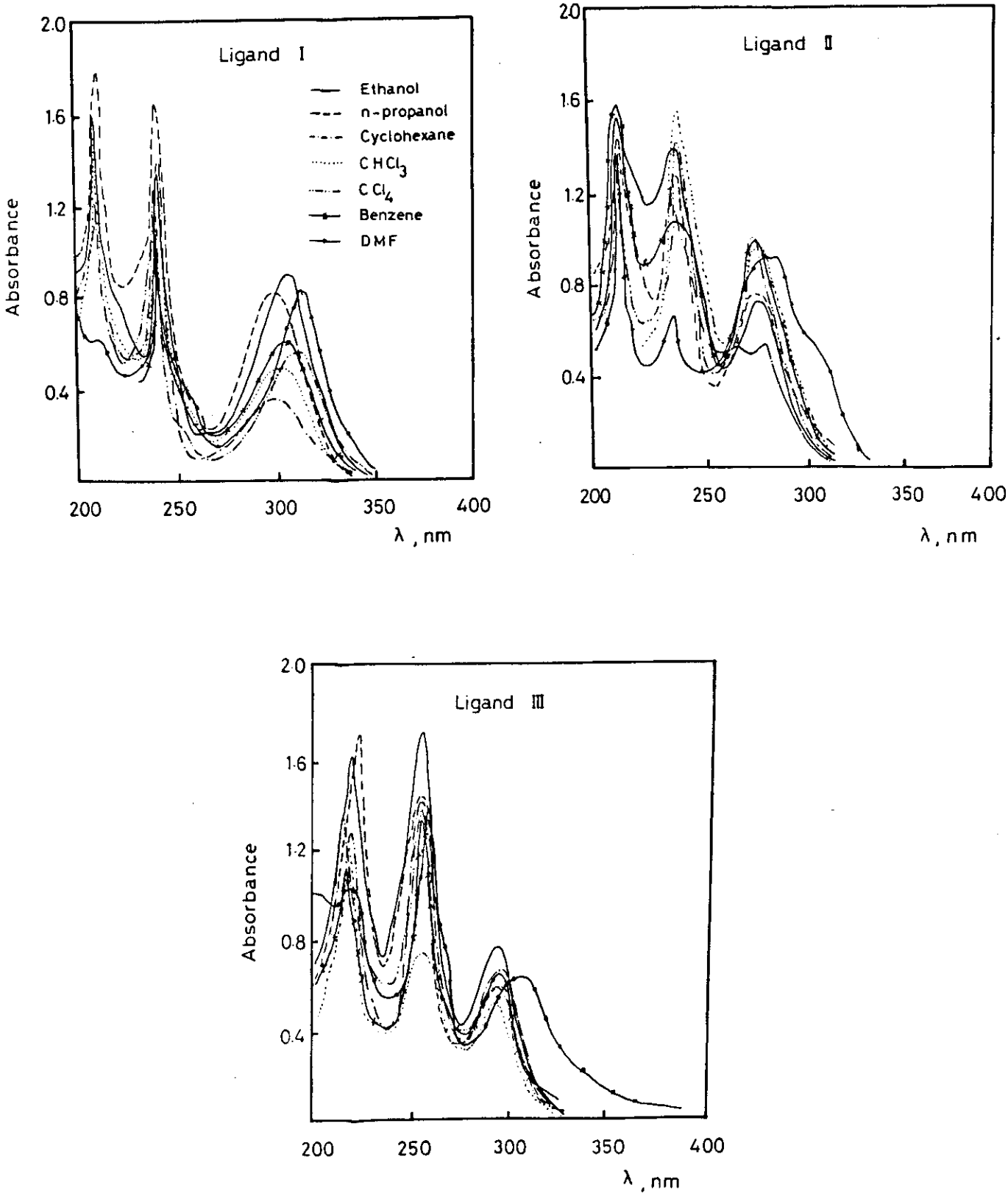

Fig. (11)

The Relation Between λ_{max} and π^* Values for CT Band of Ligand III

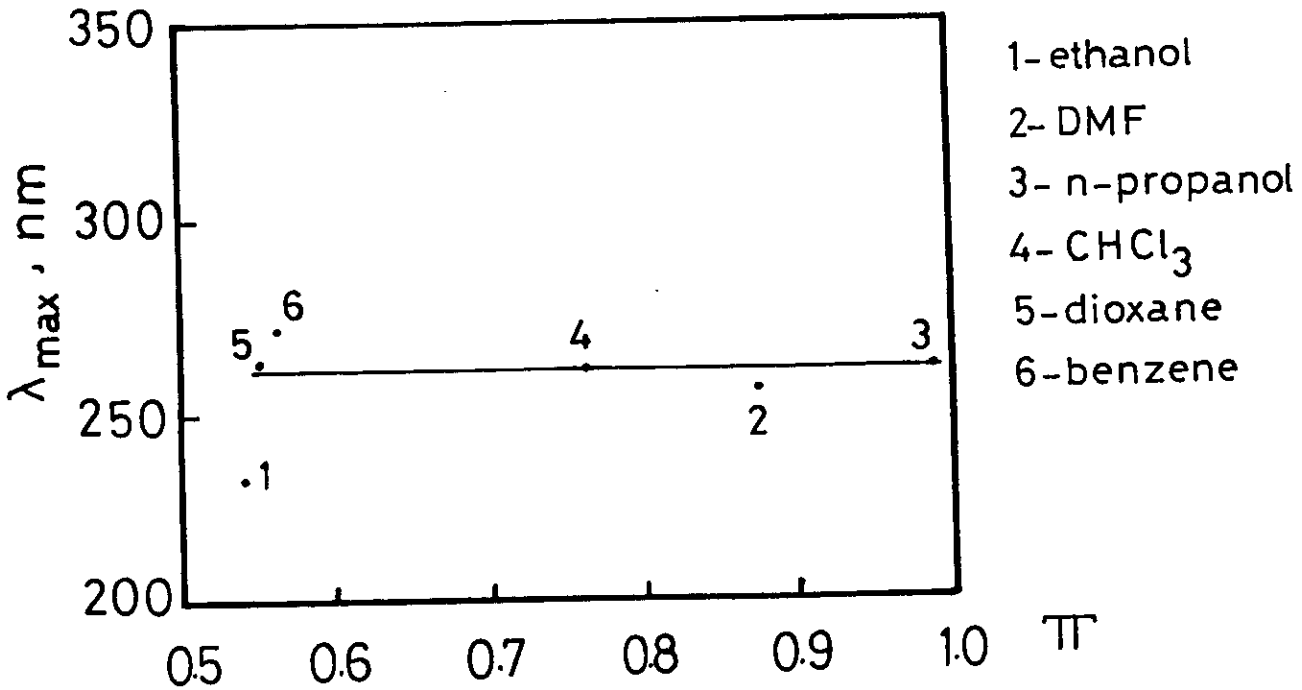

Fig. (12)

The Relation Between $\Delta\bar{\nu}$ and $\frac{D-1}{D+1}$ Values

for CT Band of Ligand III

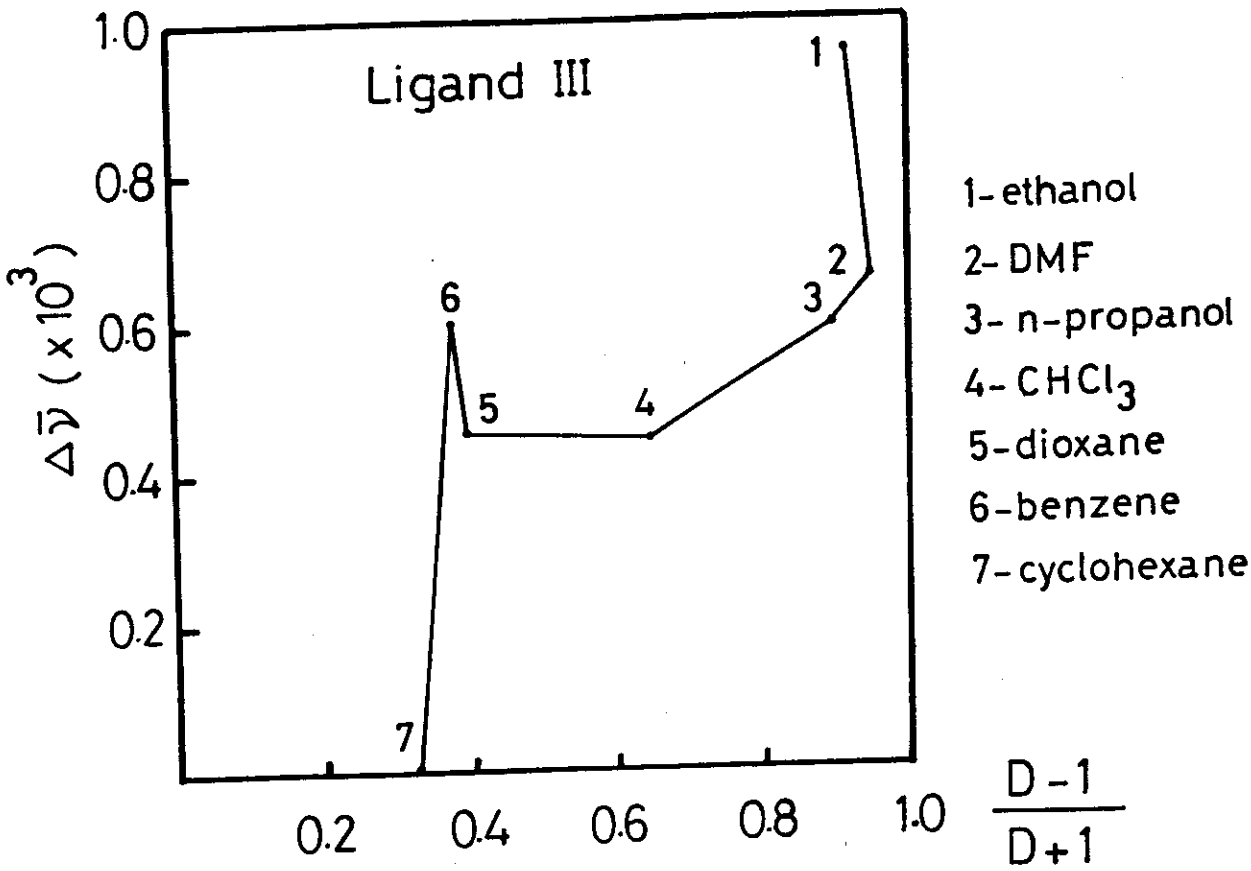

Fig. (13)

Tabe (9): Spectral data of compounds I, II and III in different organic solvents.

Ligand / Solvent	I				II				III			
	,nm			E_{CT}	,nm			E_{CT}	,nm			E_{CT}
	A	B	C		A	B	C		A	B	C	
ethyl	205	225	310	4.005	205	223	300	4.139	208	228	280	4.434
DMF	208	230	340	3.652	210	235	335	3.706	212	234	305	4.071
n-propanol	205	240	310	4.005	210	24.5	320	3.880	205	251	310	4.005
$CHCl_3$	-	258	300	4.139	-	255	320	3.880	-	250	320	3.880
Dioxan	205	250	310	4.005	208	253	330	3.763	208	260	310	4.005
benzene	-	-	320	3.880	-	-	330	3.763	-	-	320	3.880
Cyclo-hexane	203	244	370	3.356	205	253	-		208	255	380	3.267

CHAPTER III

PART (B)

STUDIES OF THE METAL CHELATES IN SOLUTION

1 - Conductometric Titration:

The stoichiometry of the complexes formed in solution between (Co^{2+}, Ni^{2+}, Cu^{2+}, La^{3+}, Gd^{3+} and Pt^{4+}) ions and ligands I, II and III was studied by conductometric titration . This method can be applied by titrating a known volume of the metal ion solution having a definite concentration ($1x10^{-5}M$) with the chelating agent as a titrant ($1x10^{-4}M$). Correction for the dilution effect should be performed by multiplying the value of the specific conductance measured by the factor $(V_1+V_2)/V_1$, where V_1 is the original volume and V_2 is the volume of the titrant.

The complex formation can be followed by studying the relationship between the conductance and the volume of the ligand added. The resulting curves are characterised by some breaks, the position of which gives information about the presence of different complexed species and denote their compositions.

The relationships between the conductance and the volume of the titrant are shown in Figs. (14-16) and

the probable stoichiometry of the complexes are collected in Table (10). The common behaviour is the increase of the conductance of the solution with the increase of the volume of the titrant. This behaviour can be expl- ained by the factors govering the chang in conductance:

(a) The increase of the volume of the metal ion on chelate formation which is accompanied by decrease in the value of diffusion coefficient of the particle. The relation between conductivity and diffusion coefficient is:

$$D^\circ = \frac{RT}{ZF^2} . \Lambda^2$$

The diffusion coefficient is related to the volume of diffusing particle by the Stocks-Einstein equation:

$$D^\circ = \frac{K}{(V_m)^{\frac{1}{3}} \eta}$$

where D° is the diffusion coefficient of the conducting species, V_m is the molar volume and η is the viscosity of the medium.

(b) The lowering of the charge on the metal ion through covalent bond formation with the ligand.

(c) The libration of H^+ ions from the ligand through bonding with the metal ion.

The first and second factors lead to lowering the conductance while the third one favours increasing the

ionic conductivity. Accordingly, the net effect will be resultant of all these factors depending on the nature of the metal ion and the medium.

Conductometric titration of acenaphthenequinone monophenylhydrazone derivatives with transition metal ions:

The conductometric titration of ligands I, II and III with Co^{2+}, Ni^{2+}, Cu^{2+}, La^{3+}, Gd^{3+} and Pt^{4+} ions are shown in Figs. (14-16) and the results gained are listed in Table (10). The data obtained indicate the probable formation of (1:1) complexes in solutions of low concentration of ligands I, II and III and (1:2) M:L complexes at relatively high ligand concentration for only ligand II with Co^{2+}, Ni^{2+}, Cu^{2+}, La^{3+} and Gd^{3+} ions.

Table (10): Stoichiometry of complexes of Co^{2+}, Ni^{2+}, Cu^{2+}, La^{3+}, Gd^{3+} and Pt^{4+} with hydrazone derivatives.

Ligand	Stoichiometry of complexes (M/L)					
	Co^{2+}	Ni^{2+}	Cu^{2+}	La^{3+}	Gd^{3+}	Pt^{4+}
I	1:1	1:1	1:1	1:1	1:1	1:1
II	1:1	1:1	1:1	1:1	1:1	1:1
	1:2	1:2	1:2	1:2	1:2	-
III	1:1	1:1	1:1	1:1	1:1	1:1

Conductometric Titration of Metal Ions with Ligand I

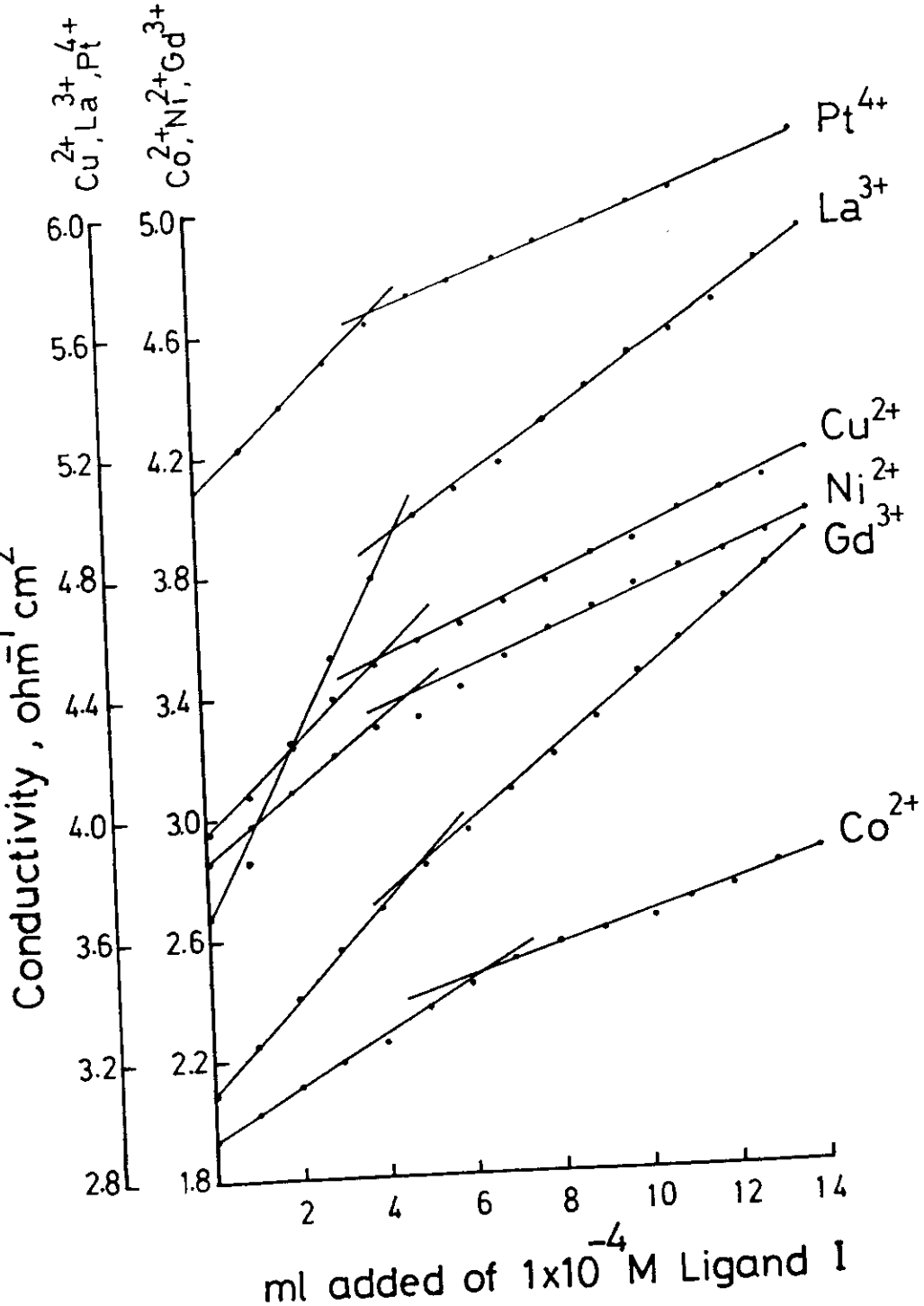

Fig. (14)

Conductometric Titration of Metal Ions with Ligand II

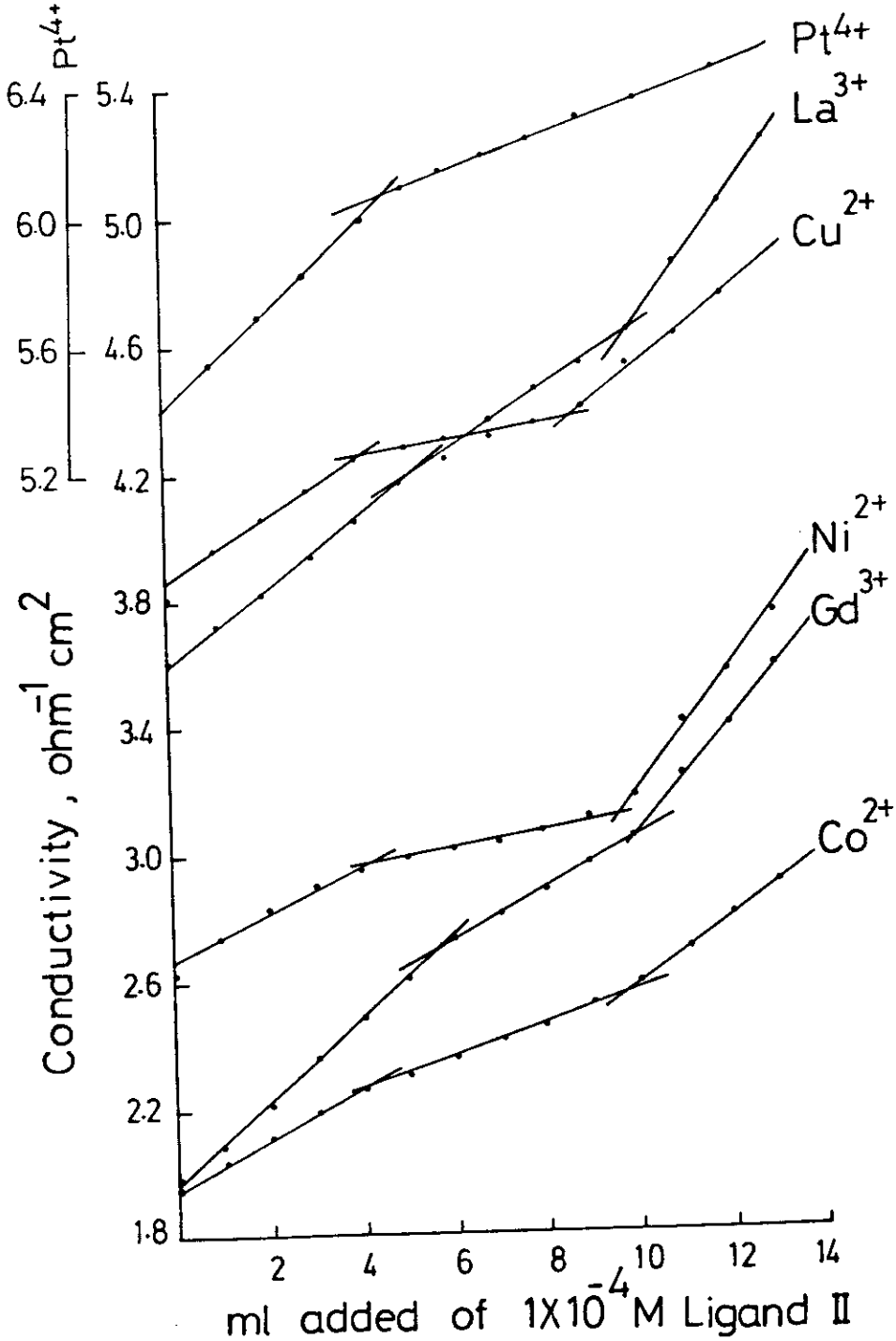

Fig. (15)

Conductometric Titration of Metal Ions with Ligand III

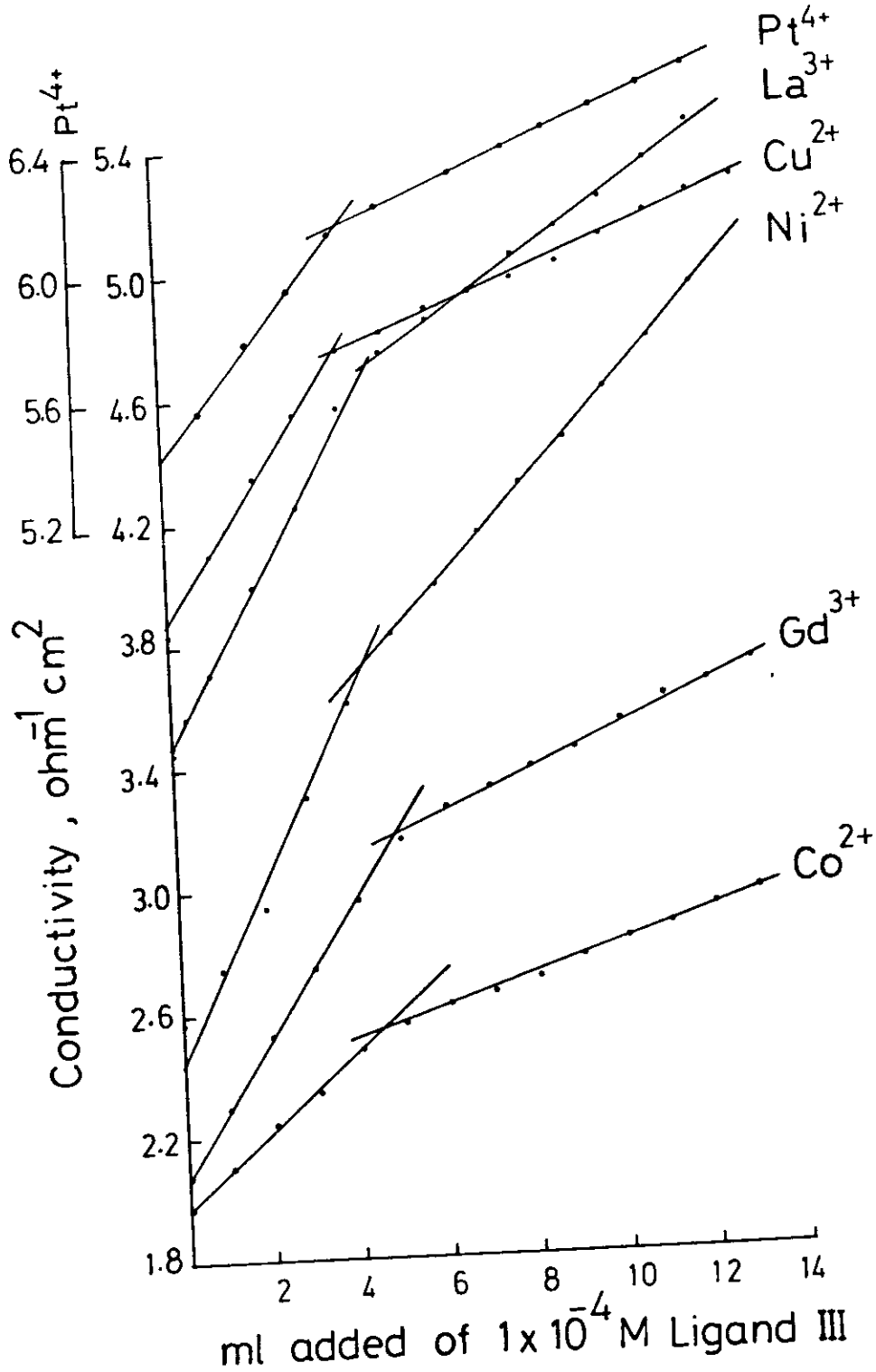

Fig. (16)

2 - Potentiometric Titration:

The potentiometric method has been used extensively in many branches of solution chemistry. It is one of the most accurate and widely applicable techniques currently available for the study of ionic equilibria.

Measurement of the free hydrogen ion concentrations of solutions of different analytical compositions may be used for studying a number of types of equilibria involving protons. Thus, for the system H^+, L, the average number of hydrogen ions bonded to the free ligand (L) can be expressed by the following relation:

$$\bar{n}_H = \frac{[H^+] - h + [OH^-]}{[L]}$$

where $[H^+]$ is the total ion concentration of dissociable hydrogen and $[OH^-]$ may usually be neglected in solutions of pH < 7. The stoichiometric equilibrium constants for the formation of the acids H_jL may be calculated from the experimental function $\bar{n}_H(h)$ by one of the usual methods[81]. The degree of formation of hydroxo-complexes of metal ions is given analogously by the equation

$$\bar{n} = \frac{[H^+] - h + [OH^-]}{[M]}$$

Measurements of hydrogen ion concentration may also be used to follow complex formation in a large number of systems M (central metal atom), L, H^+, where

the ligand L can combine with protons; the applicability of this procedure and the computation of the stability constants from the experimental function h (M, L, H^+)° was used.

The titration procedure which was used in this work is that developed by **Calvin**[82] **and Bjerrum**[83]. The computation methods of **Irving and Rossotti**[84,85] as adapted by **Fronaeus**[86] can be employed for the evaluation of proton-reagent and metal-reagent stability constants. The average number of the protons associated with the reagent molecule $\bar{n}_A$, is determined at different pH values applying the following equation:

$$\bar{n}_A = Y + \frac{(V_1-V_2)\ (N^\circ+E^\circ)}{(V^\circ+V_1)\ TC_L^\circ} \qquad (1)$$

where V_1 and V_2 are the volumes of alkali required to reach the same pH in the titration curve of perchloric acid and reagent respectively. V° the initial volume (50 ml) of the mixtures, TC_L° the total concentration of the reagent, N° normality of sodium hydroxide solution and E° the initial concentration of the free acid. The values of $\bar{n}_A$ are plotted against pH and the values of proton-ligand stability constants K_1^H and K_2^H are calculated by interpolation at half $\bar{n}_A$ values. In the complexation of metal ions and ligand, the values of the first

and second stepwise stability constants k_1 and k_2 of the complexes can be determined. The average number of the reagent molecules attached per metal ion, $\bar{n}$, and free ligand exponent, pL, can be calculated using the equations:

$$\bar{n} = \frac{(V_3-V_2)\ (N^\circ+E^\circ)}{(V^\circ+V_1)\bar{n}_A\ TC_{M^\circ}} \qquad (2)$$

and

$$pL = \log_{10} \frac{\sum_{n=0}^{n=J} \beta_n^H \left(\frac{1}{\text{anti log pH}}\right)^n}{TC_{L^\circ} - \bar{n}\ TC_{M^\circ}} \cdot \frac{V^\circ+V_3}{V^\circ} \qquad (3)$$

where TC_{M° the total concentration of the metal ions present in the solution, β_n^H overall proton-reagent stability constant. V_1, V_2 and V_3 are the volume of alkali required to reach the same pH in the titration curves of perchloric acid, organic ligand and complex respectively. On plotting the values of $\bar{n}$ against the pL and interpolation at the half $\bar{n}$ values, the stepwise stability constants of the chelates can be evaluated.

Potentiometric titration of chelates of acenaphthenequinone mono-phenylhydrazone derivatives with Co^{2+}, Ni^{2+}, Cu^{2+}, La^{3+} and Gd^{3+} ions:

The pH-metric titrations are performed in presence of acid mixture (A) as a medium consisting of 0.1M perchloric acid and 1M of sodium perchlorate as recommended

by **Bjerrum**[83] Mixture (B) is a mixture of (A) and the hydrazone ligand of concentration $5x10^{-4}M$. Mixture (B) is mixed with different metal ions of concentration $2.5x10^{-3}M$ (C). In all mixtures A, B and C (mixtures of metal ions), absolute ethanol of 50% (v/v) is enough to keep the components of the mixture in a soluble state during the titration. These mixtures are then titrated with 0.204M of NaOH free from carbonate containing 50% by volume of ethanol. The potentiometric titration curves of compounds I, II and III with different metal ions are shown in Figs. (17-19). The curves obtained are S-shaped with a sharp jump in mixtures (A) and (B) but relatively smooth curves with mixtures which contain the metal ions.

The average number of protons associated with the reagent molecule $\bar{n}_A$, at different pH values are determined using equation (1). Plotting of $\bar{n}_A$ against pH of the solution gives a proton-reagent formation curve as shown in Figs. (17-19). From these curves the proton-reagent stability constants of the organic ligands are calculated and the data obtained are recorded in Table (11).

The average number of the reagent molecules attached per metal ions, $\bar{n}$, at different pH values are calculated

with the free ligand exponent, pL, using equations (2) and (3). The metal-ligand formation curves ($\bar{n}$-pL) are given in Figs. (17-19).

Table (11): Proton-reagent stability constants and formation constants of Co^{2+}, Ni^{2+}, Cu^{2+}, La^{3+} and Gd^{3+} with acenaphthenequinone monophenylhydrazone derivatives.

Ligand	Proton ionization constants		formation constants of chelates				
			Co^{2+}	Ni^{2+}	Cu^{2+}	La^{3+}	Gd^{3+}
	$\log k_1^H$	$\log k_2^H$	pK_1	pk_1	pK_1	pk_1	pk_1
I	9.10	4.8	5.05	5.35	5.40	5.25	5.20
II	9.15	-	4.75	4.80	5.20	4.80	4.90
III	9.25	-	4.80	5.40	5.45	5.30	5.00

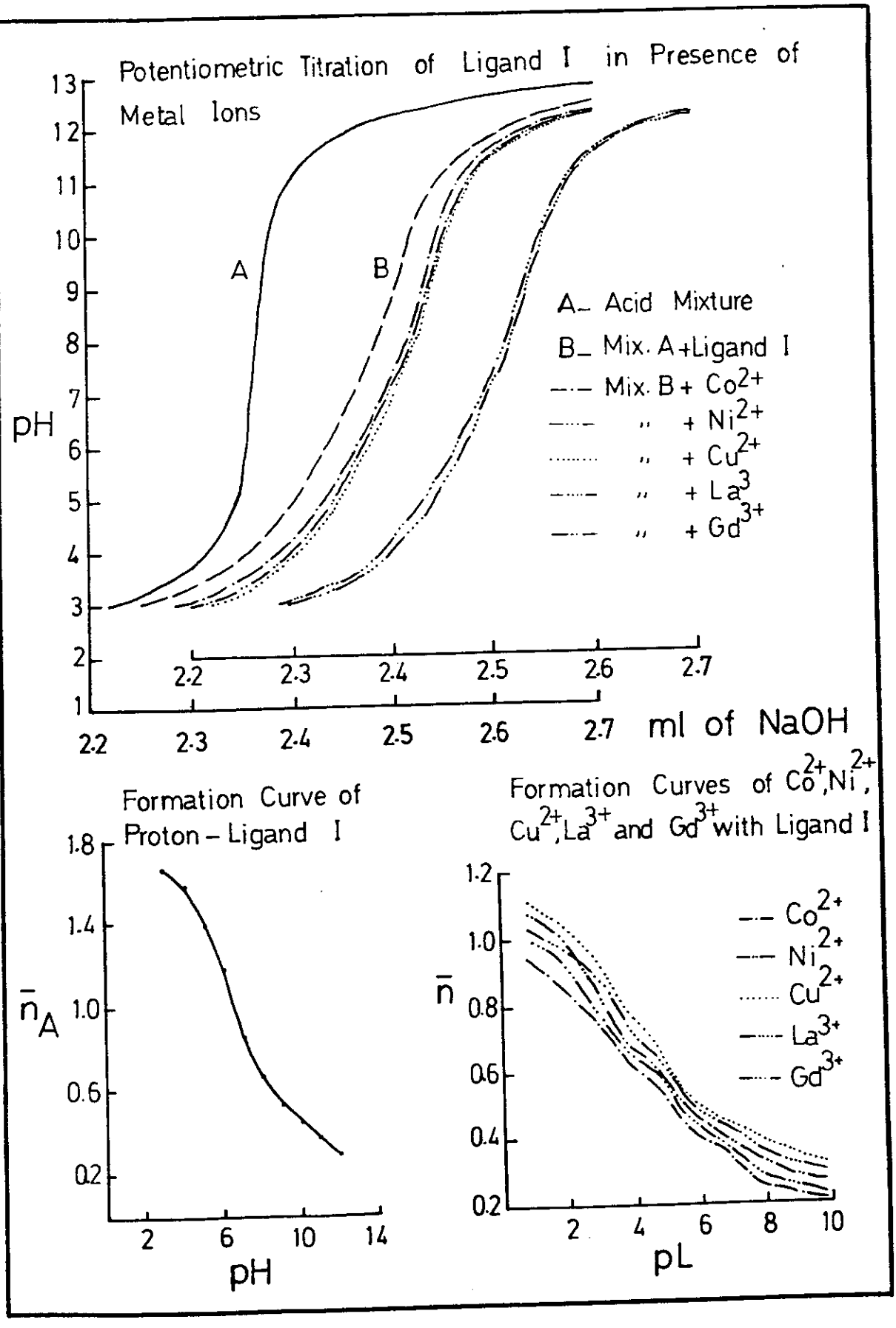
Potentiometric Titration of Ligand I in Presence of Metal Ions
pH
ml of NaOH
A
B
A– Acid Mixture
B– Mix. A+Ligand I
Mix. B + Co2+
" + Ni2+
" + Cu2+
" + La3
" + Gd3+
Formation Curve of Proton – Ligand I
n̄A
pH
Formation Curves of Co2+, Ni2+, Cu2+, La3+ and Gd3+ with Ligand I
n̄
pL
Co2+
Ni2+
Cu2+
La3+
Gd3+

Fig. (17)

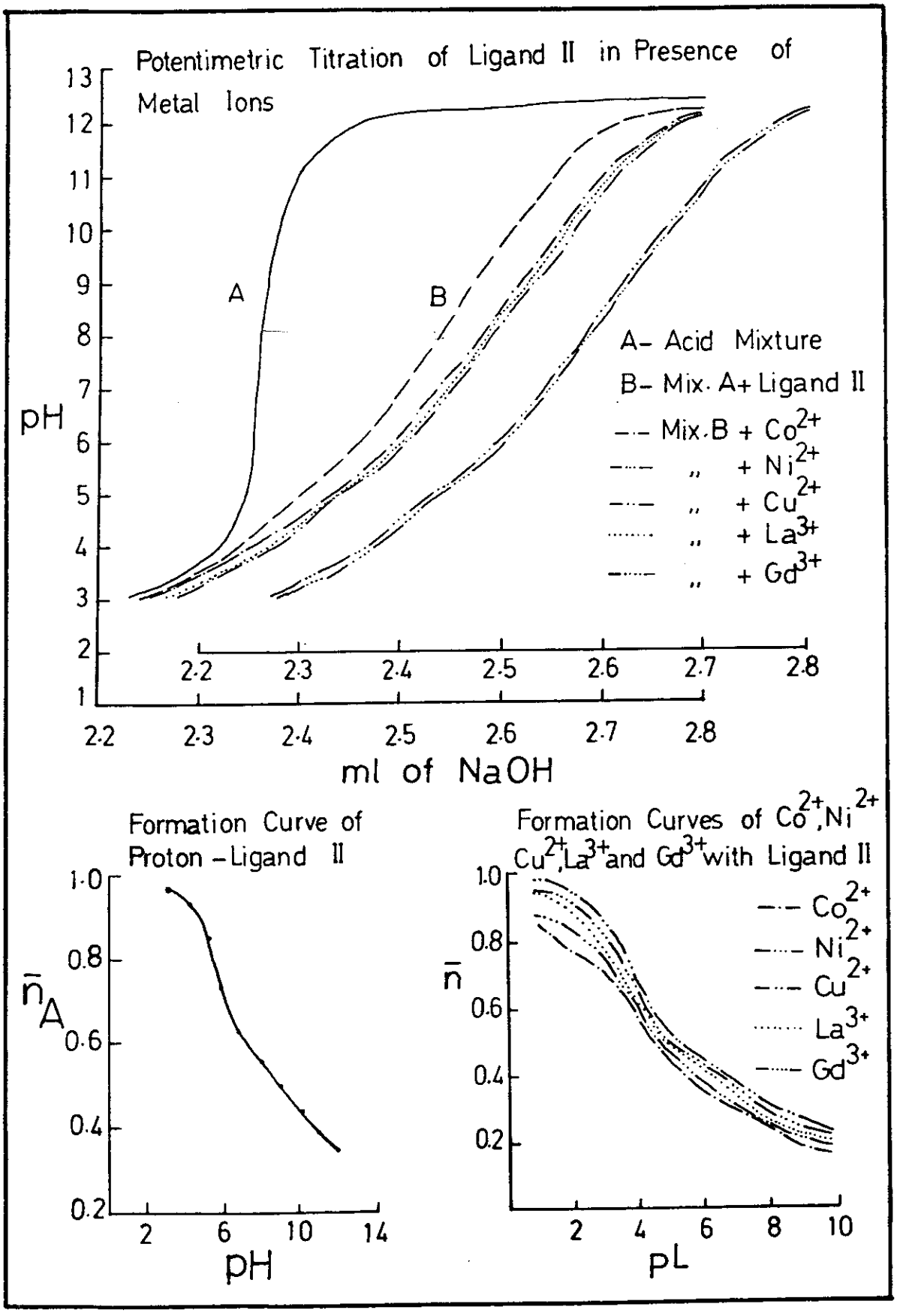
Potentimetric Titration of Ligand II in Presence of Metal Ions
pH
ml of NaOH
A
B
A– Acid Mixture
B– Mix. A+ Ligand II
Mix.B + Co2+
" + Ni2+
" + Cu2+
" + La3+
" + Gd3+
Formation Curve of Proton – Ligand II
n̄A
pH
Formation Curves of Co2+, Ni2+ Cu2+, La3+ and Gd3+ with Ligand II
n̄
pL
Co2+
Ni2+
Cu2+
La3+
Gd3+

Fig. (18)

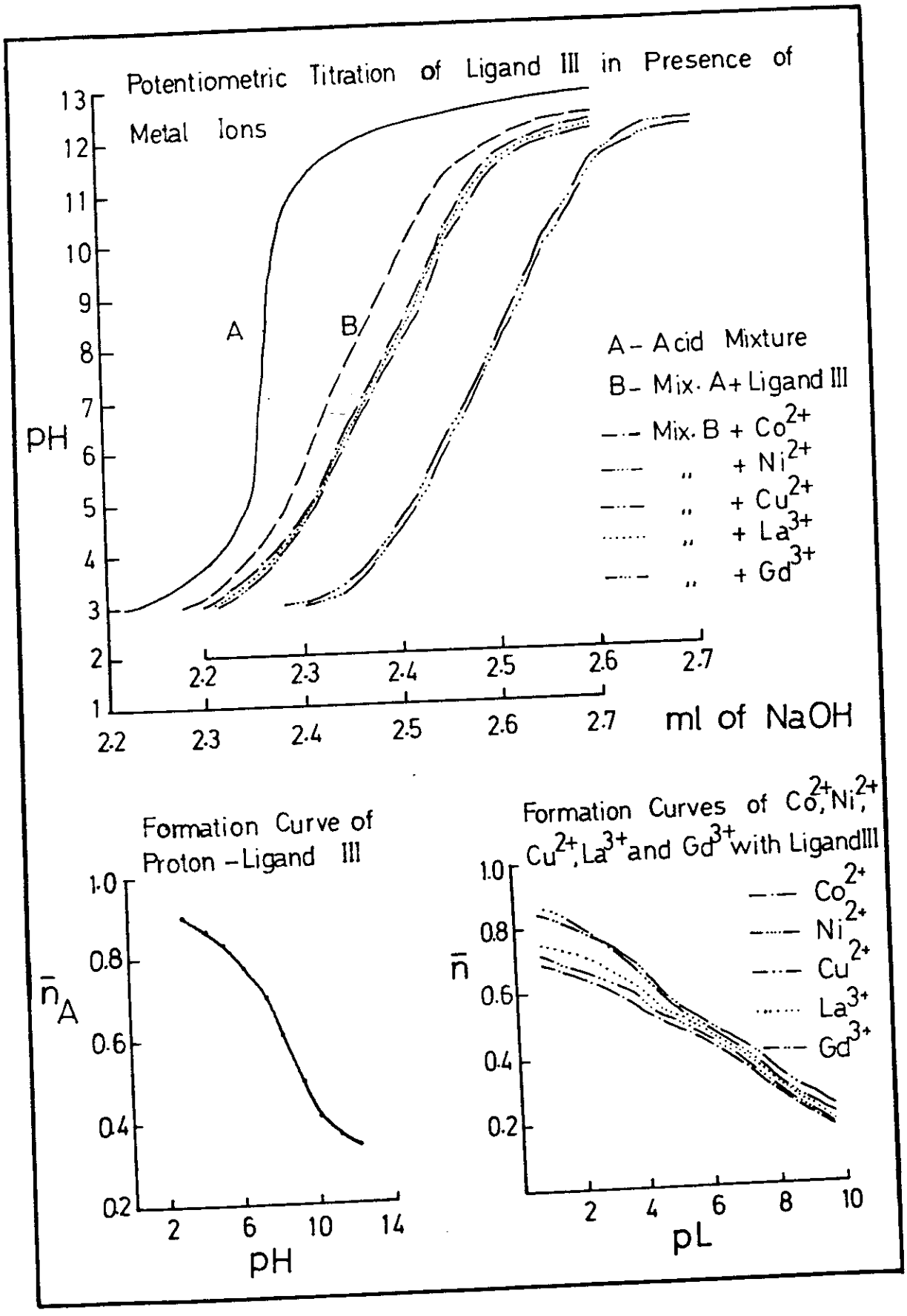
Potentiometric Titration of Ligand III in Presence of Metal Ions
pH
ml of NaOH
A
B
A – Acid Mixture
B – Mix. A + Ligand III
Mix. B + Co2+
" + Ni2+
" + Cu2+
" + La3+
" + Gd3+
Formation Curve of Proton – Ligand III
n̄A
pH
Formation Curves of Co2+, Ni2+, Cu2+, La3+ and Gd3+ with LigandIII
n̄
pL
Co2+
Ni2+
Cu2+
La3+
Gd3+

Fig. (19)

3 - **Polarographic Studies of Some Metal Chelates: Studies of comlexes of Co^{2+}, Ni^{2+} and Cu^{2+} with ligand I, II and III:**

Different concentrations of ligands I, II or III ($1x10^{-5}$M to $6x10^{-5}$M) were added to $5x10^{-5}$M of Co^{2+} or Ni^{2+} ions in the universal buffer of pH=7 containing 30% (by volume) ethyl alcohol. In case of Cu^{2+} ions, acetate buffer was used of the same pH. The polarograms obtained are sown in Figs. (20-22), which consist mainly of two waves.

As the ligand concentration increases, the $E_{\frac{1}{2}}$ shifts toward more negative potential indicating the complex formation between the metal ion and the ligand. The plot of $E_{\frac{1}{2}}$ vs. -log C_x as required by the relation[87]:

$$E_{\frac{1}{2}} = \frac{0.0591}{n} \log K - P \frac{0.0591}{n} \log C_x$$

gives a straight line. The number of ligand/metal ion, P, has been determined from the slope of the plot of $E_{\frac{1}{2}}$ vs. -log C_x, Figs. (20-22). The stability constants of different complexes have been determined using the **Lingane Method**[87]. The intercept of the plot on the ordinate axis at (-log C=0) gives the value of [(0.0591/n) log k] from which log k is then calculated, where n=2. The values of log k

for metal complexes of Co^{2+}, Ni^{2+} and Cu^{2+} with ligands I, II and III are recorded in Table (12).

The values of the stability constants runs in the order $Cu^{2+} > Ni^{2+} > Co^{2+}$ which is in accordance with the electronegativity series and the increased values of (e/r).

Table (12): Stability constants of chelates of Co^{2+}, Ni^{2+} and Cu^{2+} with ligands I, II and III calculated from polarographic measurements.

metal ion	pK		
	ligand I	ligand II	ligand III
Co^{2+}	4.78	4.82	4.66
Ni^{2+}	4.94	4.90	4.84
Cu^{2+}	5.11	5.05	5.28

The Relation Between $\Delta E_{1/2}$ and -Log C_x

for Ligand I with Co^{2+}, Ni^{2+} and Cu^{2+}

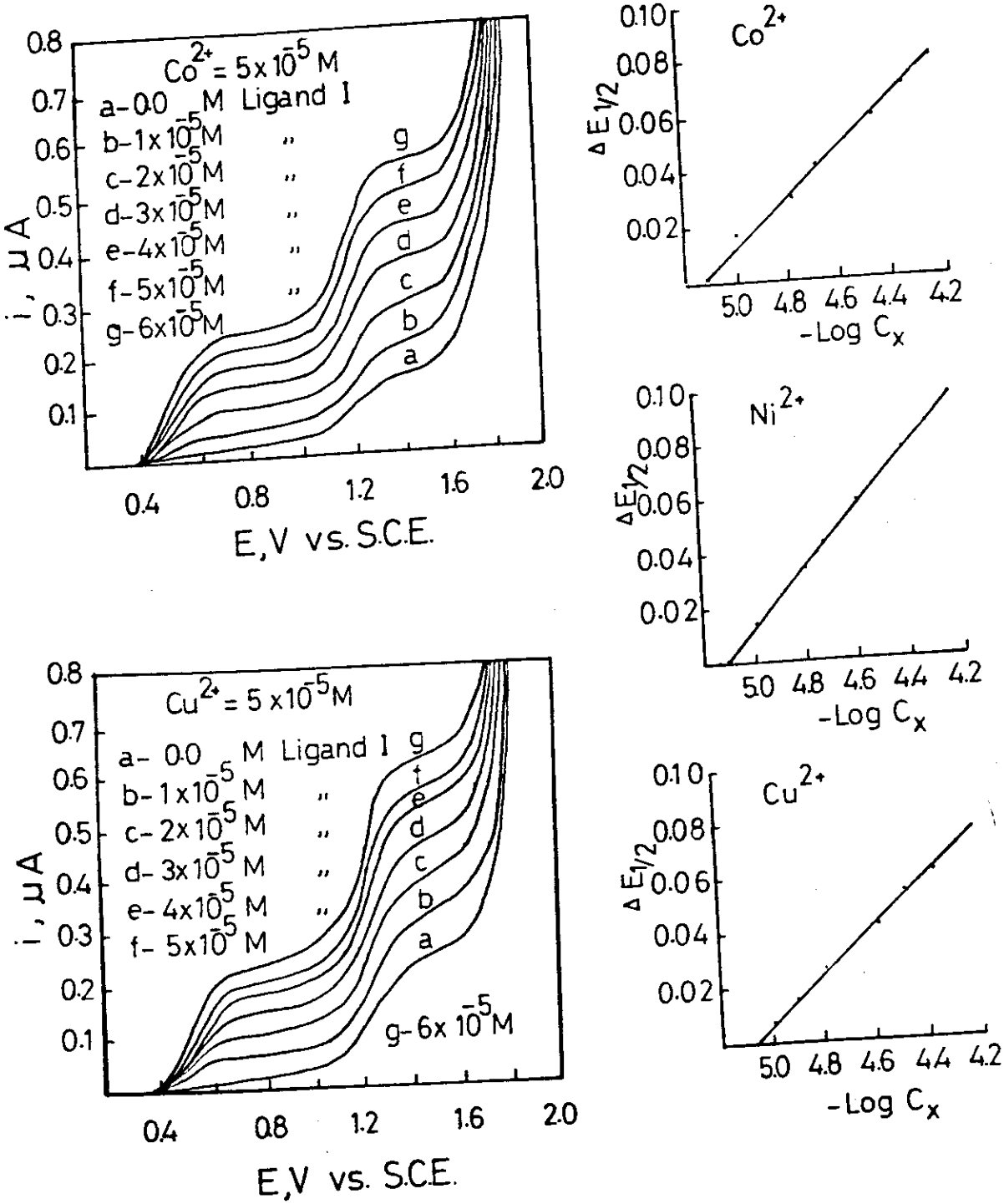

Fig.(20)

The Relation Between $\Delta E_{1/2}$ and $-\text{Log } C_x$ for Ligand II with Co^{2+}, Ni^{2+} and Cu^{2+}

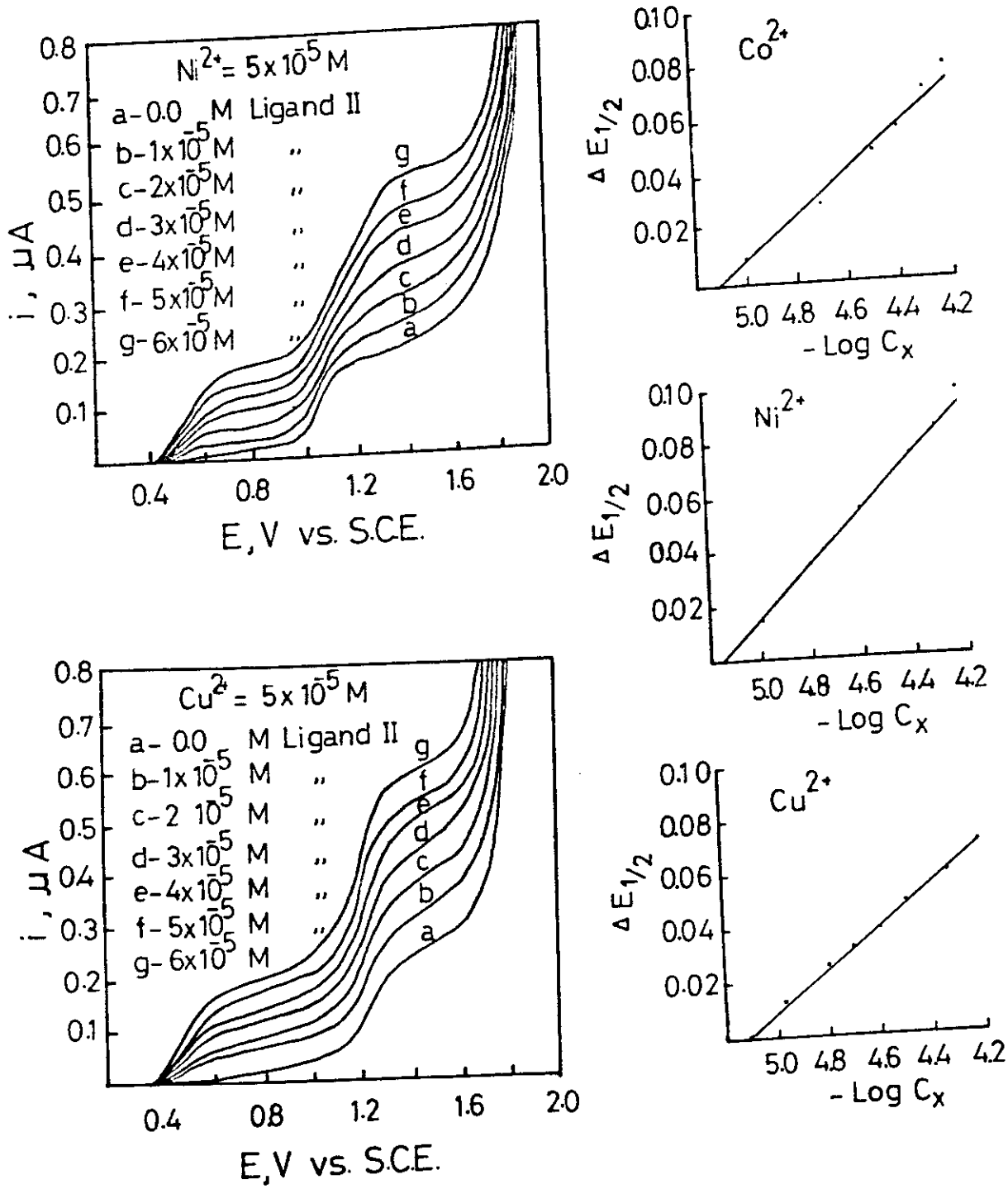

Fig. (21)

The Relation Between $\Delta E_{1/2}$ and $-\text{Log } C_x$

for Ligand III with Co^{2+}, Ni^{2+} and Cu^{2+}

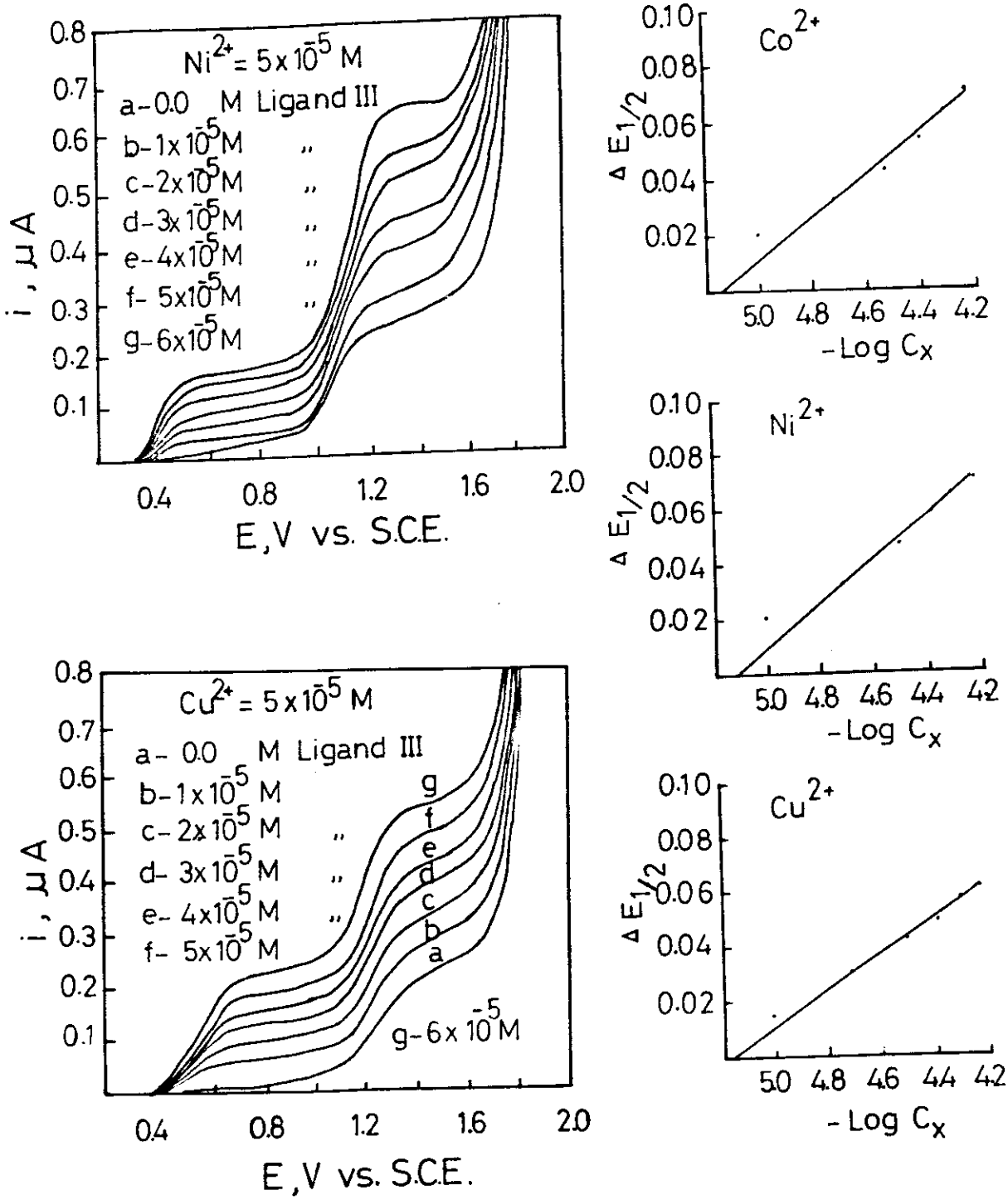

Fig. (22)

4 - **Spectrophotometric studies of metal chelates in solution :**

The spectrophotometric methods applied for detection and determination of complex formation in solution are:

1 - The molar ratio method of **Yoe and Jones**[88].

2 - The straight line method of **Asmus**[89].

3 - The continuous variation method of **Job**[90] reevaluated by **Vosburgh and Cooper**[91].

The compounds chosen as chelating agents are: acenaphthenequinone-(2-carboxyphenyl)-hydrazone (ligand I), acenaphthenequinone-(2-methoxyphenyl)-hydrazone (ligand II) and acenaphthenequinone-(2-chlorophenyl)-hydrazone (ligand III). The complexes formed between these ligands and Co(II), Ni(II), Cu(II), La(III), Gd(III) and Pt(IV) ions were examined spectrophotometrically using universal buffer in solutions containing 30% by volume ethanol. The optimum pH values of the buffer used are 7 for ligand (I) and 6 for ligands II and III.

The blank solution used in spectrophotometric measurements is an aqueous buffer containing 30% by volume ethanol.

A - The stoichiometry of complexes of acenaphthenequinone-(2-carboxyphenyl)-hydrazone with Co^{2+}, Ni^{2+}, Cu^{2+}, La^{3+}, Gd^{3+} and Pt^{4+} ions:

(1) The molar ratio method:

A series of solutions was prepared in which the metal ion concentration remained constant at $5x10^{-5}M$ while that of ligand I was varied from $1x10^{-5}M$ to $1.2x10^{-4}M$. The absorption spectra of these solutions are characterised by one band with two absorption peaks having λ_{max} at 303 and 314 nm. whereas the absorption band of the free ligand I has λ_{max} at 300 and 310 nm.

The absorbances of the solutions of different molar ratios measured at λ=303 and 314 nm are plotted vs. the molar ratio [ligand I]/[metal ion]. The results are shown graphically in Figs. (23-28). The curves are composed of two linear portions which intersect at the molar ratio (1:1) for all metal ions. This indicates the formation of one type of complexes having the stoichiometry (1 metal ion: 1 ligand I).

(2) The straight line method:

This method was first described by **Asmus**[89] for determining the stoichiometry of a complex having appreciable dissociation and was further applied by **Korkuc, Sommer and Lipiec**[92] for studying the complexes of

ferric acetylacetanilide and copper isonicotonic hydrazine. The method was verified by **Issa et al.**[93], during the study of several metal complexes. In this method, certain volume of metal ion solution (V_m) is mixed with continuously increasing volumes (V_L) of ligand I solution having the same molar concentration. The reciprocal absorbance (1/A) of these solutions measured at 303 and 314 nm is plotted vs. reciprocal volume of the ligand solution raised to a power n, ($1/V_L^n$), where n=0.5, 1, 1.5, 2 ... etc. The results obtained for metal ions Co^{2+}, Ni^{2+}, Cu^{2+}, La^{3+}, Gd^{3+} and Pt^{4+} are shown in Figs. (23-28). These plots show a linear relationship only for n=1 for all metal ions indicating the probable formation of one type of complexes (1 metal ion: 1 ligand I).

The plot of log A vs. log V_L at the same values of λ_{max} gives a linear relation with slope corresponding to the stoichiometry of the complex formed in solution, Figs. (23-28). The values obtained from these plots are 1.042 and 0.972 for Co^{2+}, 1.022 and 0.988 for Ni^{2+}, 0.943 and 0.902 for Cu^{2+}, 1.018 and 0.948 for La^{3+}, 1.013 and 0.947 for Gd^{3+} and 0.833 and 0.843 for Pt^{4+} at λ=303 and 314 nm respectively. These values confirm the existence of one complex of (1 metal ion: 1 ligand I) type.

(3) The continuous variation method:

A series of solutions was prepared by mixing equimolecular solutions of the metal ions and ligand I in varying proportions while keeping the total molar concentration constant at $1x10^{-4}$M. The plot of the absorbance of each solution measured at 303 and 314 nm vs. the mole fraction of each metal ion are shown in Figs. (23-28). These plots give peaks at mole fractions of 0.5, indicating the formation of complexes having the stoichiometry (1 metal ion: 1 ligand I).

The stoichiometries of different complexes of ligand I are collected in Table (13).

B - The stoichiometry of complexes of acenaphthenequinone-(2-methoxyphenyl)-hydrazone with Co^{2+}, Ni^{2+}, Cu^{2+}, La^{3+}, Gd^{3+} and Pt^{4+} ions:

(1) The molar ratio method:

Varying concentrations of ligand II solutions (from $1x10^{-5}$M to $1.2x10^{-4}$M) were added to constant metal ion concentration ($5x10^{-5}$M). The absorption spectra of these solutions are characterised by one band with two absorption peaks having λ_{max} at 302 and 312 nm whereas the absorption band of the free ligand II is of λ_{max} at 298 and 310 nm. The absorbances of these solutions measured at 302 and 312 nm were plotted

vs. the molar ratio [ligand II]/[metal ion]. These relationships are composed of three linear portions intersecting at the molar ratio (1:1) and (1:2) for metal ions Co^{2+}, Ni^{2+}, Cu^{2+}, La^{3+} and Gd^{3+}. This indicates the formation of two types of complexes having the stoichiometry (1 metal ion: 1 ligand II) and (1 metal ion: 2 ligand II). The absorbance-molar ratio relationship for Gd^{3+} ion is shown graphically in Fig. (29).

In case of Pt^{4+} the curve is composed of two linear portions intersecting at the molar ratio (1:1), which indicates the formation of only one complex having the stoichiometry (1 Pt^{4+}: 1 ligand II).

(2) <u>The straight line method</u>:

The reciprocal of absorbance measured at λ =302 and 312 nm is plotted vs. the reciprocal of the volume of ligand II solution raised to a power n, $(1/V_L^n)$ where n=0.5, 1, 1.5, 2 ... etc. A linear relationship is only obtained at n=1 indicating the formation of (1 metal ion: 1 ligand II) complex. This relationship is shown graphically in Fig. (29) for Gd^{3+} ion.

The plot of log A vs. log V_L gives a linear relation with slopes 1.022 and 0.972 for Co^{2+}, 1.008 and 0.949 for Ni^{2+}, 1.059 and 0.960 for Cu^{2+}, 1.078 and

0.977 for La^{3+}, 1.059 and 0.967 for Gd^{3+} and 1.087 and 0.946 for Pt^{4+} ions, for the two wavelengths respectively. The values of the slopes indicate the formation of one complex having the stoichiometry (1 metal ion: 1 ligand II). The log A - log V_L relationship is shown graphically in Fig. (29) for Gd^{3+} ion.

(3) <u>The continuous variation method</u>:

A series of solutions was prepared by mixing equimolecular solutions of the metal ions and ligand II in varying proportions while keeping the total molar concentration constant at $1x10^{-4}$M. The plot of absorbances of each solution measured at λ=302 and 312 nm vs. the mole fraction of Co^{2+}, Ni^{2+}, Cu^{2+}, La^{3+} and Gd^{3+} ions gives two peaks at mole fractions 0.5 and 0.35. This indicates the formation of two types of complexes (1 metal ion: 1 ligand II) and (1 metal ion: 2 ligand II) between these metal ions and ligand II. This relationship is shown graphically for Gd^{3+} ion in Fig. (29). In case of Pt^{4+}, there is only one peak at 0.5 which indicates the formation of one complex having the stoichiometry (1 Pt^{4+}: 1 ligand II).

The data of the stoichiometries of complexes of Co^{2+}, Ni^{2+}, Cu^{2+}, La^{3+}, Gd^{3+} and Pt^{4+} ions with ligand II are collected in Table (13).

C - **The stoichiometry of complexes of acenaphthenequinone-(2-chlorophenyl)-hydrazone with Co^{2+}, Ni^{2+}, Cu^{2+}, La^{3+}, Gd^{3+} and Pt^{4+} ions:**

(1) **The molar ratio method:**

A series of solutions was prepared in which the metal ion concentration was kept constant at 2.5×10^{-5}M while the concentration of ligand III was varied from 0.5×10^{-5}M to 0.6×10^{-4}M. The absorption spectra of each solution is characterised by one band with two peaks having λ_{max} at 302 and 314 nm. The maximum absorption of the free ligand is at 300 and 310 nm. The absorbances of solutions of different molar ratios measured at λ=302 and 314 nm are plotted vs. the molar ratio [ligand III]/[metal ion]. The resulting curves composed of two linear portions intersecting at the molar ratio 1:1 indicating the probable formation of (1 metal ion: 1 ligand III) complexes with all metal ions used. The results obtained in case of Ni^{2+} are shown graphically in Fig. (30).

(2) **The straight line method:**

The reciprocal of absorbance measured at λ=302 and 314 nm is plotted vs. the reciprocal of the volume of ligand III solution raised to a power n, $(1/V_L^n)$, where n=0.5, 1, 1.5, 2 ... etc. A linear relationship is obtained for n=1 indicating the probable formation of one complex of the type (1 metal ion: 1 ligand III) with

all metal ions. The plot of log A vs. log V gives a linear relations with slopes equal to 1.015 and 1.010 for Co^{2+}, 1.062 and 0.961 for Ni^{2+}, 0.960 and 0.906 for Cu^{2+}, 1.098 and 0.953 for La^{3+}, 1.089 and 0.926 for Gd^{3+} and 0.756 and 0.805 for Pt^{4+}, at the two wavelengths respectively. This indicates the formation of complexes having the stoichiometry (1 metal ion: 1 ligand III). The data obtained from this method in case of Ni^{2+} are represented graphically in Fig. (30).

(3) <u>The continuous variation method</u>:

A series of solutions was prepared by mixing equimolecular solutions of metal ion and ligand III in varying proportions to obtain constant molar concentration at $0.5x10^{-4}M$. The plot of the absorbances of each solution measured at 302 and 314 nm vs. the mole fraction of metal ion gives one peak at 0.5 mole fraction. This indicates the formation of one complex of the type (1 metal ion: 1 ligand III). This relationship in case of Ni^{2+} is shown graphically in Fig. (30).

The data for the stoichiometry of complexes of Co^{2+}, Ni^{2+}, Cu^{2+}, La^{3+}, Gd^{3+} and Pt^{4+} ions with ligand III are collected in Table (13).

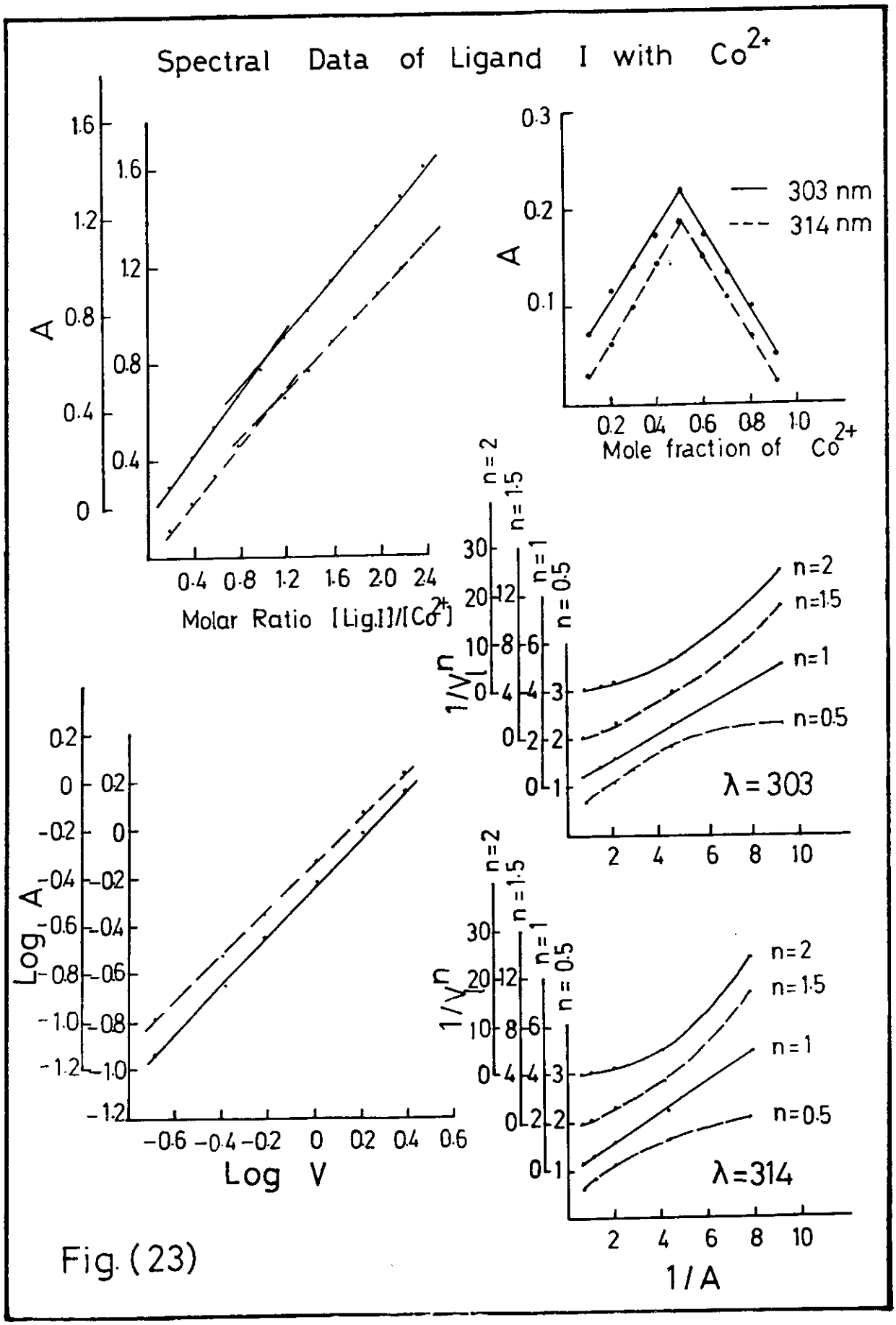
Spectral Data of Ligand I with Co^{2+}
A
Molar Ratio [Lig.I]/[Co^{2+}]
303 nm
314 nm
Mole fraction of Co^{2+}
$1/V^n$
n=2
n=1.5
n=1
n=0.5
λ = 303
λ=314
1/A
Log A
Log V

Fig. (23)

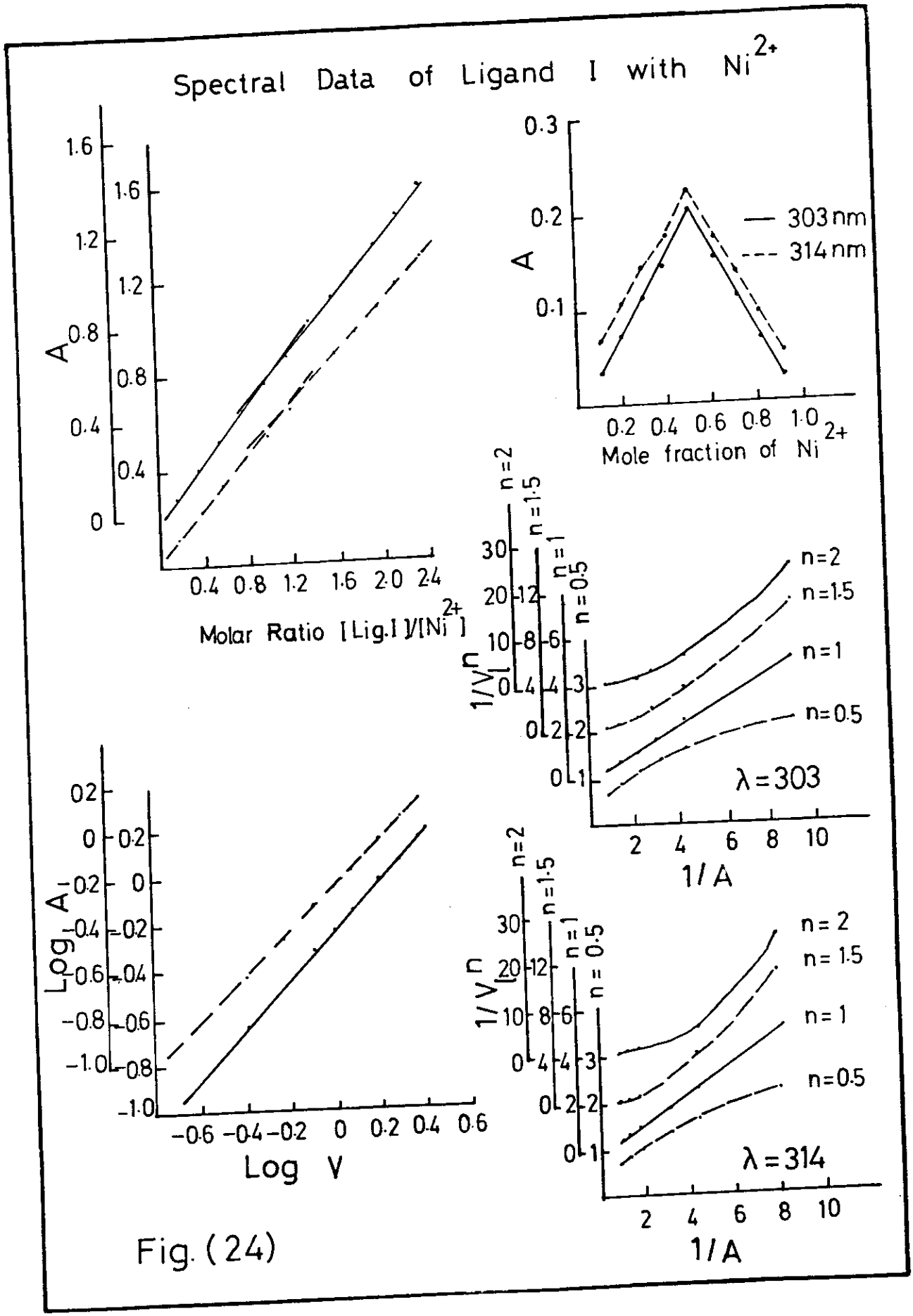
Spectral Data of Ligand I with Ni^{2+}
A
Molar Ratio [Lig.I]/[Ni^{2+}]
303nm
314nm
Mole fraction of Ni^{2+}
$1/V^n$
1/A
n=2
n=1.5
n=1
n=0.5
λ=303
λ=314
Log A
Log V

Fig. (24)

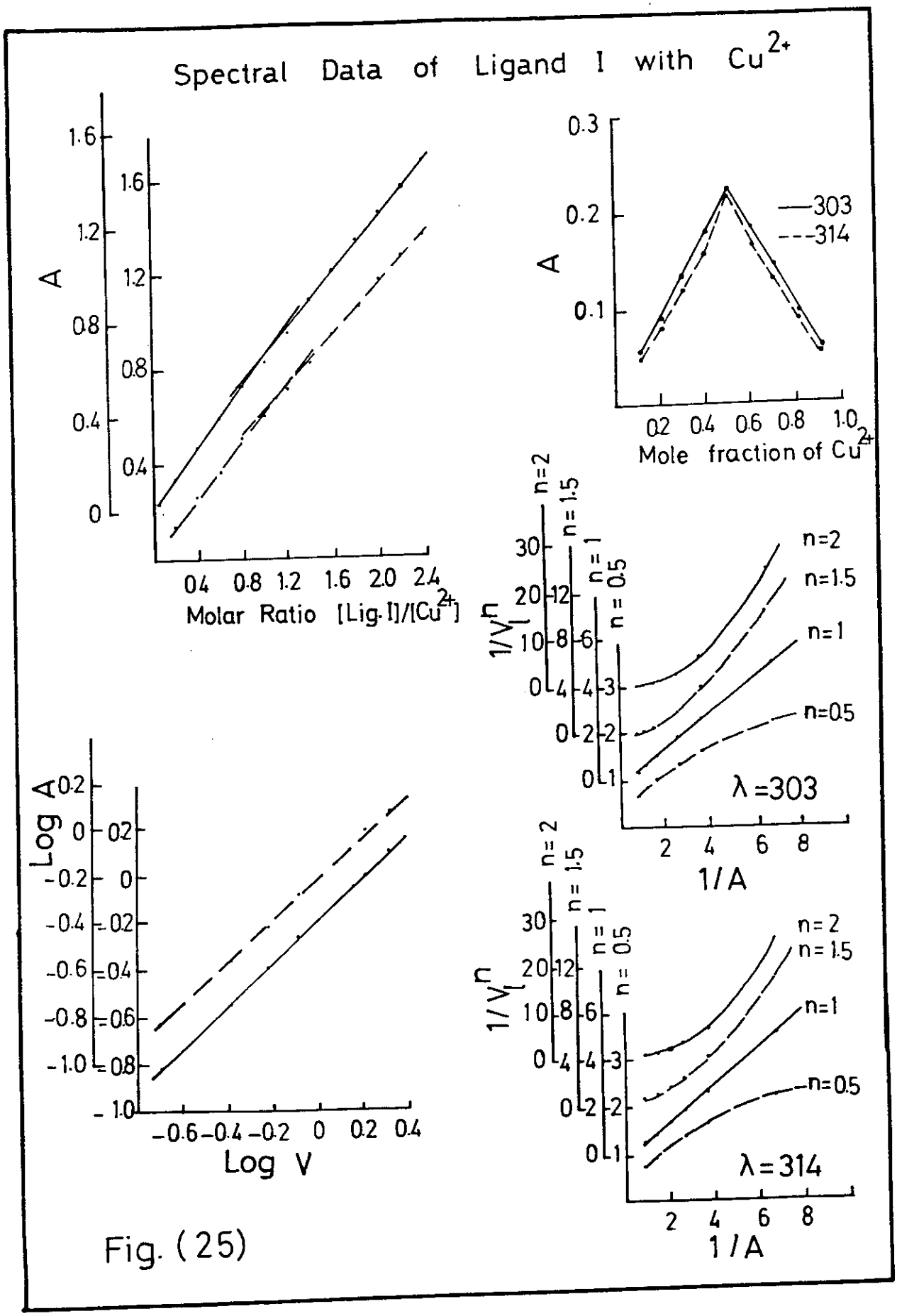
Spectral Data of Ligand I with Cu^{2+}
A
Molar Ratio [Lig. I]/[Cu^{2+}]
—303
---314
Mole fraction of Cu^{2+}
$1/V_l^n$
n=2
n=1.5
n=1
n=0.5
λ=303
1/A
λ=314
Log A
Log V

Fig. (25)

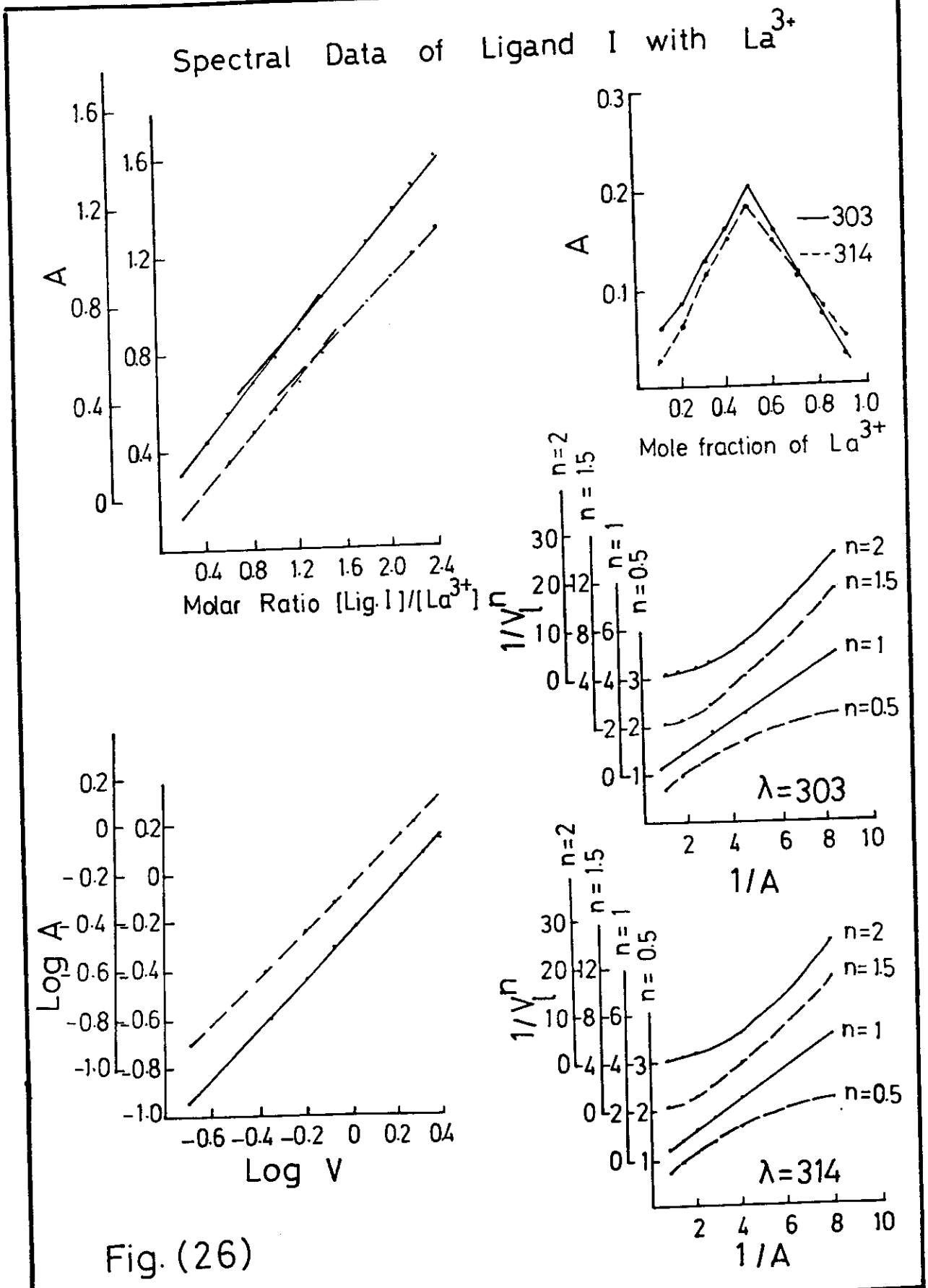
Spectral Data of Ligand I with La^{3+}
A
Molar Ratio [Lig. I]/[La^{3+}]
303
314
Mole fraction of La^{3+}
$1/V_l^n$
n=2
n=1.5
n=1
n=0.5
λ=303
1/A
λ=314
Log A
Log V

Fig. (26)

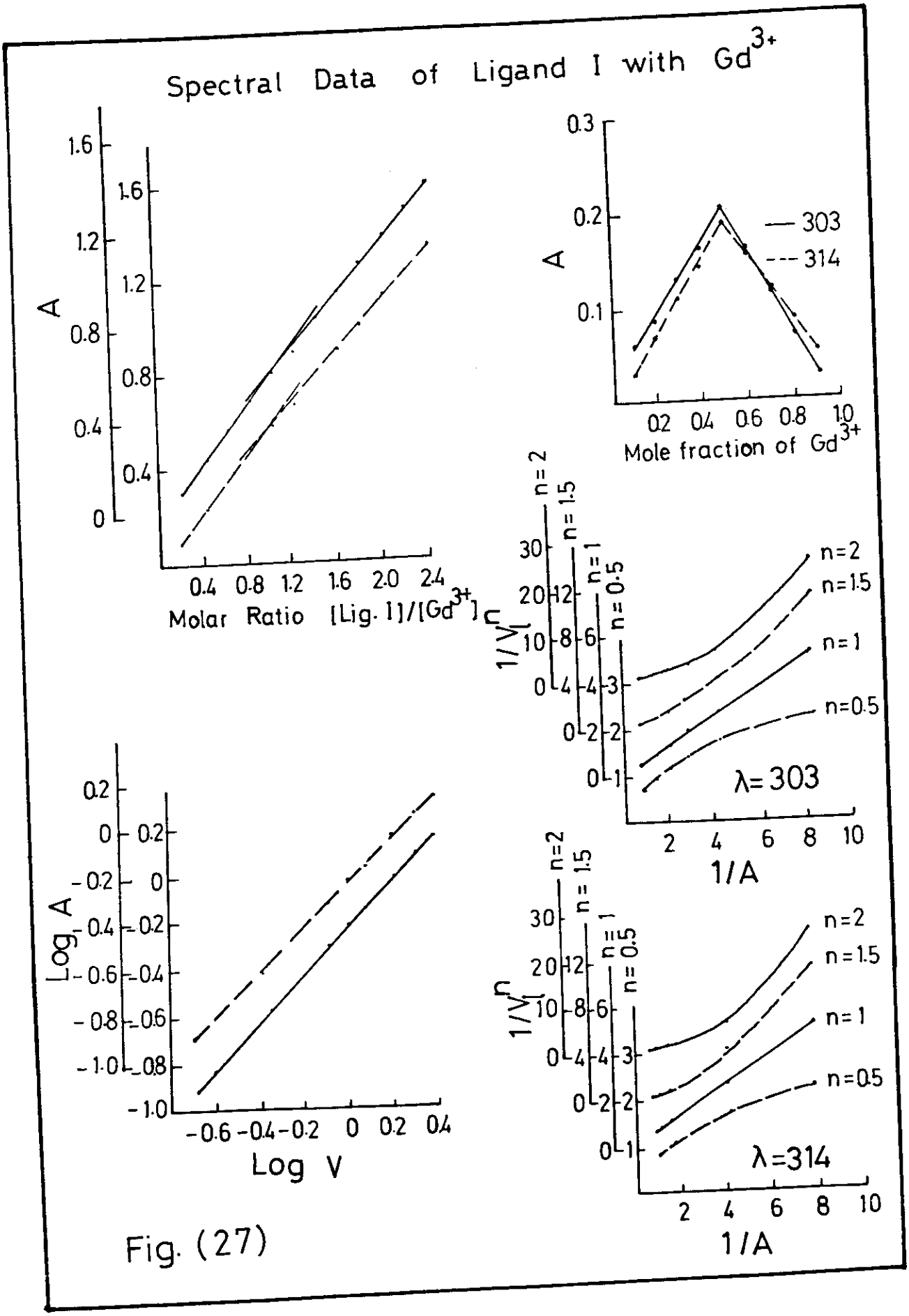
Spectral Data of Ligand I with Gd^{3+}
A
Molar Ratio [Lig. I]/[Gd^{3+}]
303
314
Mole fraction of Gd^{3+}
$1/V_l^n$
n=2
n=1.5
n=1
n=0.5
λ=303
1/A
λ=314
Log A
Log V

Fig. (27)

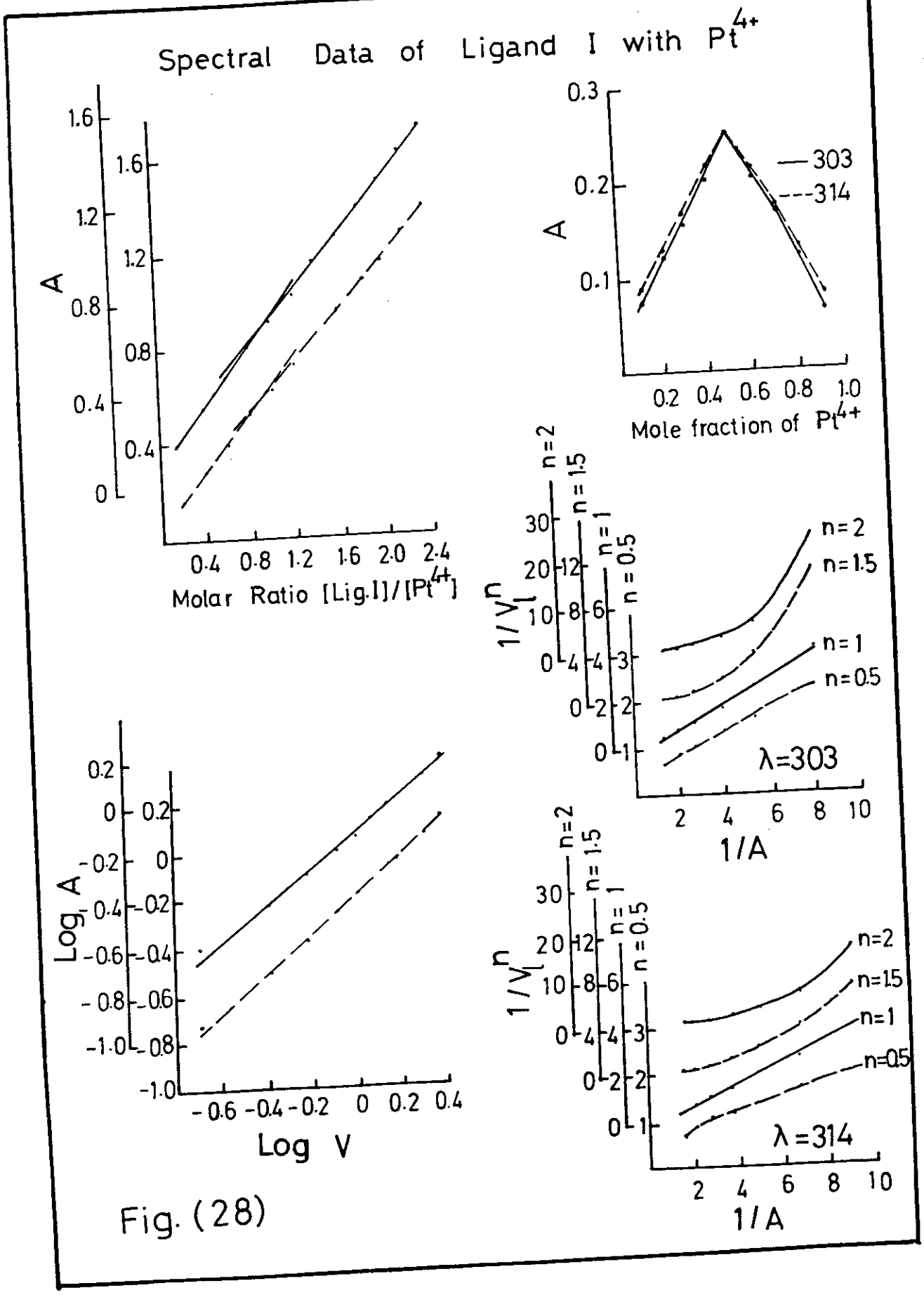
Spectral Data of Ligand I with Pt^{4+}
A
Molar Ratio [Lig.I]/[Pt^{4+}]
303
314
Mole fraction of Pt^{4+}
$1/V_l^n$
n=2
n=1.5
n=1
n=0.5
λ=303
1/A
λ=314
Log A
Log V

Fig. (28)

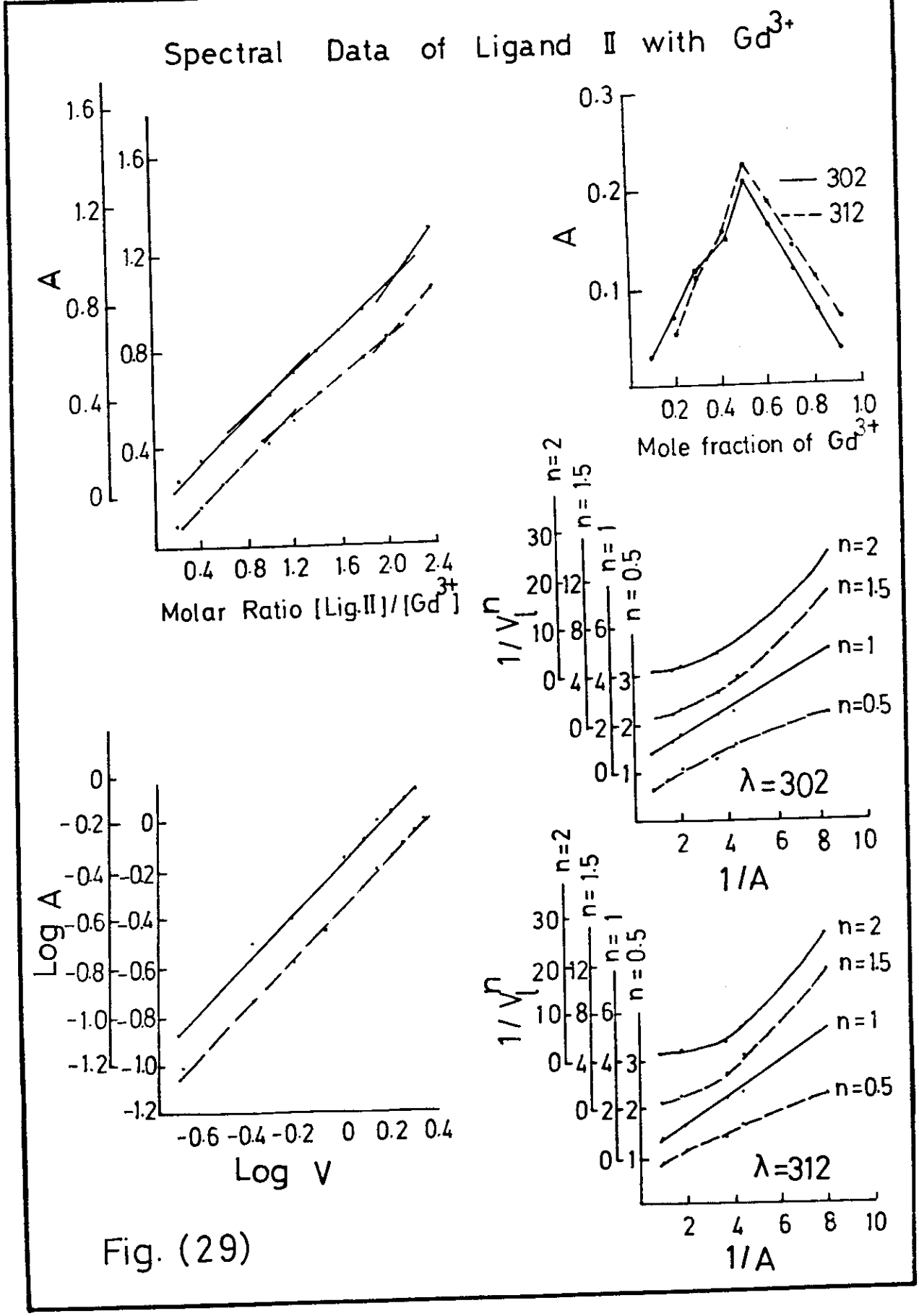
Spectral Data of Ligand II with Gd^{3+}
A
Molar Ratio [Lig.II]/[Gd^{3+}]
302
312
Mole fraction of Gd^{3+}
Log A
Log V
$1/V^n$
n=2
n=1.5
n=1
n=0.5
λ=302
λ=312
1/A

Fig. (29)

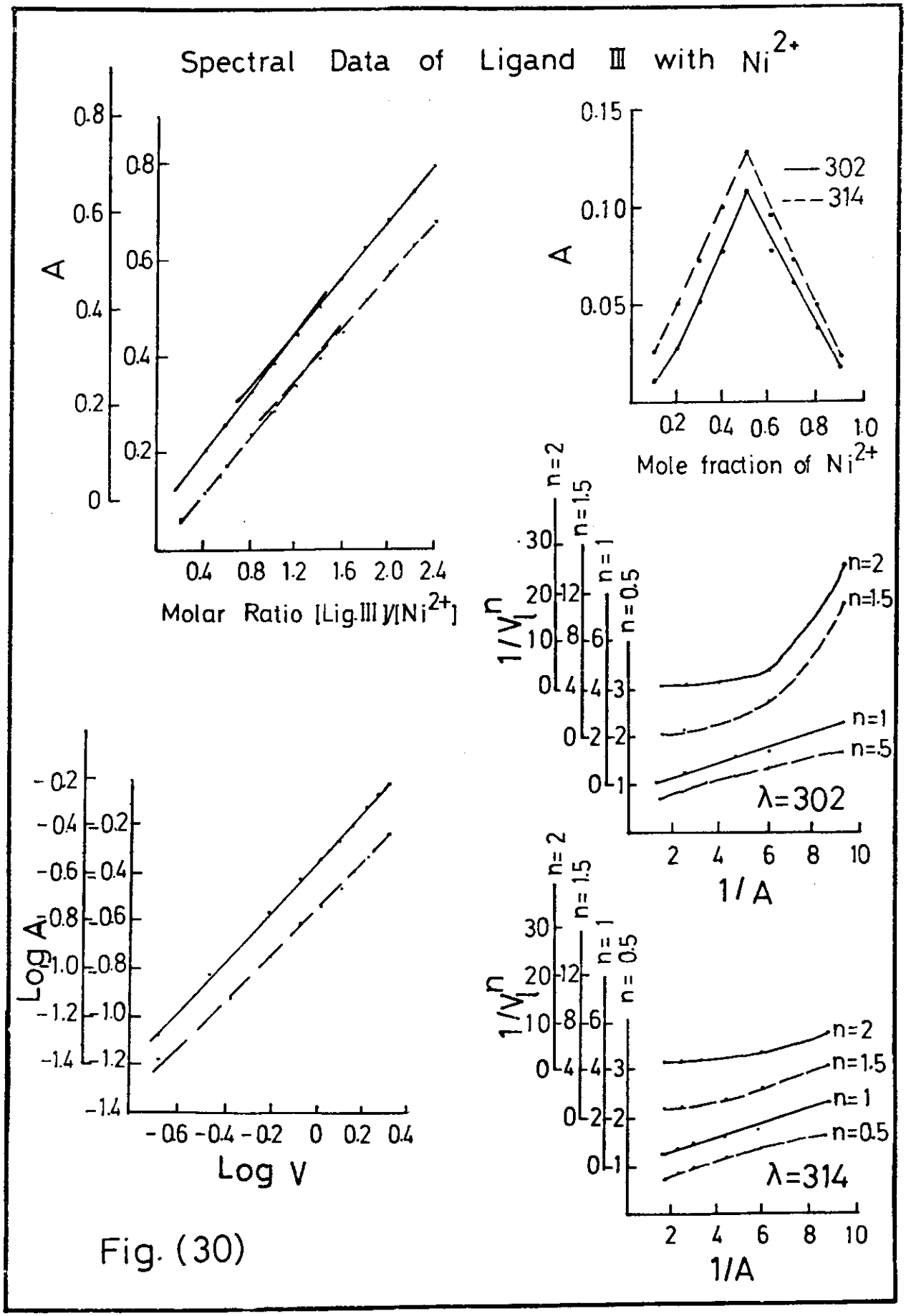
Spectral Data of Ligand III with Ni^{2+}
A
Molar Ratio [Lig.III]/[Ni^{2+}]
A
302
314
Mole fraction of Ni^{2+}
$1/V_l^n$
n=2
n=1.5
n=1
n=0.5
λ=302
1/A
λ=314
Log A_i
Log V

Fig. (30)

Table (13): Stoichiometry of metal chelates obtained from different spectrophotometric methods.

Ligand	Co^{2+}			Ni^{2+}			Cu^{2+}			La^{3+}			Gd^{3+}			Pt^{4+}		
	M.R.	S.L.	C.V.	M.R.	S.L.	C.V.	M.R.	S.L.	C.U.	M.R.	S.L.	C.V.	M.R.	S.L.	C.V.	M.R.	S.L.	C.V.
I	1:1	1:1	1:1	1:1	1:1	1:1	1:1	1:1	1:1	1:1	1:1	1:1	1:1	1:1	1:1	1:1	1:1	1:1
II	1:1	1:1	1:1	1:1	1:1	1:1	1:1	1:1	1:1	1:1	1:1	1:1	1:1	1:1	1:1	1:1	1:1	1:1
	1:2		1:2	1:2		1:2	1:2		1:2	1:2		1:2	1:2		1:2			
III	1:1	1:1	1:1	1:1	1:1	1:1	1:1	1:1	1:1	1:1	1:1	1:1	1:1	1:1	1:1	1:1	1:1	1:1

M.R. : Molar Ratio

S.L. : Straight Line

C.V. : Continuous Variation

Evaluation of the stability constants of the metal chelates from spectrophotometric measurements:

The spectrophotometric methods used for establishment of the stoichiometry of the complexes formed in solution were also utilised for the determination of their stability constants. The overall formation constants of the complexes were colculated from the data obtained from the molar ratio[88], continuous variation[90] and straight line method[93].

The following equation was used for the determination of the stability constants (K_n) for the different complexes:

$$K = \frac{A/A_M}{[1 - (A/A_m)]^{n+1} C_L^n n^2} \qquad (1)$$

where A is the absorbance at ligand concentration C_L

A_m is the absorbance at full colour develope.

n is the stoichiometric ratio of the complex.

Evaluation of the stability constants of the chelates of Co^{2+}, Ni^{2+}, Cu^{2+}, La^{3+}, Gd^{3+} and Pt^{4+} ions with acenaphthenequinone-(2-carboxyphenyl)-hydrazone by spectrophotometric methods:

The spectrophotometric data obtained from the molar ratio and continuous variation methods are used for the determination of the stability constants of

chelates of the different ions involved in the present work with ligand I. The data are evaluated applying equation (1). The values of log K calculated for the chelates of ligand I are given in Table (14).

Evaluation of the stability constants of the chelates of Co^{2+}, Ni^{2+}, Cu^{2+}, La^{3+}, Gd^{3+} and Pt^{4+} ions with acenaphthenequinone-(2-methoxyphenyl)-hydrazone by spectrophotometric methods:

The data obtained from the molar ratio and continuous variation methods are applied to equation (1). The values of the stability constants of the chelates are evaluated and collected in Table (14).

Evaluation of the stability constants of the chelates of Co^{2+}, Ni^{2+}, Cu^{2+}, La^{3+}, Gd^{3+} and Pt^{4+} ions with acenaphthenequinone-(2-chlorophenyl)-hydrazone by spectrophotometric methods:

The spectrophotometric data of the molar ratio and continuous variation methods are utilised for evaluation of stability constants of the corresponding complexes using equation (1). The values of the stability constants are evaluated and depicted in Table (14).

Table (14): Stepwise formation constants of metal ions with different ligands.

Metal ion	ratio (M/L)	Ligand I				Ligand II				Ligand III			
		M.R.	C.V.	S.L.	Mean	M.R.	C.V.	S.L.	Mean	M.R.	C.V.	S.L.	Mean
Co^{2+}	1:1	5.047	5.029	4.96	5.012	5.008	5.079	5.03	5.039	4.989	4.956	4.82	4.92
	1:2					8.913	9.064						
Ni^{2+}	1:1	5.080	5.044	5.01	5.044	5.014	5.089	5.03	5.044	5.055	5.063	4.95	5.086
	1:2					8.931	9.090						
Cu^{2+}	1:1	5.168	5.243	5.15	5.187	5.030	5.179	5.08	5.096	5.073	5.254	5.14	5.155
	1:2					8.950	9.155						
La^{3+}	1:1	5.082	5.084	5.02	5.062	5.031	5.104	5.07	5.068	5.031	5.036	5.20	5.089
	1:2					8.960	9.132						
Gd^{3+}	1:1	5.026	5.044	4.92	4.996	5.047	5.106	5.08	5.077	5.010	5.024	5.01	5.014
	1:2					8.951	9.148						
La	1:1	5.256	5.274	5.18	5.236	5.042	5.164	5.12	5.108	5.296	5.70	5.35	5.448

CHAPTER III

PART (C)

STUDIES OF THE SOLID COMPLEXES

(i) Elemental analysis and molar conductivities of the metal chelates:

a) Elemental analysis:

The chemical composition and the percent of the metal ion, chloride ion and water molecules in the solid chelates can be determined by elemental analysis. The determination of chloride ion content was performed by **Volhard's method**[94], the metal ions concentration were estimated by EDTA titration[95] under the appropriate conditions and the number of water molecules attached to the metal chelate is determined by the dehydration method. The results of analysis are given in Tables (15-17). The corresponding probable constitutional formula for different complexes are thereby suggested based on the results obtained.

b) Molar conductivities:

Conductivity measurements in nonaqueous solutions have frequently been used in structural studies of metal chelates within the limits of their stabilities.

of the chloride ion (the anion) inside or outside the coordination sphere is detected by its precipitation as AgCl by the addition of $AgNO_3$ to the solubilized chelates in DMF. Accordingly, the anions and cations of the complexes can be represented as given in Tables (15-17).

Table (15): Elemental analysis, melting points and molar conductances of some chelates of ligand I.

Complex	% C		% H		% N		% M		m.p.	Λ_m
	Calc.	Found	Calc.	Found	Calc.	Found	Calc.	Found		
$[CoL(H_2O)_3]$	53.06	53.24	2.79	2.92	5.58	6.08	13.70	13.21	244-46	13.2
$[NiL(H_2O)_3]$	53.06	53.66	2.79	3.00	6.52	6.77	13.66	13.70	252-54	8.4
$[CuL(H_2O)_3]$	52.46	52.68	2.76	2.56	6.44	2.89	14.63	14.02	240-42	11.4
$[LaL(H_2O)_3]^+Cl^-$	41.80	41.08	2.20	2.72	5.13	5.72	25.46	26.38	254-56	50.0
$[GdL(H_2O)_3]^+Cl^-$	40.43	41.03	2.12	2.44	4.97	5.07	27.9	26.21	250-52	38.8
$[PtL(H_2O)_3]^{2+}2Cl^-$	37.93	37.11	2.00	2.34	4.65	5.02	32.62	31.50	230-32	111.3

Table (16): Elemental analysis, melting points and molar conductances of some chelates of ligand II.

Complex	% C		% H		% N		% M		m.p.	Λ_m
	Calc.	Found	Calc.	Found	Calc.	Found	Calc.	Found		
$[CoL(H_2O)_3]^+Cl^-$	50.50	49.88	3.10	3.30	6.20	5.92	13.04	12.89	158-60	47.31
$[NiL(H_2O)_3]^+Cl^-$	50.53	50.03	3.10	2.91	6.21	6.00	13.01	13.21	241-43	47.22
$[CuL(H_2O)_3]^+Cl^-$	49.99	50.21	3.07	2.87	5.26	6.01	13.94	13.62	234-36	51.21
$[LaL(H_2O)_3]^{2+}2Cl^-$	40.21	40.72	2.46	2.62	4.93	5.00	24.50	25.00	243-45	130.20
$[GdL(H_2O)_3]^{2+}2Cl^-$	38.95	39.00	2.39	2.91	4.78	4.62	26.87	26.21	240-42	110.11
$[PtL(H_2O)_3]^{3+}3Cl^-$	34.61	35.03	2.12	1.88	4.25	4.32	29.62	29.11	204-06	220.20
$[Co(L)_2(H_2O)]$	33.15	34.00	2.03	1.98	4.07	4.11	8.56	8.23	252-54	7.00
$[Ni(L)_2(H_2O)]$	33.39	33.26	2.05	2.31	4.10	3.98	8.60	9.02	170-72	9.32
$[Cu(L)_2(H_2O)]$	33.15	33.62	2.03	2.42	4.07	4.27	9.24	9.33	198-20	8.22
$[La(L)_2(H_2O)]^+Cl^-$	28.55	27.92	1.75	2.10	3.50	3.70	17.39	17.02	182-84	37.12
$[Gd(L)_2(H_2O)]^+Cl^-$	27.90	25.88	1.71	1.95	3.42	3.02	19.25	21.72	178-80	115.20

Table (17): Elemental analysis, melting points and molar conductances of some chelates of ligand III.

Complex	% C		% H		% N		% M		m.p.	Λ_m
	Calc.	Found	Calc.	Found	Calc.	Found	Calc.	Found		
$[CoL(H_2O)_4]^+Cl^-$	45.32	45.22	2.30	2.53	5.87	6.13	12.35	12.30	235-37	57.25
$[NiL(H_2O)_4]^+Cl^-$	45.79	46.21	2.33	2.76	5.93	5.22	12.44	12.02	238-40	40.33
$[CuL(H_2O)_4]^+Cl^-$	45.77	45.91	2.33	3.02	5.93	6.70	13.47	12.93	221-23	72.14
$[LaL(H_2O)_2Cl_2]$	39.17	40.11	1.99	2.50	5.07	5.22	25.19	25.40	237-39	15.55
$[GdL(H_2O)_2Cl_2]$	37.90	38.25	1.93	2.21	4.91	5.31	27.60	27.02	226-28	12.30
$[PtL(H_2O)_3Cl]^{2+}2Cl^-$	32.67	33.31	1.66	2.01	4.23	4.81	29.51	30.10	207-09	120.15

(ii) Thermogravimetric and Differential Thermal Analysis of Some Metal Chelates:

Thermal methods of analysis open up a new possibility for the investigation of metal chelates[97-102]. They include such technique as thermogravimetric analysis (TGA), differential thermal analysis (DTA) and thermometric titration (TT).

From TGA curves, one can calculate the percentage of water molecules and metal ions in the chelates, whereas those of DTA make it possible to characterize thermographically the process of phase transformation in the examined system. To understand the mechanism of complex formation and the stability of the complexes formed, it is of interest to observe the intermediate products formed by the oxidative action of heat on the investigated metal chelates.

The TGA and DTA curves give information about the various unexpected phenomena observed during heat treatment. It is important to take into account that the TGA curve reveals the variation in weight, whereas the DTA is connected with calorific phenomena which often occur with no detectable weight change. The present investigation is a study of the thermogravical behaviour of some selected chelates.

a) **TGA and DTA of chelates of acenaphthenequinone-(2-carboxyphenyl)-hydrazone with some metal ions:**

Fig. (31) shows the TGA and DTA curves of Ni^{2+}, Cu^{2+}, Gd^{3+} and Pt^{4+} (1:1) complexes with ligand I . Each endothermic or exothermic peak on the DTA curve, corresponding to certain phase transformation, is accompanied by an inflection on the TGA curve from which the corresponding weight loss can be calculated. The DTA curves of these complexes show endothermic peaks at the temperature range 40-130°C which are due to the removal of humidity, namely physically combined water molecules from the crystal lattice. The endothermic peaks at 130-270°C are due to the dehydration of coordinated water molecules whose percentage were calculated from the corresponding inflections on the TGA curves and given in Table (18).

The DTA curves of these complexes exhibit strong exothermic peaks within the range 360-435°C which are due to the phase transformation accompaning melting of the metal chelates and oxidation of the organic products. Finally, the small exothermic peaks (endothermic for Pt^{4+}: ligand I complex) at 480-520°C are due to some sorts of lattice rearrangments leading to the formation of the final products which were found to be NiO, CuO, Gd_2O_3 and PtO_2. The percentage of water molecules,

metal ions and metal oxides of these complexes were calculated from the TGA curves and tabulated with those of their theoritical values Table (18) where a satisfactory agreements is obtained.

As example of the thermal degradation reaction taking place through thermal analysis of Gd^{3+}: Ligand I complex, the thermal decompposition of $[GdL(H_2O)_3]^+ Cl^-$ can be formulated as follows:

$$[Gd(L)(H_2O)_3]^+Cl^- \xrightarrow[-\text{humidity } H_2O]{40 - 125°C} [Gd(L)(H_2O)_3]^+Cl^-$$

wet dry

$$\text{———}[Gd(L)] \xleftarrow[-Cl]{260°C} [Gd(L)]^+Cl^- \xleftarrow[-3\ H_2O]{240°C} \text{———}$$

$$\xrightarrow{435\text{-}480°C} Gd_2O_3$$

b) <u>TGA and DTA of chelates of acenaphthenequinone-(2-methoxyphenyl)-hydrazone with some metal ions</u>:

The DTA and TGA curves of Ni^{2+} (1:1) and (1:2), La^{3+} (1:1), Gd^{3+} (1:1) and (1:2) [M:L] complexes of ligand II are given in Fig. (32). The experimental values of the weight percent of water molecules and metal ions present, calculated from the TGA curves, are given and compared to those of the calculated values in Table (18). The removal of lattice water is represented by the endothermic peaks at 65-105°C while the endothermic peaks (exothermic for Ni^{2+} and La^{3+} (1:1)

complexes) within the range 130-240°C are due to the elemination of coordinated water molecules. The strong exothermix peak at 340-480°C on the DTA curves corresponds to the phase transformation due to the melting of the anhydrous complexes taking place as an initial step to the formation of NiO, La_2O_3 and Gd_2O_3 as final products. As example; the thermal decomposition of mono-nuclear Gd^{3+} complex can be represented as follows:

$$\underset{\text{wet}}{[Gd(L)(H_2O)_3]^{2+}2Cl^-} \xrightarrow[-\text{humidity } H_2O]{60 - 105°C} \underset{\text{dry}}{[Gd(L)(H_2O)_3]^{2+}2Cl^-}$$

$$.Gd_2O_3 \xleftarrow{430-450°C} [Gd(L)] \xleftarrow[-2Cl]{375°C} [Gd(L)]2Cl \xleftarrow[-3H_2O]{225°C}$$

c) <u>TGA and DTA of chelates of acenaphthenequinone-(2-chlorophenyl)—hydrazone with some metal ions</u>:

Fig. (33) comprises the DTA and TGA curves of mono-nuclear Co^{2+}, Ni^{2+}, Cu^{2+} and Pt^{4+} complexes with ligand III. The removal of phsically combined water molecules attached to te crystal lattice of the complexes is represented by the endothermic peak at 50-120°C, while that of the coordinated water molecules is represented by the endothermic peaks within the temperature range 120-125°C. The dechloronation of the complexes[103] is represented by endothermic peaks at 210-225°C. The exothermic peaks at 350-410°C are due to the phase transformation taking place during the melting of the

anhydrous complexes which is followed by the formation of metal oxides as final products. The experimental and calculated values of water molecules, metal oxides and metal ions in the solid complexes were determined from the inflections on the TGA curves and are given in Table (18).

TGA and DTA curves of chelates of Ligand I

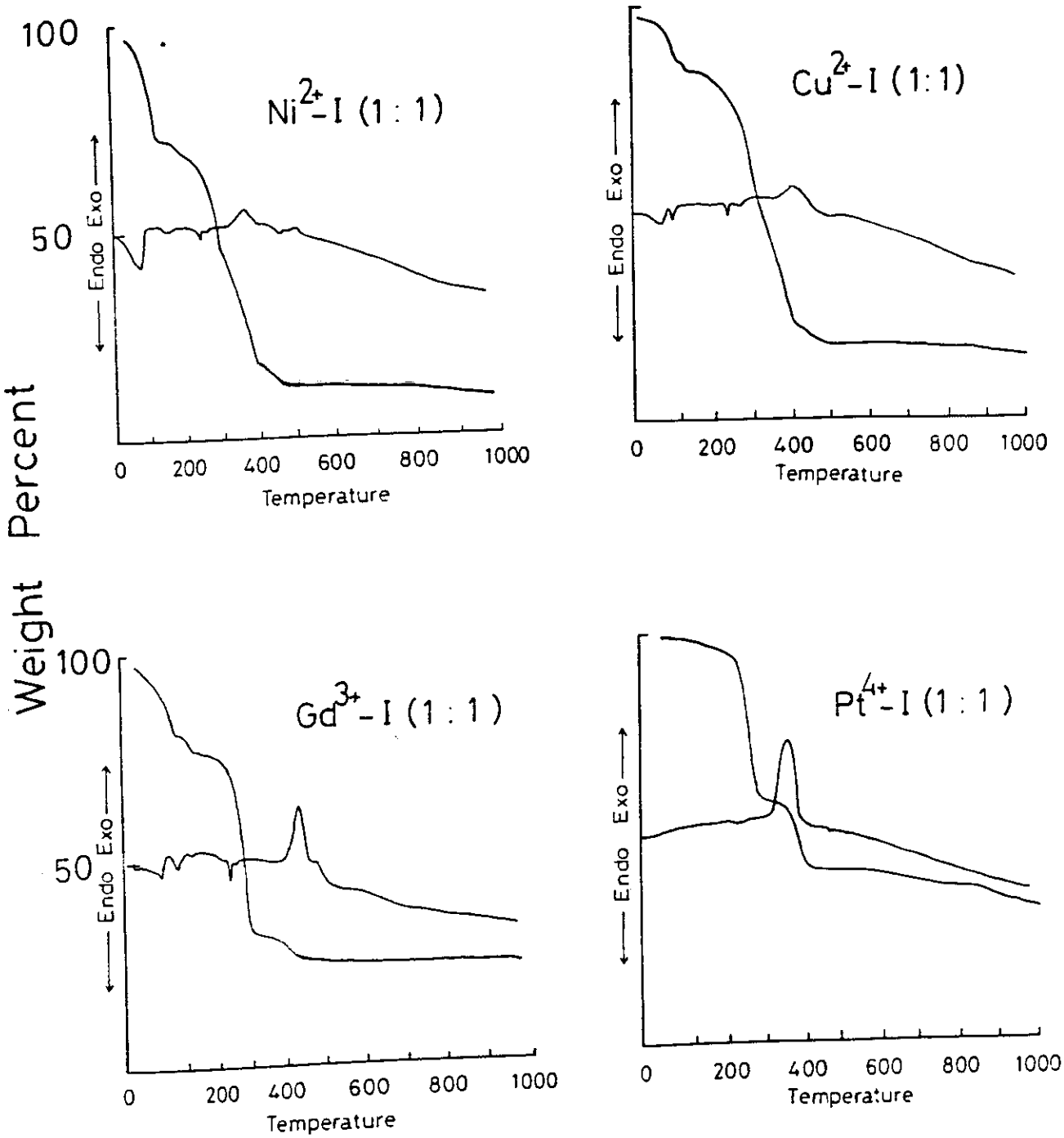

Fig. (31)

TGA and DTA curves of chelates of Ligand II

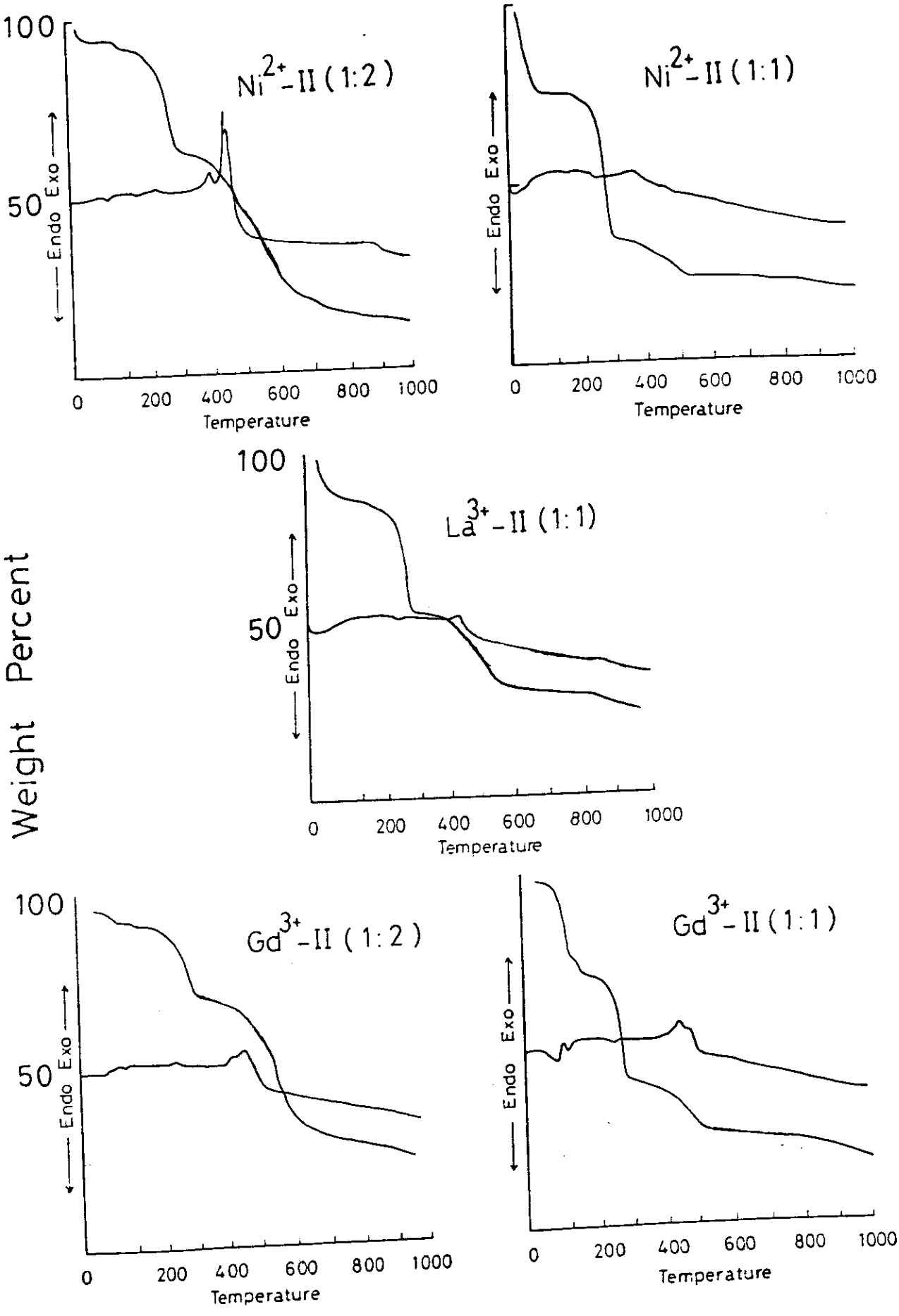

Fig. (32)

TGA and DTA curves of chelates of Ligand III

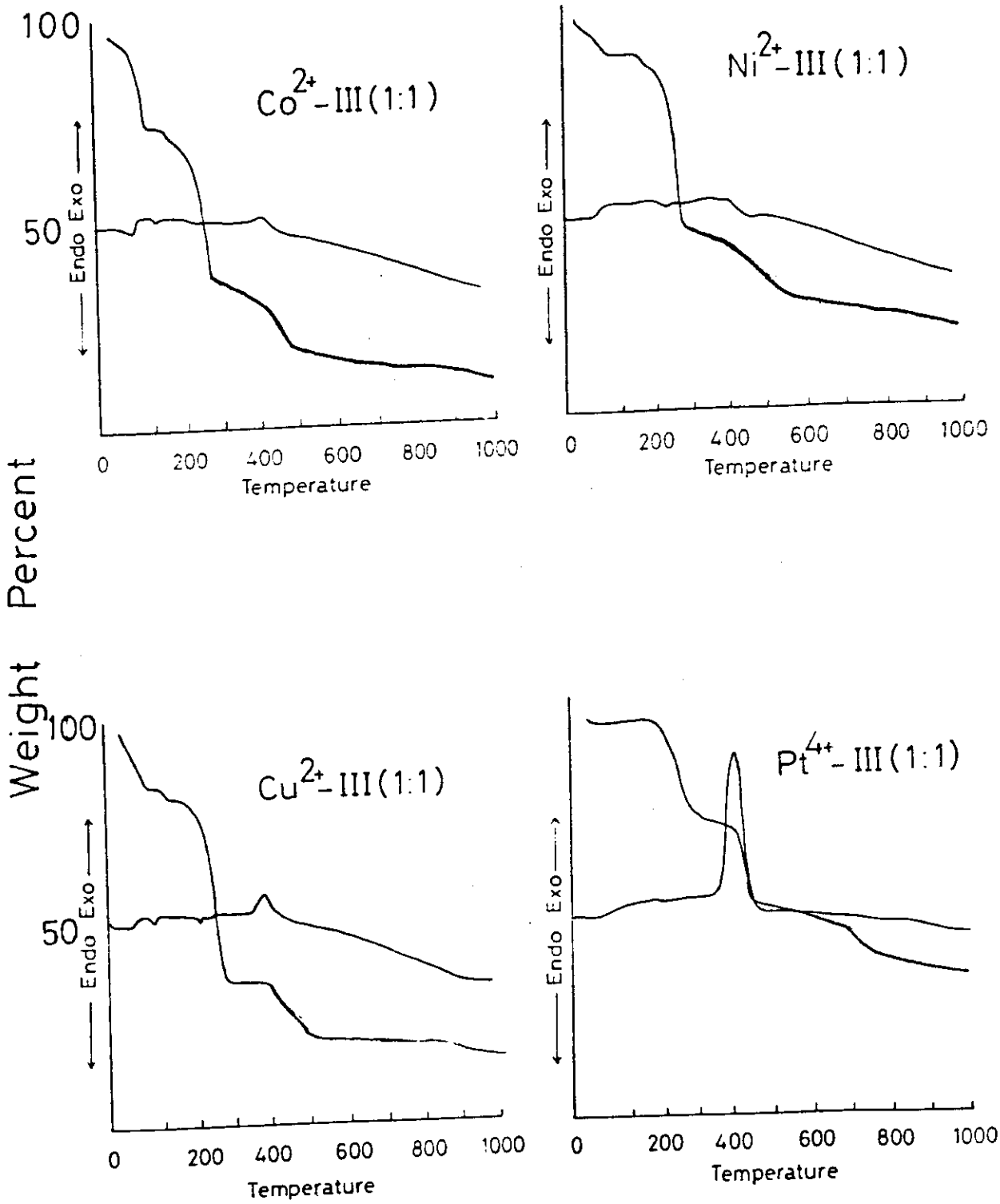

Fig.(33)

Table (18): Weight percent of water molecules, metal oxide and metal ion in some metal chelates.

Chelate	Ratio M:L	H_2O		Metal Oxide		M^{n+}	
		Found	Calc.	Found	Calc.	Found	Calc.
Ni-I	1:1	12.2	11.97	17.22	17.43	13.86	13.66
Cu-I	1:1	12.3	11.84	17.98	18.31	14.82	14.63
Gd-I	1:1	10.9	10.33	20.52	30.21	26.89	27.90
Pt-I	1:1	10.3	9.82	36.21	36.70	32.90	32.62
Ni-II	1:1	12.3	11.97	15.99	16.56	13.42	13.01
Ni-II	1:2	2.9	2.64	12.03	11.48	8.85	8.60
La-II	1:1	12.3	11.96	30.11	29.32	25.20	24.50
Gd-II	1:1	10.3	9.23	30.78	30.21	26.92	26.87
Gd-II	1:2	3.4	2.21	21.92	21.69	18.38	19.25
Co-III	1:1	15.2	15.11	16.00	15.64	12.58	12.35
Ni-III	1:1	16.0	15.26	15.75	15.30	12.67	12.44
Cu-III	1:1	15.6	15.26	16.34	16.19	13.66	13.47
Pt-III	1:1	9.3	8.17	35.41	35.04	30.18	29.51

(iii) Infrared Spectra of the Solid Metal Chelates:

A substantial part of the knowledge concerning the mode of bonding in metal chelates can be gained by applying infrared spectrophotometry either in absorption or reflactance arrangements. A verification of the mode of bonding between the organic ligands and the metal ions in the complexes can be easily achieved by comparing the ir-spectra of the free ligands with those of the complexes[104,105].

The ir absorption spectra of the solid chelates produced from acenaphthenequinone-(2-X phenyl)-hydrazones where X=COOH (I), OCH_3 (II) and Cl (III) with Co^{2+}, Ni^{2+}, Cu^{2+}, La^{3+}, Gd^{3+} and Pt^{4+} ions were studied and compared to those of their free ligands, the spectra are shown in Figs. (34-36). The complexes are studied to show whether the free ligands interact with metal ions through their hydrazone form, for which the following mode of bonding may be found:

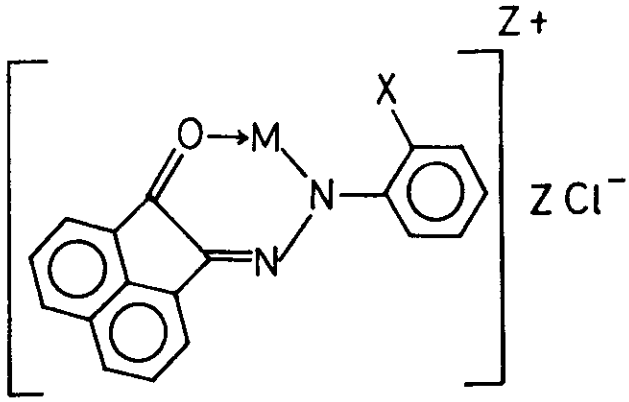

Structure I

or through their azo form, for which the following bonding can be given:

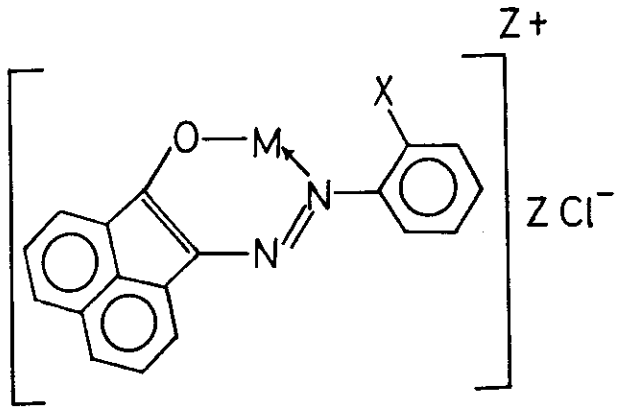

Structure II

The spectra of the free ligands exhibit the $\nu_{C=O}$, $\nu_{C=N}$, ν_{N-H} and $\nu_{N=N}$ at 1715, 1678-1680, 3420 and 1419-1410 cm^{-1} respectively, indicating that these ligands are present in hydrazone $\rightleftharpoons$ azo tautomeric forms. On the other hand, the ir-spectra of the solid chelates showed the presence of the C=N and C=O bands at 1678-1680 and 1715-1732 cm^{-1} and as well the absence of the stretching frequencies of the N=N bands indicating that the ligands participate in chelate formation through their hydrazone form; and structure (I) would then be the predomenate one.

(1) **Complexes of Co^{2+}, Ni^{2+}, Cu^{2+}, La^{3+}, Gd^{3+} and Pt^{4+} ions with acenaphthenequinone-(2-carboxyphenyl)-hydrazone:**

The ir-spectra of Co^{2+}, Ni^{2+}, Cu^{2+}, La^{3+}, Gd^{3+} and Pt^{4+} with ligand I are shown in Fig. (34) and the important bands are listed in Table (19). Inspection of these spectra reveals that:

i - The $\nu_{C=O}$ band of the carboxyl group located at 1732 cm^{-1} in the spectrum of the free ligand is shifted to higher frequency in the spectra of metal complexes (1765-1770 cm^{-1}).

ii- The $\nu_{C=O}$ band of the hydrazone form present at 1715 cm^{-1} in case of free ligand displays a shift to higher frequencies from 15 to 20 cm^{-1}. It is worthy to mention that the carbonyl group in the free ligand was strongly hydrogen bonded leading to the appearance of the $\nu_{C=O}$ at relatively lower frequency than expected[106]. The contribution of this group in complex formation will lead to the cleavage of the hydrogen bond and a coordination M ⟵ O bond will be formed, concequently a higher frequency shift would be expected to appear

iii- The $\nu_{C=N}$ band was shifted also to the higher frequency side by 30-35 cm^{-1}.

iv- The ν_{NH} and $\nu_{N=N}$ bands of the free ligand present

at 3420 and 1418 cm^{-1} respectively disappeared in case of the solid complexes. The ν_{OH} of the carboxylic group not accuratly detected due to the broad band of the coordinated water molecules.

v - The ν_{COO^-} band of the free ligand at $1600_{(S)}$ cm^{-1} was found to be greatly affected by chelate formation and shifted to 1575-1580 cm^{-1}.

vi- The two new bands appearing at 450-510 and 360-365 cm^{-1} are assigned to the ν_{M-O} and ν_{M-N} stretching modes, respectively. Based on these data and those obtained from elemental analysis, the bonding in the solid complexes with this ligand can be formulated as follows:

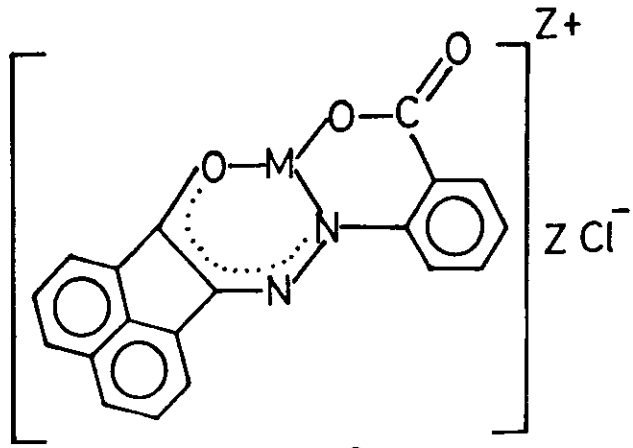

$Z = (0 \text{ for } M^{2+}, 1 \text{ for } M^{3+} \text{ and } 2 \text{ for } M^{4+})$

(2) **Complexes of Co^{2+}, Ni^{2+}, Cu^{2+}, La^{3+}, Gd^{3+} and Pt^{4+} with acenaphthenequinone-(2-methoxyphenyl)-hydrazone:**

The ir absorption spectra of the solid chelates

produced from ligand II with Co^{2+}, Ni^{2+}, Cu^{2+}, La^{3+} and Cd^{3+} ions of stoichiometric ratios (1:1) and (1:2) [M:L], and (1:1) only in case of Pt^{4+}, were studied and compared to that of their free ligand. The spectra are shown in Fig. (35) while the assignment of the important bands are given in table (20). From the carful study of these spectra, the following aspects can be pointed out:

i - The two bands located at 3330 and 1418 cm^{-1} due to the ν_{OH} and $\nu_{N=N}$ vibrations respectively, disappeared on complex formation indicating that this ligand participate in complex formation via its hydrazone form rather than the azo one.

ii- The band located at 3420 cm^{-1} due to ν_{NH} vibration also disappeared in the spectra of the solid chelates, the fact which indicates that this compound acts as a monobasic ligand and a simple covalent bond is formed (M-N) through proton elimination. This fact was previously supported from conductometric titration curves from which a steady increase in conductance was obtained due to the liberation of H^+ as a result of the complexation process.

iii- The shift of the $\nu_{C=O}$ band (present at 1715 cm^{-1}) to higher frequencies in both 1:1 and 1:2 [M:L]

complexes by 15-50 cm^{-1} suggests that this group has contributed, to chelate formation. The presence of this band denotes that the hydrazone structure and not the azo form of the ligand is involved in complex formation.

iv- The bands due to ν_{C-O} and ν_{O-CH_3} at 1275 and 1210 cm^{-1} respectively display some shifts to lower frequency. Also this band exhibits some decrease in intensity and broadening in comparison to the free ligand indicating a sort of coordination bond between the metal ion and the oxygen otom of the methoxy group.

v - The two new bands observed at 510-530 and 407-435 cm^{-1}, Table (20) for all the solid complexes and are not observed in the ir spectrum of the free ligand and can be assigned to ν_{M-O} and ν_{M-N} respectively.

Based on the knowledge gained from this investigation as well as that obtained from elemental analysis and molar conductance, bonding of metal ions to this ligand can be formulated as follows:

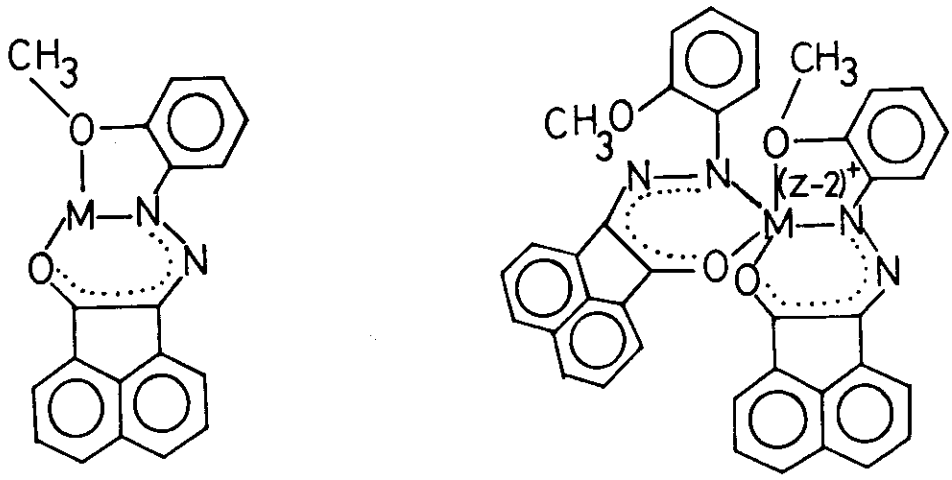

z = (1 for M^{2+}, 2 for M^{3+} and 3 for M^{4+})

(1:1) (1:2)
[M:L]

(3) <u>Complexes of Co^{2+}, Ni^{2+}, Cu^{2+}, La^{3+}, Gd^{3+} and Pt^{4+} with acenaphthenequinone-(2-chlorophenyl)-hydrazone</u>:

The ir spectra of the solid complexes are recorded and compared to that of the free ligand, Fig. (36). Such comparison shows that this compound acts as a monobasic bidentate ligand and the complex formation proceedes through a simple covalent, (M-N) with one proton eleminated from the NH group and a coordinated bond (M ⟵ O) between metal ion and the carbonyl group of the hydrazone form of the ligand. This was gathered from the shift in band position due to $\nu_{C=O}$ and the

disappearance of the band due to ν_{NH} vibration, Table (21). The presence of the $\nu_{C=N}$ band of the free ligand as well for all solid chelates indicates that chelate formation precludes the azo $\rightleftharpoons$ hydrazone tautomerism. The data obtained from elemental analysis and molar conductance measurements give a great deal of information about the structure of the complexes and the number of charges present in. Based on these data and those obtained from ir-spectra, the bonding in the solid chelates of this ligand can be represented as follows:

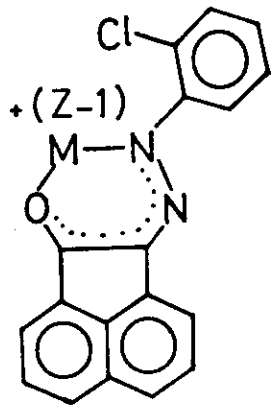

z = (1 for M^{2+}, 2 for M^{3+} and 3 for M^{4+})

(1:1)

Infrared Spectra of Ligand II and its Chelates

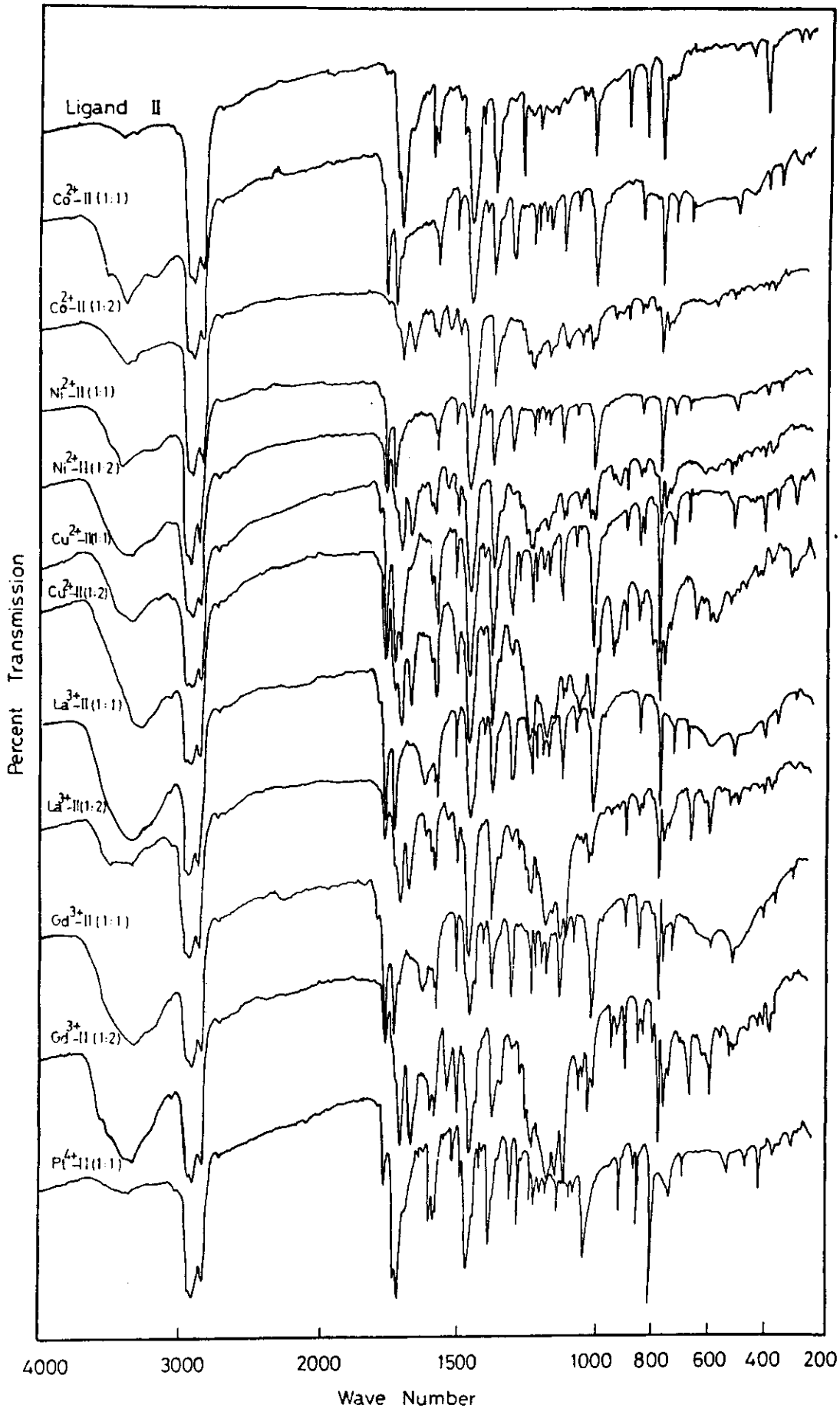

Fig. (35)

Infrared Spectra of Ligand III and its Chelates

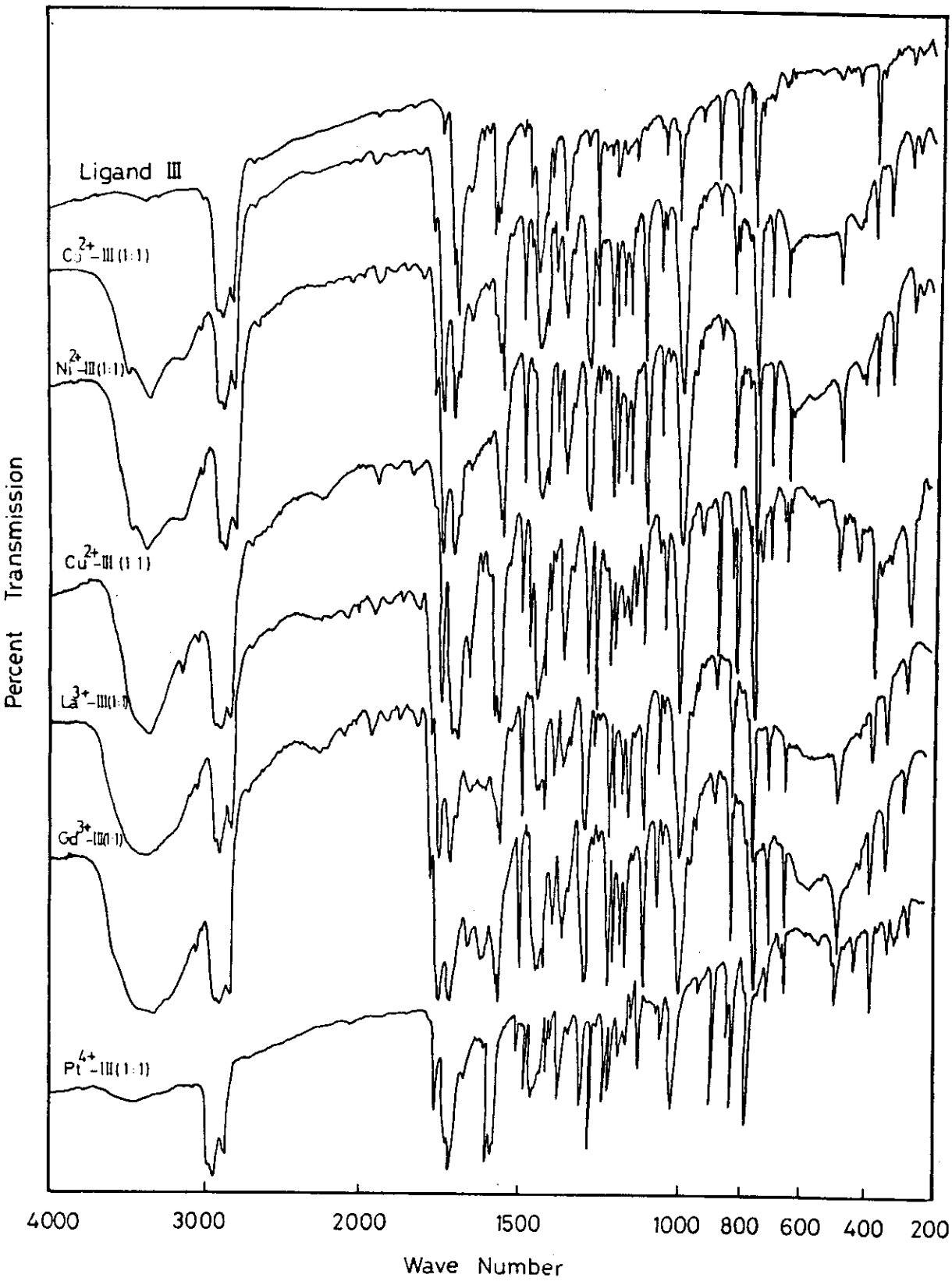

Fig. (36)

Table (19): The ir-vibrational spectra of some function groups (cm^{-1}) of ligand I and its metal chelates:

Compound	ν_{NH}	ν_{OH}	$\nu_{C=O}$	$\nu_{C=O}$	$\nu_{C=N}$	ν_{COO^-}	M-O	M-N
I	3420	2560	1732	1715	1680	$1600_{(s)}$	-	-
Co^{2+}-I (1:1)	-	-	1765	1730	1710	$1575_{(s)}$	448	360
Ni^{2+}-I (1:1)	-	-	1765	1732	1712	1575	445	360
Cu^{2+}-I (1:1)	-	-	1768	1730	1712	1578	445	357
Cu^{2+}-I (1:1)	-	-	1768	1730	1712	1578	445	357
La^{3+}-I (1:1)	-	-	1770	1735	1715	1575	410	360
Gd^{3+}-I (1:1)	-	-	1765	1735	$1715_{(sh)}$	1580	510	360
Pt^{4+}-I (1:1)	-	-	1765	1732	1712	1577	512	365

Table (20): The ir-vibrational spectra of some function groups (cm^{-1}) of ligand II and its metal chelates:

Compound	Ratio M:L	ν_{NH}	$\nu_{C=N}$	$\nu_{C=O}$	ν_{C-O}	ν_{O-CH_3}	M-O	M-N
II	-	3420_w	1678	1715	1275	1210	-	-
Co^{2+}-II	1:1	-	1732	1770	1300	1215	515	410
	1:2	-	1670	1710	1280	1212	523	408
Ni^{2+}-II	1:1	-	1735	1768	1302	1215	525	407
	1:2	-	1665	1710	1302	1210	530	415
Cu^{2+}-II	1:1	-	1715	1733	1300	1215	525	410
	1:2	-	1675	1710	1305	1230	525	410
La^{3+}-II	1:1	-	1730	1769	1301	1215	525	407
	1:2	-	1675	1710	1305	1230	510	425
Gd^{3+}-II	1:1	-	1730	1770	1300	1218	510	410
	1:2	-	1670	1710	1345	1230	510	410
Pt^{4+}-II	1:1	-	1715	1735	1305	1215	515	410

Table (21): The ir-vibrational spectra of some function groups (cm^{-1}) of ligand III and its metal chelates:

Compound	ν_{N-H}	$\nu_{C=N}$	$\nu_{C=O}$	C-Cl	M-O	M-N
III	3420	1680	1715	775	-	-
Co^{2+}-III (1:1)	-	1735	1770	772	510	360
Ni^{2+}-III (1:1)	-	1730	1768	773	515	362
Cu^{2+}-III (1:1)	-	1715	1732	773	518	380
La^{3+}-III (1:1)	-	1732	1765	770	518	375
Gd^{3+}-III (1:1)	-	1735	1770	775	515	366
Pt^{4+}-III (1:1)	-	1718	1765	778	520	370

(iv) Proton Magnetic Resonance spectra of La^{3+}-chelates:

^{1}H-nmr spectroscopy is considered now as a very helpfull tool for investigation of the metal chelates. It can be used to determine the position of the replacable protons of the function groups that contribute in complex formation[107].

The ^{1}H-nmr spectra of La^{3+}-chelates of compounds I, II and III are given in Figs. (37-39) and compared to those of the free ligands. Such ligands were found to exhibit hydrazone $\rightleftharpoons$ enol tautomerism, which was previously supported from the ir-spectra:

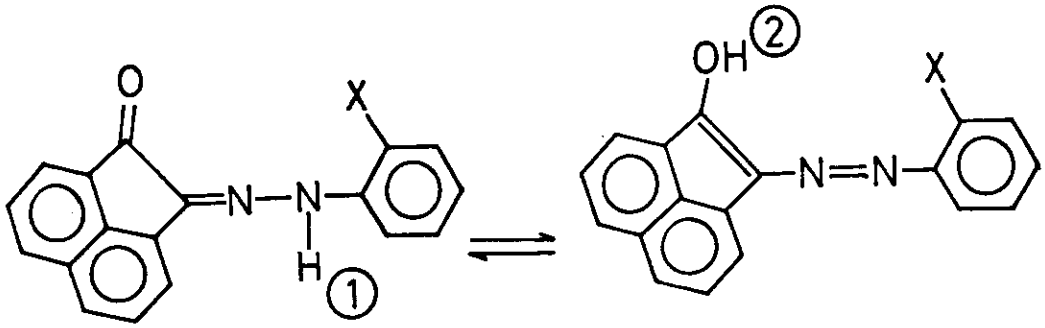

where X = COOH (3)-I, OCH_3 (4)-II and Cl-III.

The ^{1}H-nmr spectra of the compounds I, II and III show a singlet signals at δ = 11.20, 11.34 and 10.45 ppm respectively corresponding to the proton (1) of the imino group. The slight broadening of this signal is due to the hydrazone $\rightleftharpoons$ enol tautomerism, which leads to the appearance of proton (2) of the hydroxyl group.

Also, the down field shift in the position of this signal in compounds I and II compared to that of compound III is attributed to the contribution of this proton in an intramolecular hydrogen bond[108].

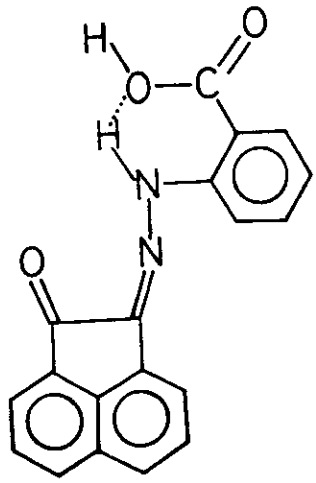

Proton (3) of the carboxylic group in compound (I) gave its own signal at δ= 8.43 ppm, while the signal at δ= 0.96-1.33 ppm is due to the three protons of the methoxy group (4), in compound II. The ^{1}H-nmr spectra of all compounds showed multiple signals at δ= 7.75-8.61 ppm with integration amounting to 10 protons corresponding to the aromatic moeities of the molecules.

On comparing the ^{1}H-nmr spectra of La^{3+}-chelates with those of the free ligands, it was found that the signals of protons (1) (NH) completely disappeared indicating that complex formation takes place through proton elemination from the imino group. Also, the

signals of proton (3) of the carboxylic group of compound I disappeared indicating that the bonding leading to chelate formation in this compound is as follows:

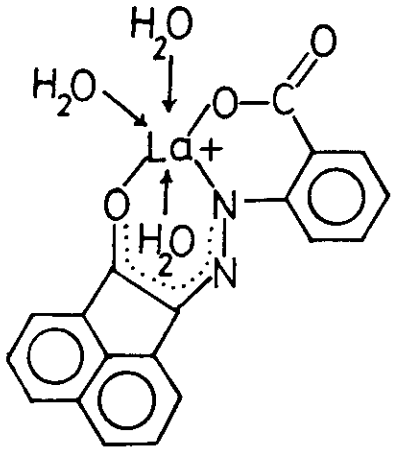

On the other hand, the signals of all aromatic protons are shifted downfields direction with an obvious decrease and broadening in their envelope as a result of the deshielding of the π-electrons of the rings due to the formation of a covalent bond between La^{3+} ion and the oxygen and nitrogen atoms of the hydrazone form. This shift of the aromatic signals is expected since the formation of La-N or La-O bond withdraws electrons from the aromatic ring, and this is in accordance with the data obtained from ir-studies.

In all the ^{1}H-nmr spectra of La^{3+}-chelates, a new broad signal within the range 3.18-3.36 ppm is observed, which is due to water molecules coordinated to the metal complex.

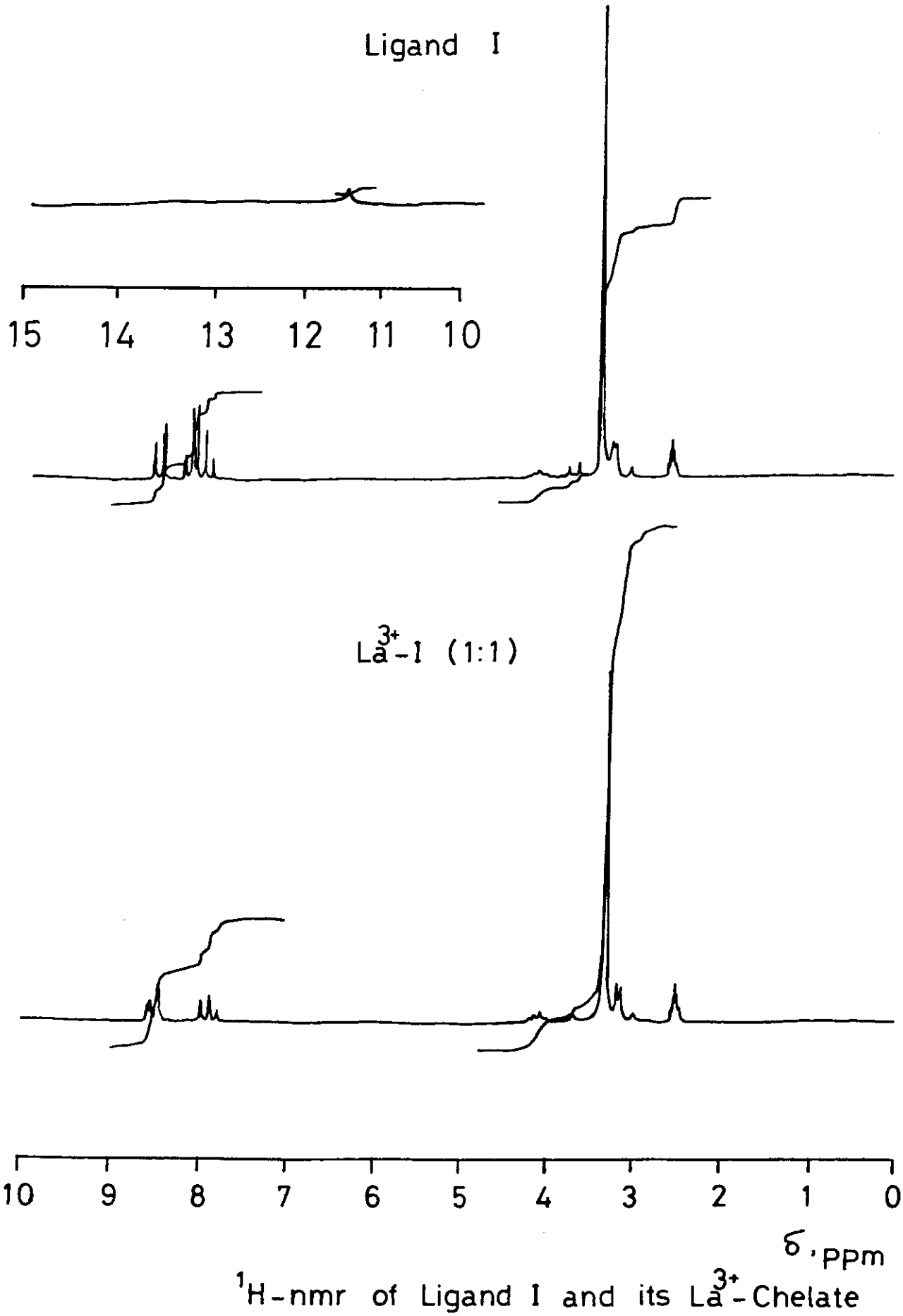

^{1}H-nmr of Ligand I and its La^{3+}-Chelate

Fig. (37)

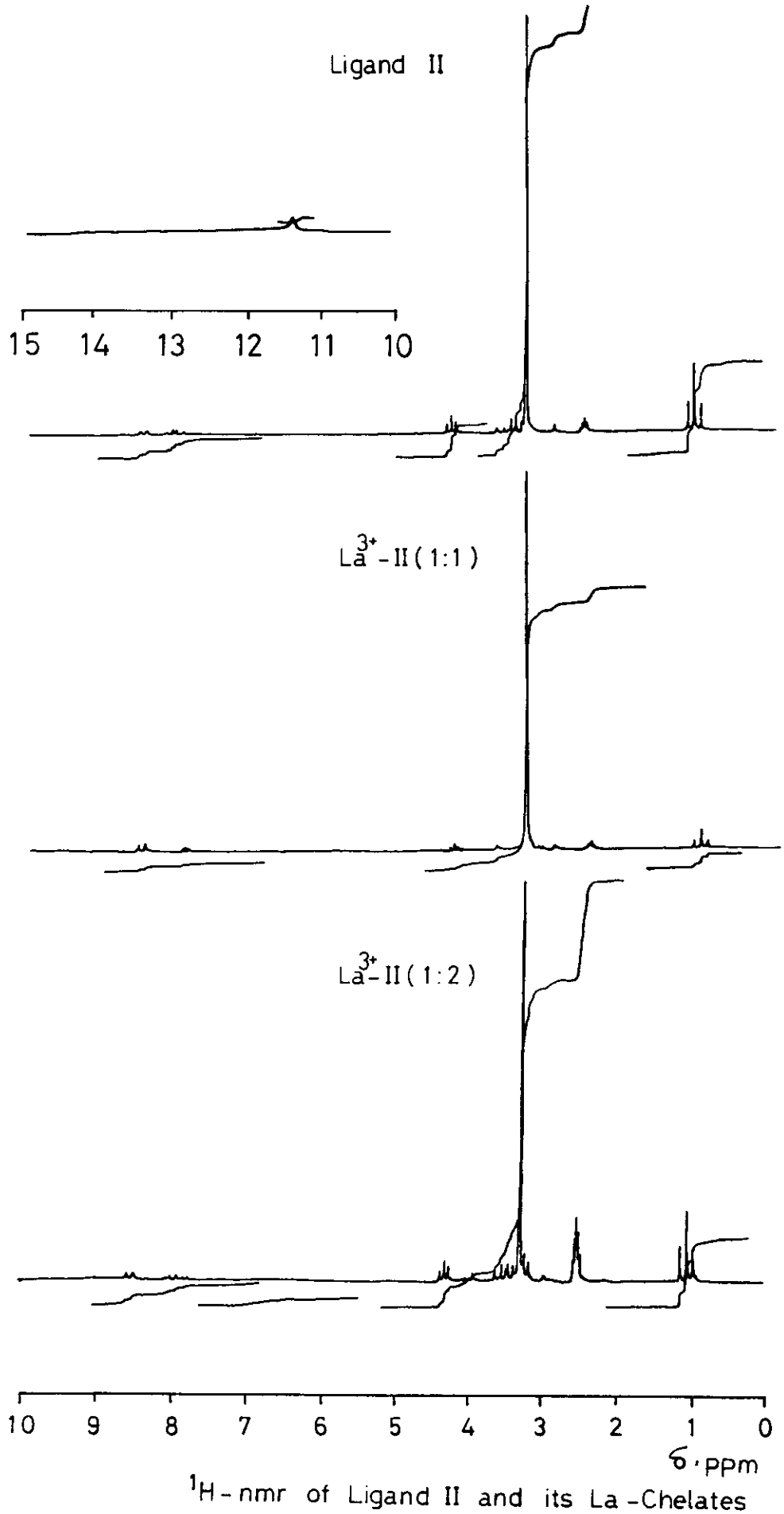

^{1}H-nmr of Ligand II and its La-Chelates

Fig. (38)

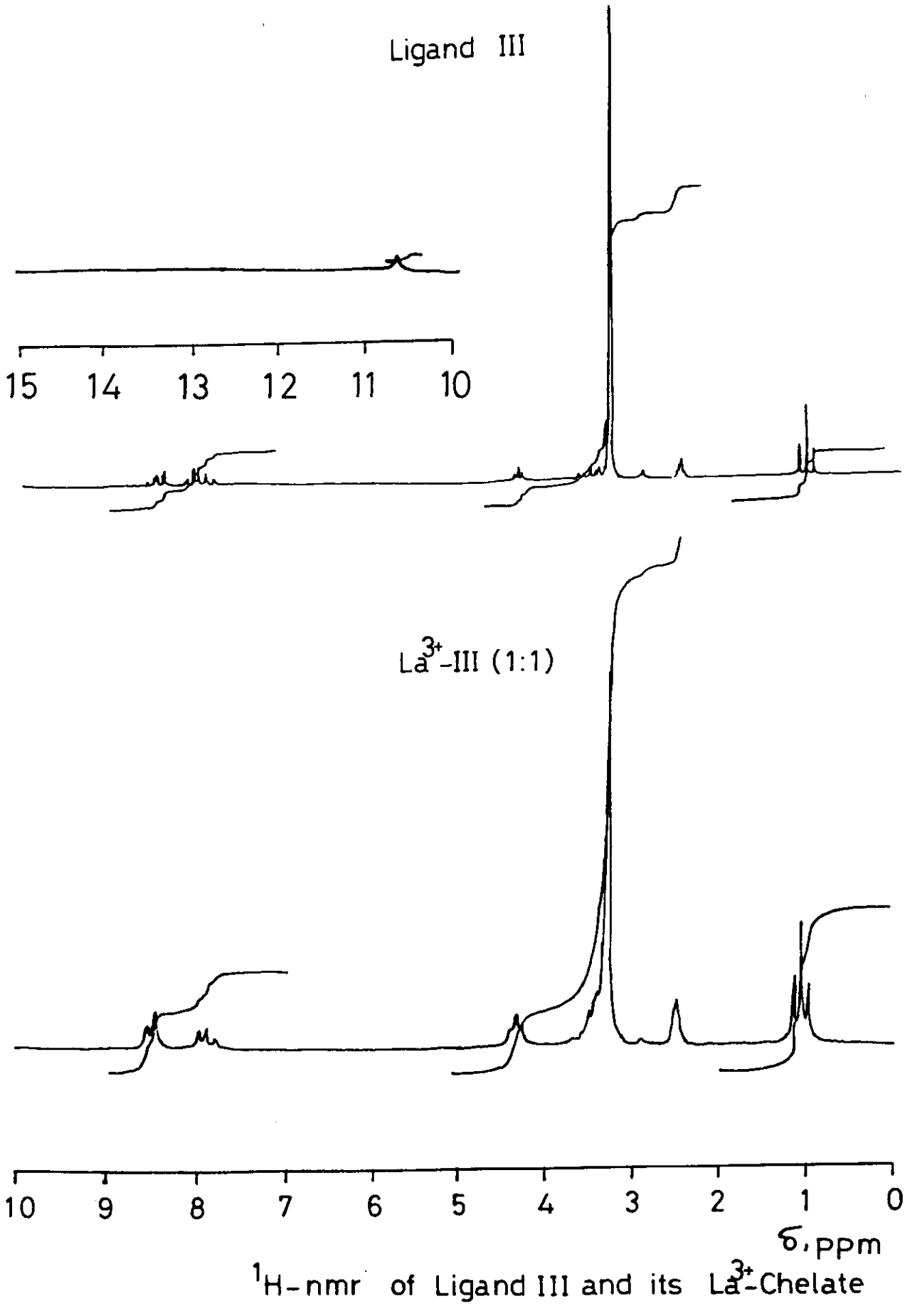

^{1}H-nmr of Ligand III and its La^{3+}-Chelate

Fig. (39)

(v) Electronic spectra and magnetic properties of metal chelates:

I - Electronic absorption spectra of metal chelates:

Electronic spectra of transition metal ions and complexes are observed in the visible and uv regions (50000 to 10000 cm^{-1}) in which electronic excitation takes place. The radiant energies of this region of spectrum is absorbed by a complex for a variety of reasons:

(1) ligand spectra (L ⟶ L)

(2) charge-transfer spectra (CT)

(3) ligand-field spectra

These arise from electronic transitions within the d- or f- orbitals of the metal that have been splited in a ligand field. The lanthanide ions all show absorptions in the visible or near uv regions of the spectrum. These colours arise from f-f transitions. Since the f orbitals are deep inside the atom, they are largely shielded from invironmental factors such as forming complexes (which affects the outer electrons). External fields only split the various spectroscopic states by ~100 cm^{-1}, so the absorption bands are usually sharp. This is in marked contrast to the transition elements where d-d spectra give broad absorption bands because of the very considerable effect of the environment.

Based on the fact that electronic absorption spectra are very diagnostic of the stereochemistry of metal chelates, the electronic absorption spectra of the solid chelates prepared in the present work are measured as Nujol mull and in solution using DMF as solvent within the range 200-850 nm.

The electronic spectra for d^7 system are well defined for different configurations. The Co (II) in d^7 is known to exist in four coordinate as tetrahedral and six coordinate as octahedral geometries. The spectrum of tetrahedral Co (II) complex is more intense than that of the octahedral one and is characterised by a more strongly structured peak in the visible region. There are three electronic transitions depicted from the ground state. The first band appears in the region 30000-50000 cm^{-1} for most complexes, yet it has been observed[109] in few cases. The second band is usually a broad one appearing in the near ir-region. The third band in intense, broad and usually excure in the region of 15000-20000 cm^{-1} with obvious splitting[109-112].

The absorption spectra of Co^{2+} complexes both in DMF and nujol mull show mainly the M-L or L-M charge transfer transitions with an obvious change in their $\bar{\nu}_{(cm^{-1})}$ compared to those of the free ligands, also a

d-d transition within the range 29586-31545 cm^{-1} corresponding to the $^4A_2 \longrightarrow 4\ T_1$ transition.

It is well known that Ni (II) forms a large number of chelates whose coordination number varies from four to six[113]. The structure of the six coordinated chelates is generally octahedral and often with slight distortion, while those with coordination number four may have tetrahedral or square planar arrangement. Trigonal bipyramidal or square-pyramidal structures are usually assigned for many penta coordinated Ni (II) chelates as well as Co (II) chelates.

The absorption spectra of these complexes exhibit some d-d transitions, Table (22) at $\bar{\nu}_{max}$ positions which can be assigned either to $^3A_{2g} \longrightarrow {}^3T_{1g}$ (F) or $^3A_{2g} \longrightarrow {}^3T_{1g}$ (P) transitions. The charge transfer band (Metal $\longrightarrow$ Ligand or Ligand $\longrightarrow$ Metal) is observed which was shifted to lower or higher energy on complex formation.

Cu (II) chelates commonly exist in tetrahedral, squar planar or distorted octahedral symmetry and in less common cases in five coordinate geometry for five coordinate Cu (II) complexes. There are two possible geometrical arrangements for the ligands around the

metal ion via (a) trigonal bipyramidal (D_3h) with ground state d_z2 or (b) square pyramidal (C_4V) with ground state $d_{x^2-y^2}$. Actually, one can distinguish between these two cases based on the visible spectrum. In case of trigonal bipyramidal type, the spectrum displays a band around 10000 cm^{-1} which sometimes exhibits a shoulder in the near ir-region[114-116]. The square pyramidal type show one band in the visible region around 13000 cm^{-1} and a shoulder in the near ir side.

The majority of six coordinated Cu (II) complexes are tetragonally distorted and their spectra exhibit one absorption band in the visible region (>15380 cm^{-1}), while the square planar, trigonally distorted Cu (II) complexes give rise to two absorption bands in the visible region around 15380 cm^{-1}. Usually the square planar structure shows a broad band around 16000-14280 cm^{-1} range[115].

The electronic absorption spectra of Cu^{2+} complexes with the organic ligands under investigation in nujol mull and DMF show mainly their CT bands with a slight deviation when compared to the free ligands. Also, some d-d bands appeared as weak peaks within the range 20080-31250 and 20618-29586 cm^{-1} using DMF and nujol mull as a medium respectively which can be assigned

to the $^2T_{2g} \longrightarrow {}^2E_g$ octahedral and $^2B_{1g} \longrightarrow {}^2A_{1g}$ tetrahedral chelates.

The electronic absorption spectra of the organic ligands and their metal chelates using nujol mull and DMF techniques are shown in Figs. (40-42). The spectral data of the metal chelates in comparison to those of the corresponding free ligands are given in Table (22).

It can be concluded from these spectral data that $\bar{\nu}(cm^{-1})$ of the CT band of metal chelates displays red or blue shift compared to those of the free ligands. This generally confirms that such ligands interact with the metal ion in some sort of chelation, and the metal ion environments are different leading to the formation of different geometrical types of complexes. The change in $\bar{\nu}(cm^{-1})$ values of the CT band on going from nujol mull to DMF results from the destruction of the crystalline state hence the environment differs in the solid state than that in solution.

II - Magnetic properties of some metal chelates:

The study of the magnetic properties of the solid complexes in addition to spectral studies provide informations that can throw considerable light on their structure and geometry.

A combination of spectral and magnetic studies of the solid complexes enables to determine the stereochemistry of a chelate and may also give an idea about the extent of distortion therein. The magnetic properties are concerned with the nature of states very close in energy to the ground state whereas the spectral studies are concerned with the electronic transitions between the ground and the excited states of the molecule.

For many transition elements of the first series, experimental results show that orbital contribution to the magnetic moment is almost completely queniched and the magnetic moment is given by the equation:

$$\mu_{eff} = \sqrt{n(n+2)}$$

where n is the number of unpaired electrons.

The magnetic susceptibilities of some selected solid chelates were determined at room temperature using Gouy method, from which the magnetic moments and the number of unpaired electrons in the d-orbital were calculated[117].

The values of magnetic moments of (Co^{2+}-I), (Co^{2+}-II) and (Co^{2+}-III) (1:1) complexes were found to be 3.89, 3.94 and 3.75 BM, respectively (theoritical spin value is 3.87 BM) indicating the presence of three

unpaired electrons in d-orbital, so the complex formed is high-spin octahedral having sp^3d^2 hybridization.

All the studied Ni^{2+} complexes (d^8) are paramagnetic with magnetic moment values amounting to $\simeq$ 2.82 - 2.88 BM indicating the presence of two unpaired electrons in d-orbital.

The Cu^{2+} complexes show paramagnetic behaviour with a magnetic moments nearly equal to that of the theoritical spin only value of Cu^{2+} (1.72). So, the geometry of Cu^{2+}-complexes with ligands I, II and III would be octahedral taking place through sp^3d^2 hydridization.

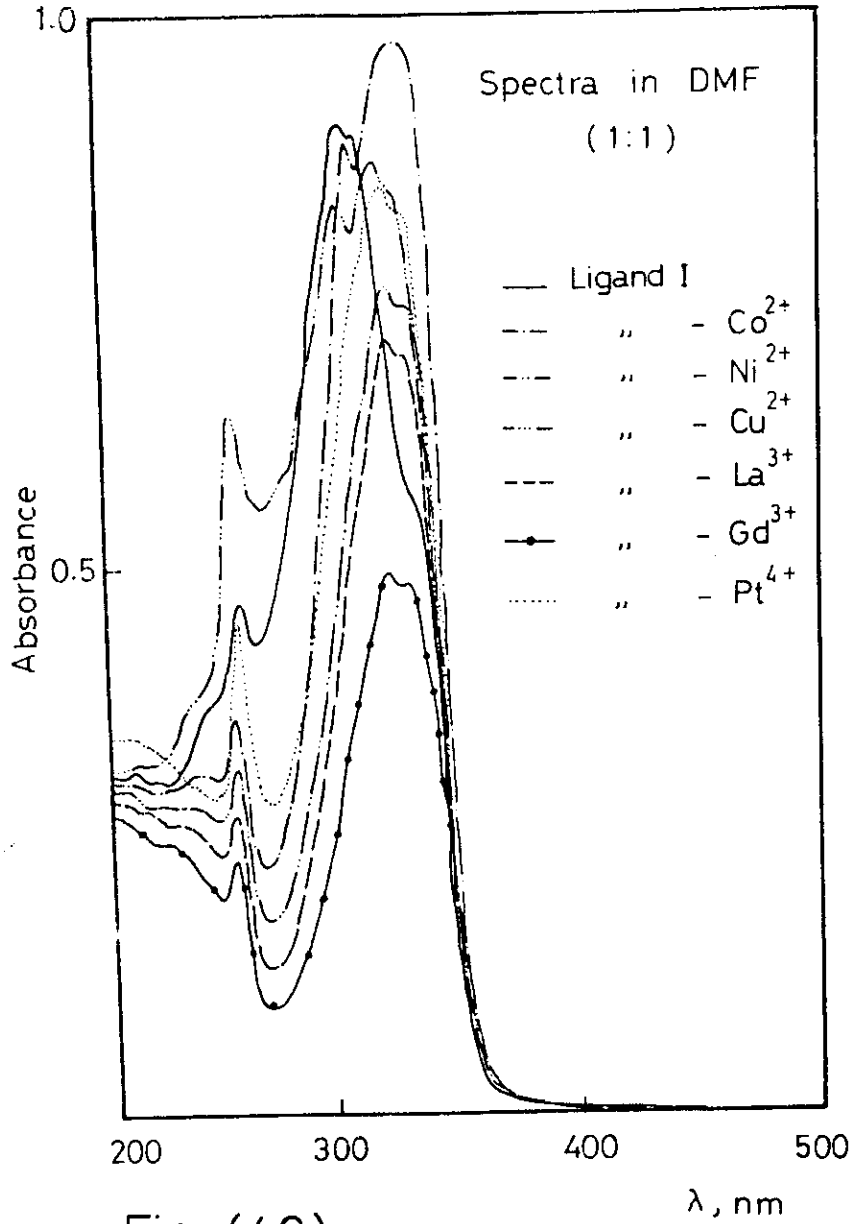
1.0
0.5
Absorbance
Spectra in DMF
(1:1)
Ligand I
" - Co^{2+}
" - Ni^{2+}
" - Cu^{2+}
" - La^{3+}
" - Gd^{3+}
" - Pt^{4+}
200
300
400
500
λ, nm

Fig. (40)

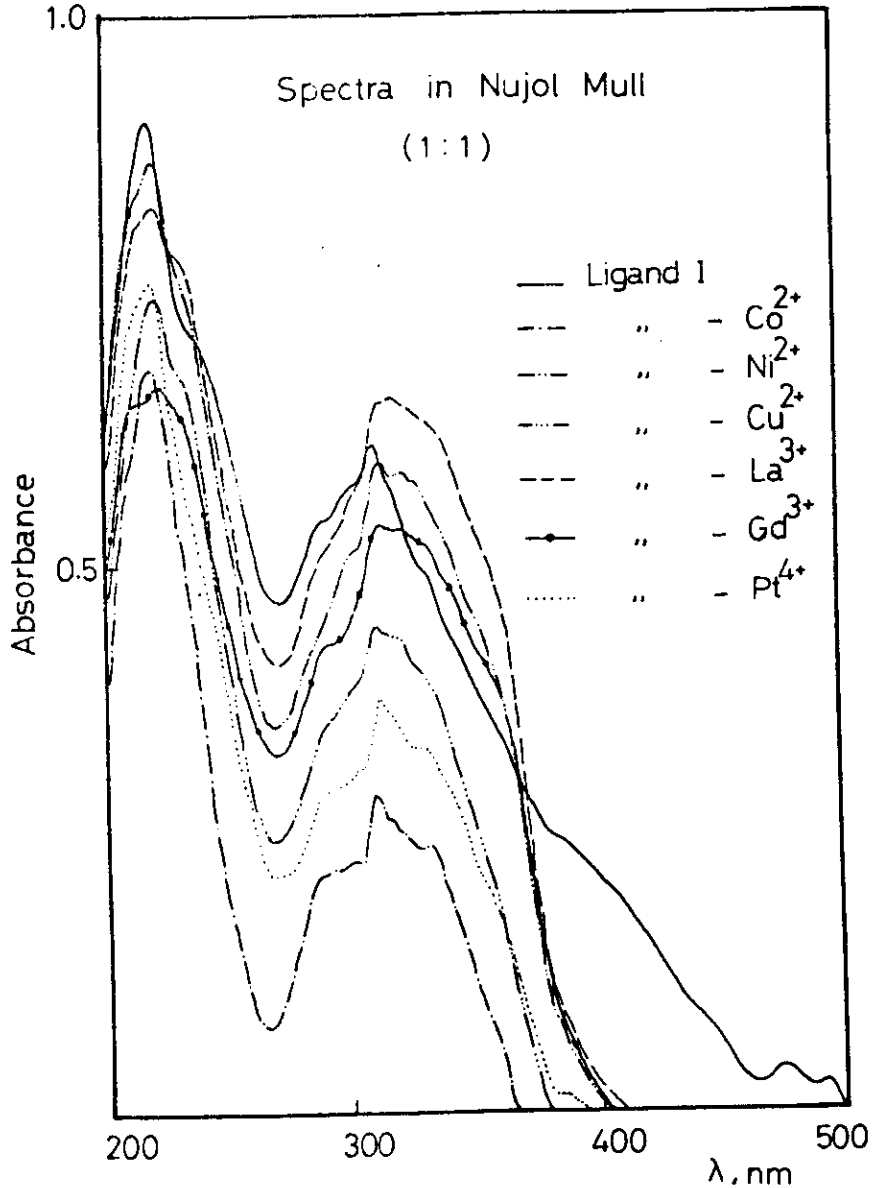
1.0
0.5
Absorbance
Spectra in Nujol Mull
(1:1)
Ligand I
" - Co^{2+}
" - Ni^{2+}
" - Cu^{2+}
" - La^{3+}
" - Gd^{3+}
" - Pt^{4+}
200
300
400
500
λ, nm

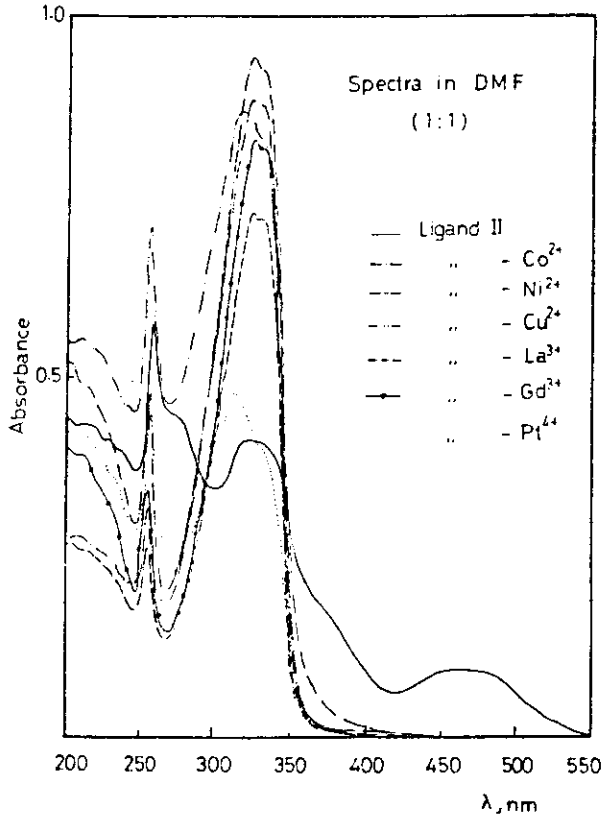
Spectra in DMF
(1:1)
Ligand II
" - Co^{2+}
" - Ni^{2+}
" - Cu^{2+}
" - La^{3+}
" - Gd^{3+}
" - Pt^{4+}
Absorbance
1.0
0.5
200 250 300 350 400 450 500 550
λ, nm

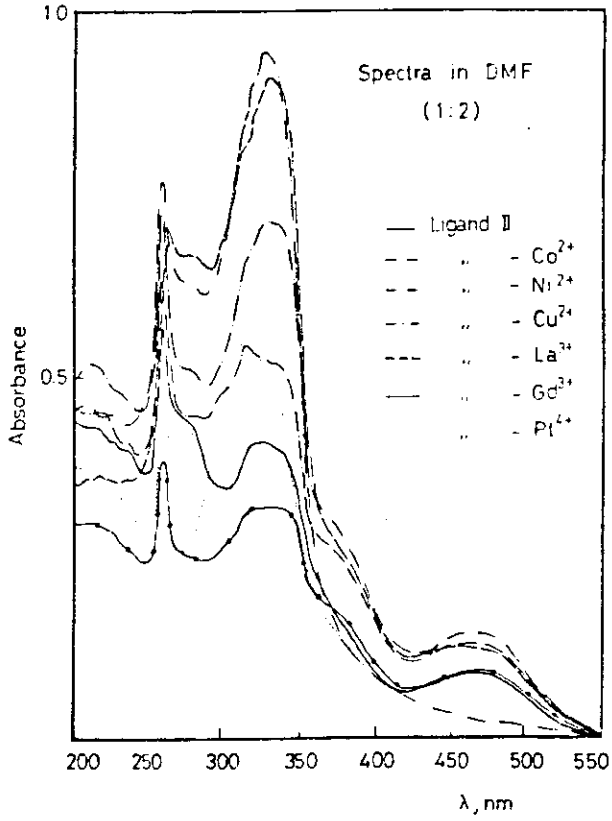
Spectra in DMF
(1:2)
Ligand II
" - Co^{2+}
" - Ni^{2+}
" - Cu^{2+}
" - La^{3+}
" - Gd^{3+}
" - Pt^{4+}
Absorbance
1.0
0.5
200 250 300 350 400 450 500 550
λ, nm

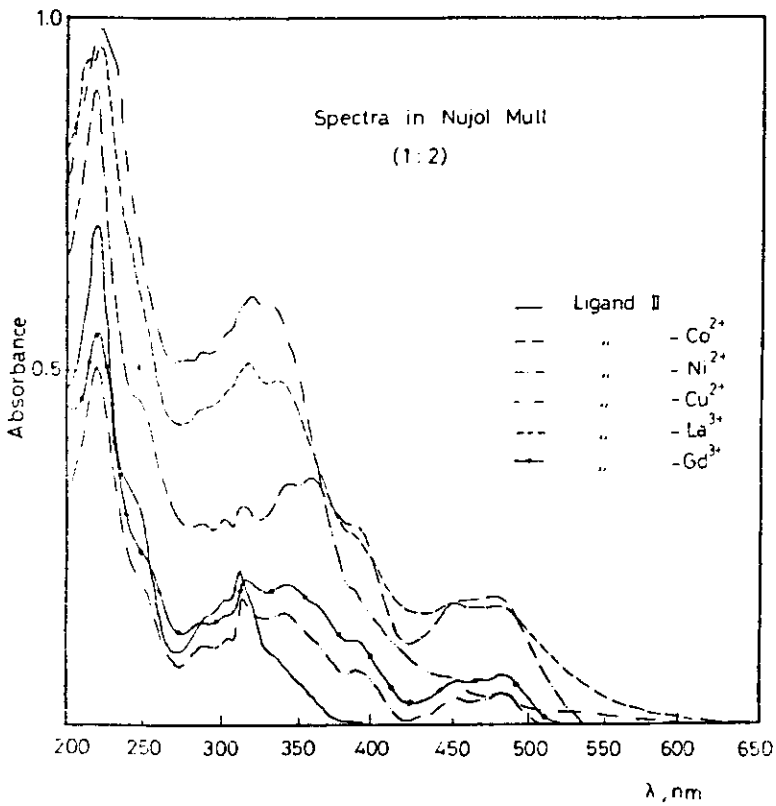
Spectra in Nujol Mull
(1:2)
Ligand II
" - Co^{2+}
" - Ni^{2+}
" - Cu^{2+}
" - La^{3+}
" - Gd^{3+}
Absorbance
1.0
0.5
200 250 300 350 400 450 500 550 600 650
λ, nm

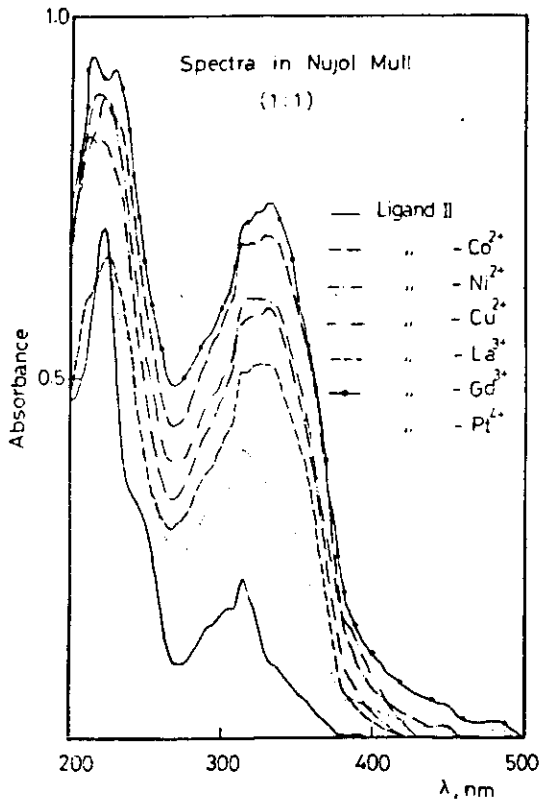
Spectra in Nujol Mull
(1:1)
Ligand II
" - Co^{2+}
" - Ni^{2+}
" - Cu^{2+}
" - La^{3+}
" - Gd^{3+}
" - Pt^{4+}
Absorbance
1.0
0.5
200 300 400 500
λ, nm

Fig. (41)

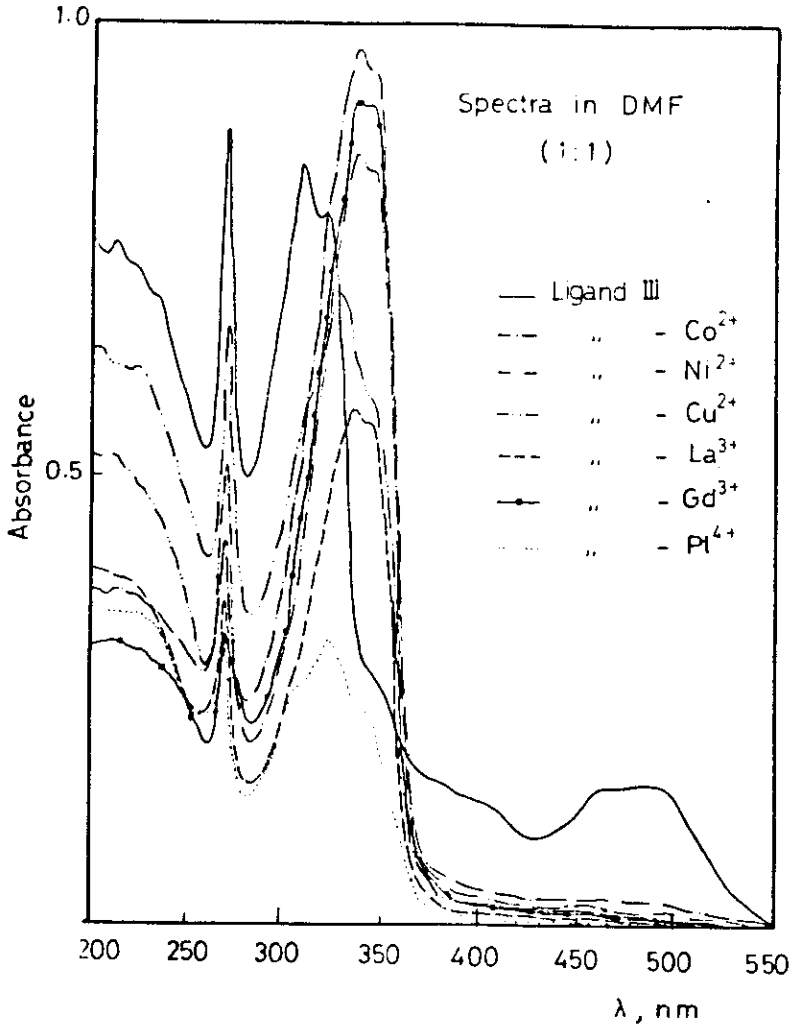
1.0
0.5
Absorbance
Spectra in DMF
(1:1)
Ligand III
" - Co^{2+}
" - Ni^{2+}
" - Cu^{2+}
" - La^{3+}
" - Gd^{3+}
" - Pt^{4+}
200 250 300 350 400 450 500 550
λ, nm

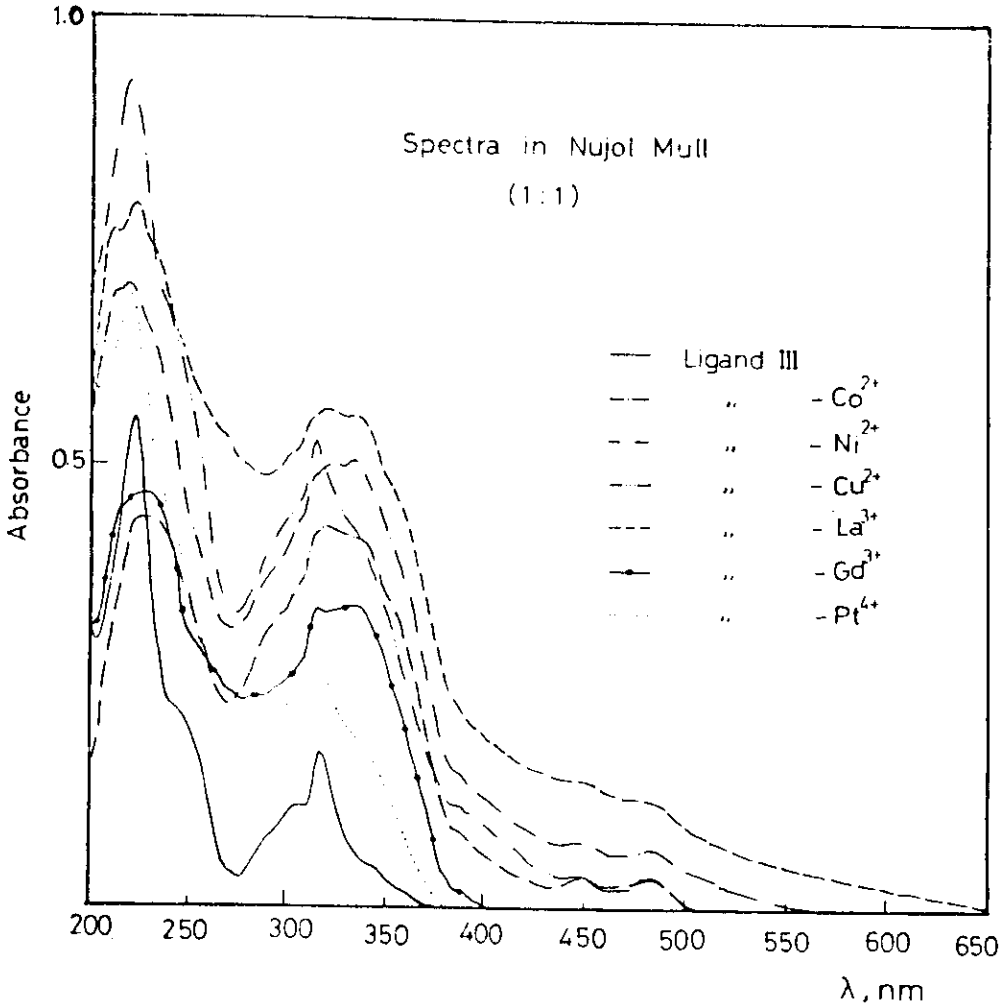
1.0
0.5
Absorbance
Spectra in Nujol Mull
(1:1)
Ligand III
" - Co^{2+}
" - Ni^{2+}
" - Cu^{2+}
" - La^{3+}
" - Gd^{3+}
" - Pt^{4+}
200 250 300 350 400 450 500 550 600 650
λ, nm

Fig. (42)

Table (22): The electronic absorption spectral data of some metal chelates in DMF and Nujol Mull.

Ligand	M^{Z+}	Ratio	Band Maxima (cm^{-1})	
			DMF	Nujol Mull
I	-	-	35714-33333	45450-33003
	Co^{2+}	1:1	30303	35714-32467-30120
	Ni^{2+}	1:1	30675-29586(sh)	34014(sh)-3333-31446
	Cu^{2+}	1:1	33784-31250	35461-32787-31250-29586(sh)
	La^{3+}	1:1	30769-29851	31546-29586
	Gd^{3+}	1:1	30657-29586	35211-32467-30303(sh)
	Pt^{4+}	1:1	30769-29412	35211-31546-30303
II	-	-	30864-21276	43350-32258
	Co^{2+}	1:1	30303-29850	33333-29586-22222
		1:2	31546-29498	27778-22421-20833
	Ni^{2+}	1:1	30120-29851	31446-29586
		1:2	31056-27027-21276	29586-25316-22222-20747
	Cu^{2+}	1:1	33333-29586	33333-29851-25773
		1:2	35700-31250	31250-25000(sh)-22222-20618
	La^{3+}	1:1	31446-31056	33333-31250
		1:2	30303-26316-21276	32258-30120-22222-20747
	Gd^{3+}	1:1	31847-31250	33333-31250-22222-20661
		1:2	29586-26881-21276	31250-29412-25316-22222-20408
	Pt^{4+}	1:1	32679-30303	32051-22222-20833
III	-	-	33333-22026	33333-31250
	Co^{2+}	1:1	30769-20000	31545-22222-20747
	Ni^{2+}	1:1	30488-28571-21739	31250-22222-20619
	Cu^{2+}	1:1	30675-28571-25000-20080	31746-25974-22222-20703
	La^{3+}	1:1	29762-28735	33333-22222-20833
	Gd^{3+}	1:1	30769-28985	31446-29412-25773
	Pt^{4+}	1:1	30864-28902	33557-31446

(vi) Structural Elucidation of The Solid Complexes:

From the preceeding discussion and based on the data obtained from the different methods of analysis, the mode of bonding within the metal chelates and their structures can be formulated taking into account the following aspects:

(i) The prepared complexes were subjected to elemental analysis whose values are in good agreement with the suggested formula. Also, the molar conductance measurements gave satisfactory informations about the number of charges present and the position of Cl^- (anion) in-or out-the coordination sphere.

(ii) TGA-DTA measurements of some solid complexes showed that they lose their water of coordination above 120°C and all the unhydrated complexes show thermal stabilities up to 350°C above which decomposition of the complex species took place with an inflection at $\sim$ 500°C indicating the melting of the unhydrous complexes.

(iii) (a) The ir spectra of the solid complexes were recorded and compared to those of the free ligands. Such compparison showed that the two bands located at 3420 and 1410-1419 cm^{-1} due to the stretching vibrations of the NH and N=N groups respectively disappear on complex formation. Also the shift of

the $\nu_{C=O}$ and $\nu_{C=N}$ to higher frequencies observed on complex formation suggests that these ligands contribute to chelate formation through their hydrazone form.

(b) The bands due to ν_{COO^-} in ligand (I) and ν_{OCH_3} in ligand (II) found at 1600 and 1210 cm^{-1} respectively display some shift to lower frequencies in the spectra of the solid complexes, indicating their participatation in chelate formation.

(c) The two new bands observed at 448-520 and 360-425 cm^{-1} for all solid complexes can be assigned to ν_{M-O} and ν_{M-N} respectively.

(iv) The ^{1}H-nmr spectra of La^{3+}-chelates showed the disapparance of the signals found at 11.34-10.45 and 8.43 ppm due to the NH and COOH (in ligand I) indicating their elimination on complex formation. The signals of the aromatic protons (7.75-8.61 ppm) of the free ligands show some shifts downfields in the spectra of the solid chelates due to the deshielding effect of the metal ion on the ligand protons as a result of coordination.

(v) The electronic absorption spectra of Co^{2+}, Ni^{2+} and Cu^{2+} complexes in the solid state (nujol mull technique) show a d — d transition bands at 29586-31545, 22222-34014 and 20618-29586 cm^{-1} due to $^4A_2$

$\longrightarrow {}^4T_1$, ${}^3A_{2g} \longrightarrow {}^3T_{1g}$ (F) and ${}^3A_{2g} \longrightarrow {}^3T_{1g}$ (P) and ${}^2T_{2g} \longrightarrow {}^2E_g$ within the octahedral complexes in Co^{2+}, Ni^{2+} and Cu^{2+} complexes respectively. The data derived from the magnetic susceptibility measurements were in satisfactory agreement indicating sp^3d^2 or d^2sp^3 hydridization within the octahedral complexes.

Based on the knowledge gained from the preceeding discussion, the structure of the solid complexes can be represented as follows:

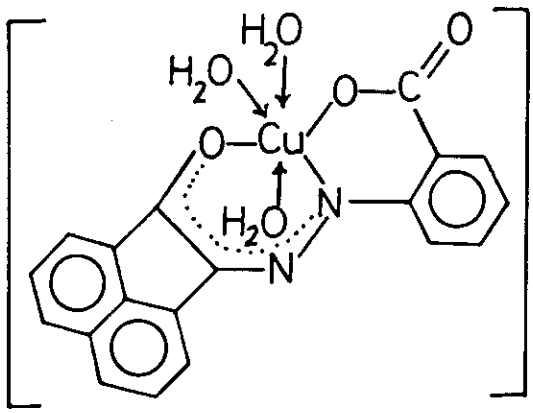

Cu^{2+}:I (1:1)

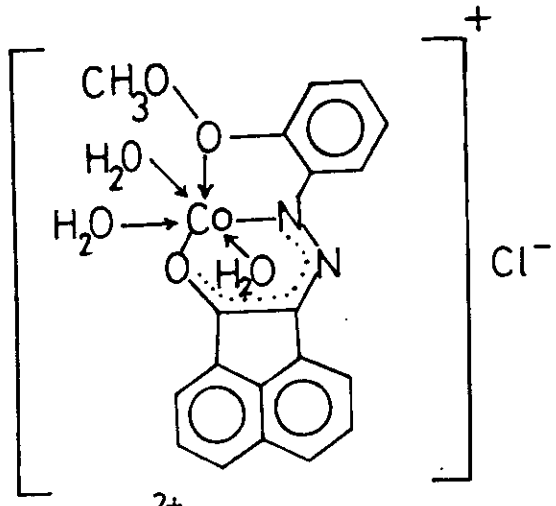

Co^{2+}: II (1 : 1)

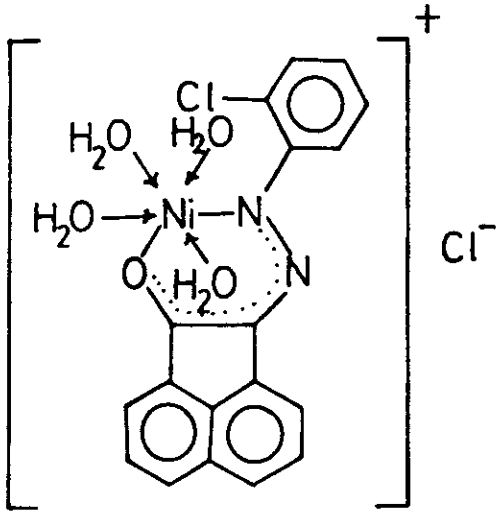

Ni^{2+}: III (1 : 1)

CHAPTER III

PART (D)

(1) Polarographic micro determination of Co^{2+}, Ni^{2+} and Cu^{2+}:

The polarographic reduction of a series of solutions of constant concentration ($5x10^{-5}M$) in suitable ethanolic buffer solution and of metal chloride concentrations ranging between $1x10^{-5}$ to $7x10^{-5}M$ is performed from 0 to 1.8 V. Universal buffer used for the reduction of ligands I, II and III with Co^{2+} and Ni^{2+}, while acetate buffer was used for the reduction of the different ligands with Cu^{2+}. Calibration curves for Co^{2+}, Ni^{2+} and Cu^{2+} ions with different ligands are obtained by plotting the concentration of metal ion (µg) vs. the wave height (nA).

Polarographic determination of Co^{2+}, Ni^{2+} and Cu^{2+} using ligand I:

The polarograms obtained for ligand I with Co^{2+} and Cu^{2+} in 30% (v/v) at pH = 7 are shown in Fig. (37). The polarograms show two waves, the first one being due to the reduction of the ligand while the second involves the reduction of the metal ion. This is suggested by the fact that the height of the second of them increases with increasing the metal ion concentration. The increase of the wave height was found to be directly proportional to the concentration of the metal ions. Calibration curves are given in Fig. (37). From the calibration curve, the metal ion can be estimated under these conditions. A concentration of 70 µg of Co^{2+}, Ni^{2+} and Cu^{2+} can be determined.

Polarographic determination of Co^{2+}, Ni^{2+} and Cu^{2+} using ligand II:

The polarograms obtained for ligand II with Co^{2+} and Cu^{2+} in 30% (v/v) at pH = 7 are shown in Fig. (38). It shows that two waves appeared corresponding to the reduction of the ligand and the metal ion respectively. The increase in the height of the second wave is directly proportional to the concentration of the metal ion. The second wave is used to prepare the calibration curves shown in Fig. (38). Under these conditions,

concentrations of 70 µg for Co^{2+} and 50 µg for both Ni^{2+} and Cu^{2+} ions can be detected.

Polarographic determination of Co^{2+}, Ni^{2+} and Cu^{2+} using ligand III:

The polarograms shown in Fig. (39) were obtained for ligand III with Ni^{2+} and Cu^{2+} in 30% (v/v) ethanol at pH = 7. The polarograms show two waves, the first of which corresponds to the reduction of the ligand while the second one represents the reduction of the metal ion complex. The increase in the height of the second one is directly proportional to the concentration of the metal ion. The calibration curves, Fig. (39) show that 70 µg of Co^{2+} or Ni^{2+} and 50 µg of Cu^{2+} can be determined by this ligand.

Calibration Curves For Co^{2+}, Ni^{2+} and Cu^{2+}
With Ligand I

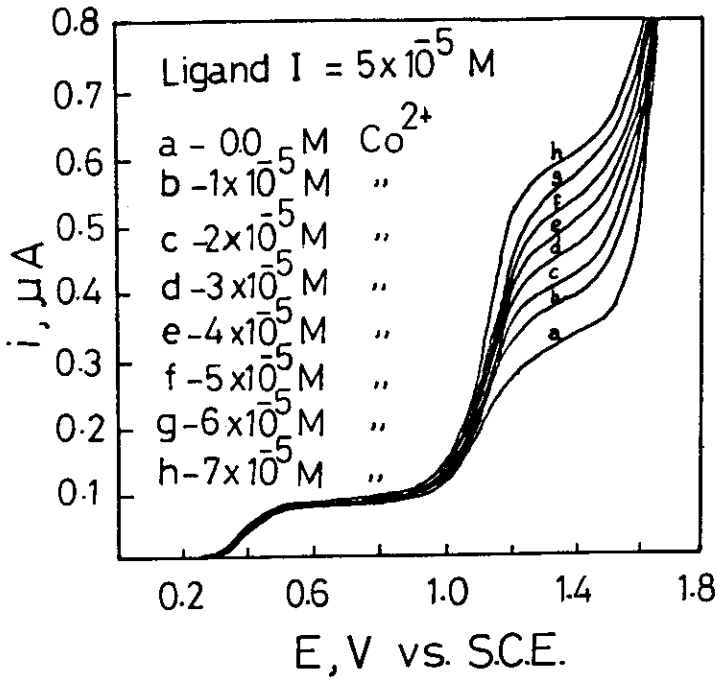

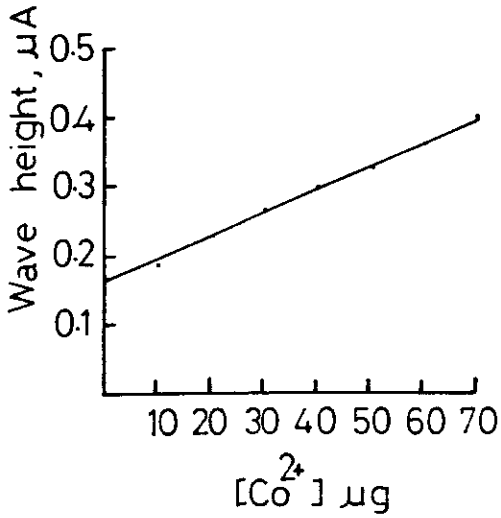

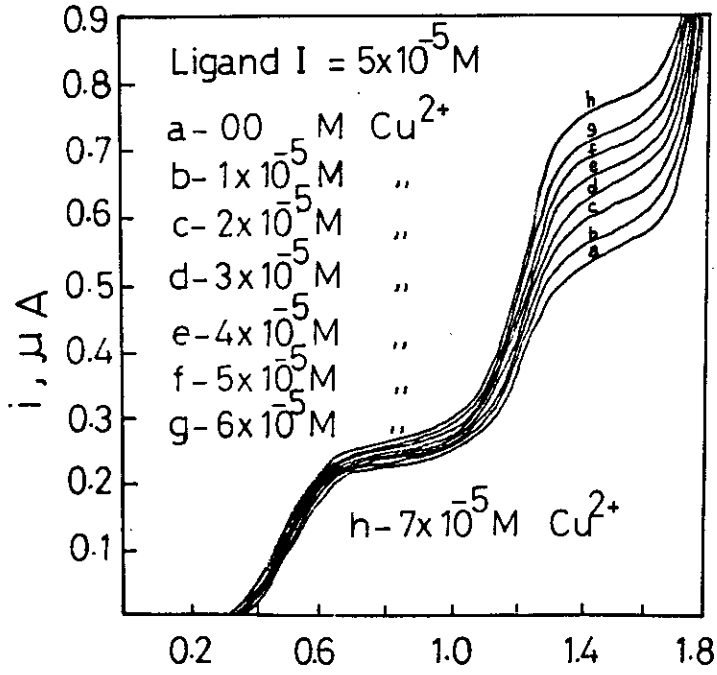

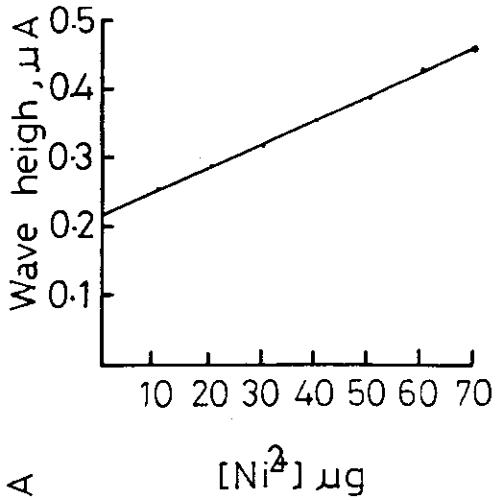

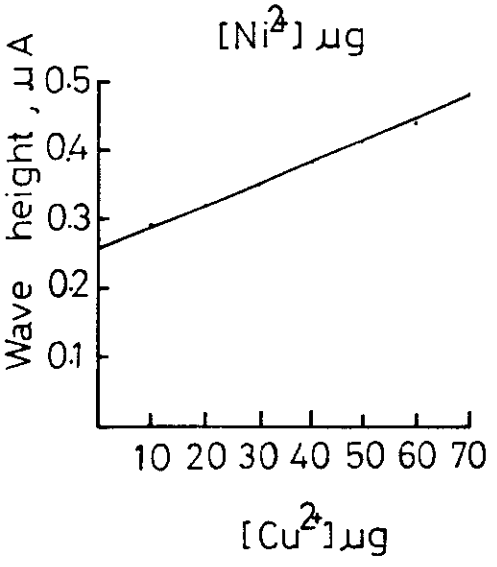

Fig.(43)

Calibration Curves For Co^{2+}, Ni^{2+} and Cu^{2+}
With Ligand II

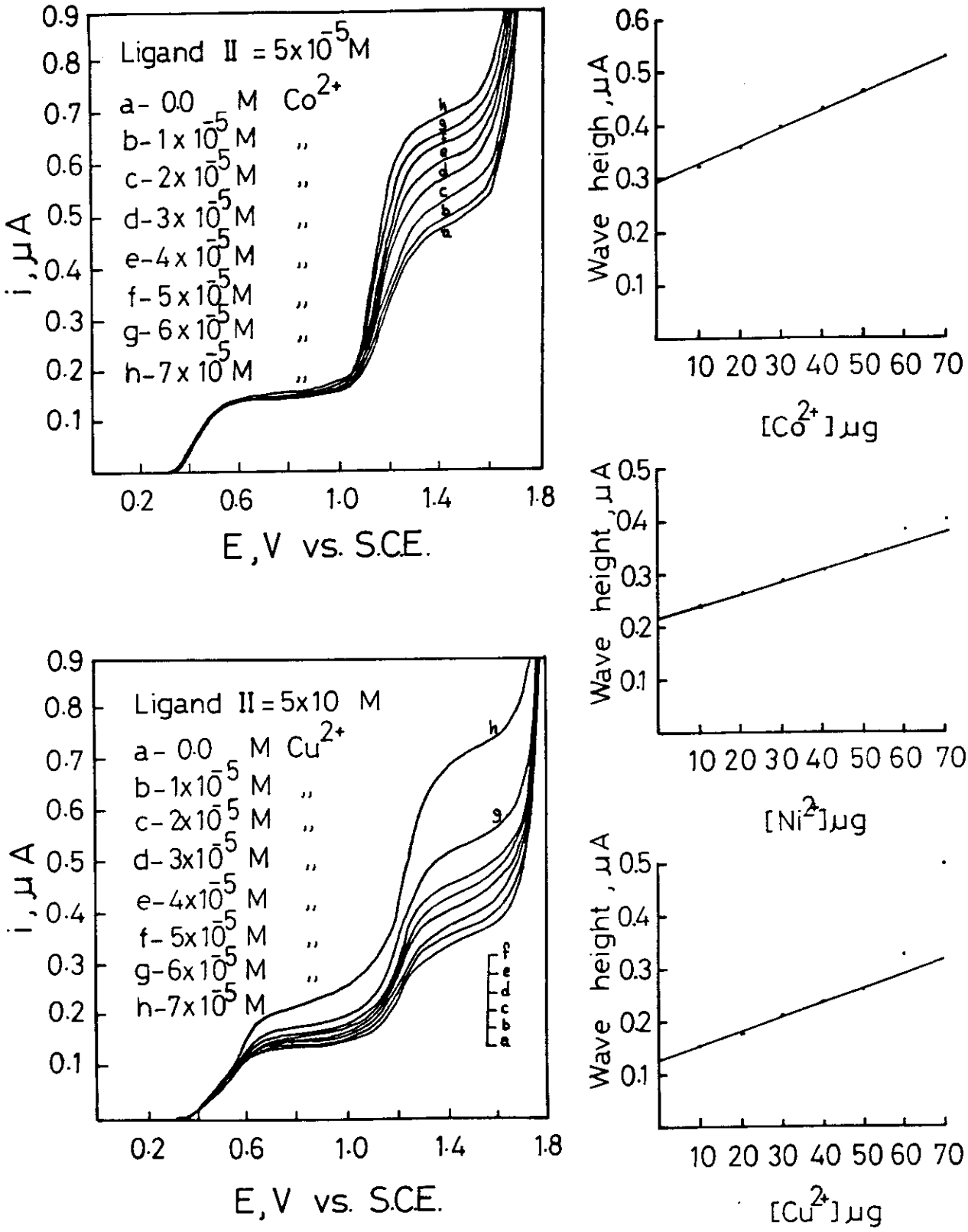

Fig. (44)

Calibration Curves For Co^{2+}, Ni^{2+} and Cu^{2+}
With Ligand III

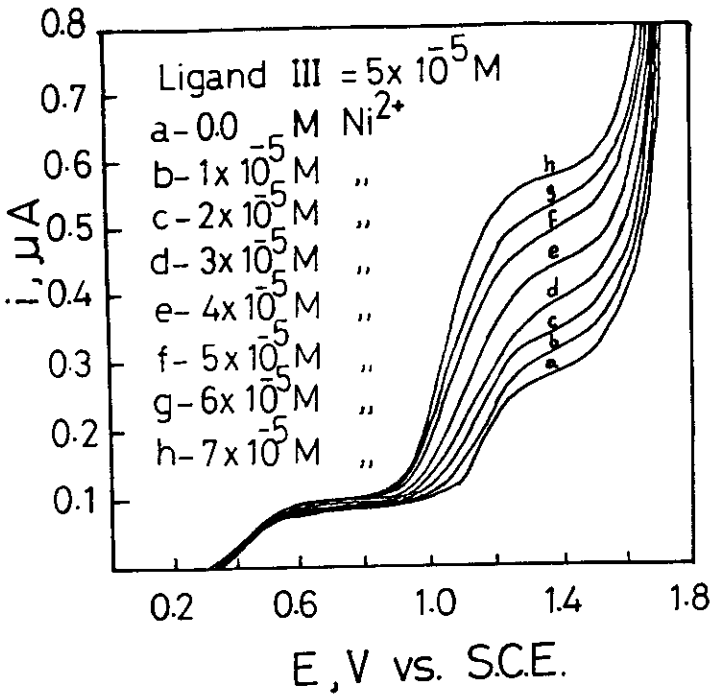

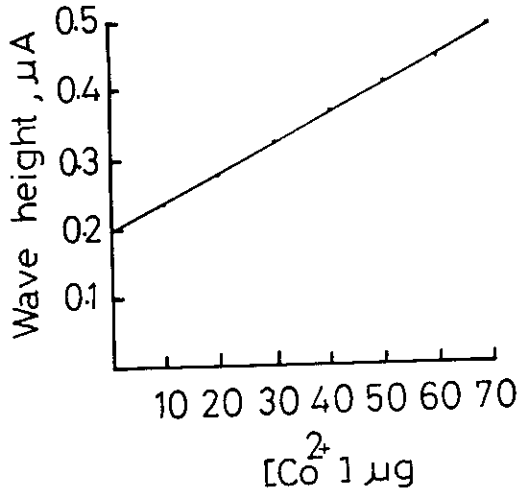

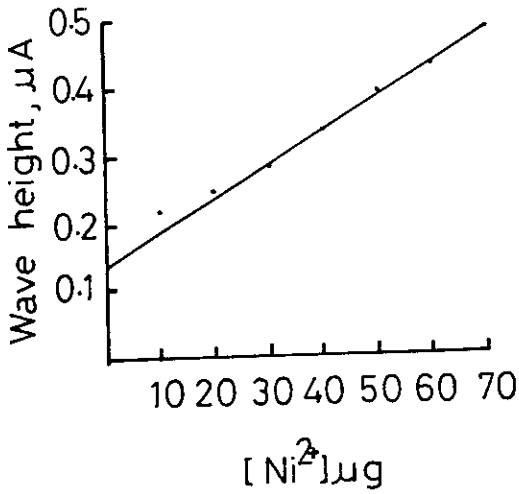

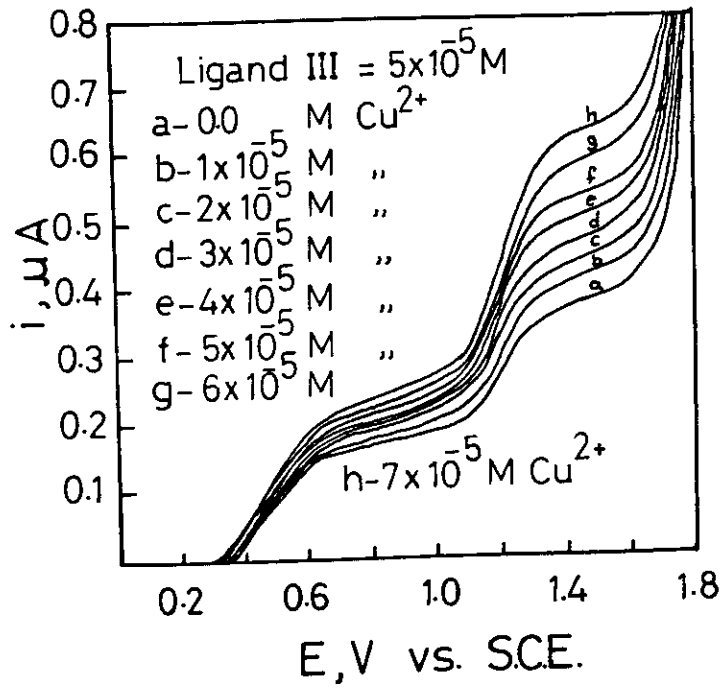

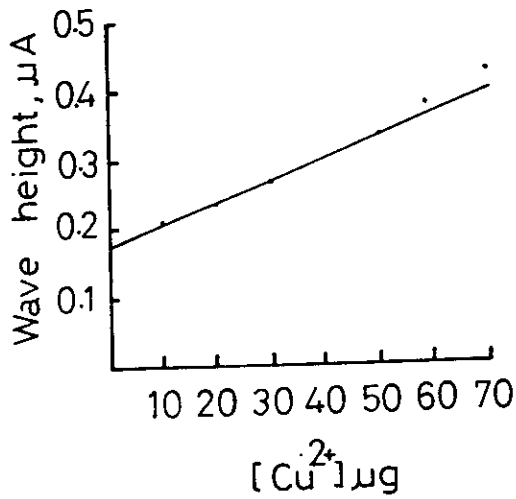

Fig.(45)

(2) Micro determination of the free metal ions spectrophotometrically:

When a chelate solution absorbs in a region far from that characteristic for the ligand, a blank containing the same concentration of the ligand as that in the test solution is used to compensate the absorption due to the colouring ligand. In case of the present investigation, this will lead to incorrect results because the absorption acquires negative values. This behaviour was ascribed to the existence of lower concentration of the free ligand in the test solution than in the blank one[118]. Therefore, to obtain the proper absorption values of the complex, the absorption due to the free ligand should be exactly compensated.

The spectrophotometric method for determination of Co^{2+}, Ni^{2+}, Cu^{2+}, La^{3+}, Gd^{3+} and Pt^{4+} ions using ligands I, II and III has been carried out in which case the concentration of the ligand is kept constant at $1x10^{-4}M$, while that of metal ion is regularly increased from $1x10^{-5}M$ to $1x10^{-4}M$. The corresponding blank solutions used containing ligand concentration was also varied from $9x10^{-5}M$ to $1x10^{-5}M$.

Spectrophotometric determination of Co^{2+}, Ni^{2+}, Cu^{2+}, La^{3+}, Gd^{3+} and Pt^{4+} using acenaphthenequinone-(2-carboxy-phenyl)-hydrazone as chelating agent:

The plot of the absorbance of each solution, measured at 303 and 314 nm, vs. the concentration of metal ion gives a straight line passing through the origin, Fig. (46-a,b). The values of the molar extinction coefficient, which was evaluated from the slopes of the curves, are given in Table (23). The high values of the extenction coefficient permit the micro determination of such ions spectrophotometrically using ligand I as a colouring agent. The linearity of the A-[M] relationship is satisfied up to 60 µg for Co^{2+}, Ni^{2+}, 57 µg for Cu^{2+}, 139 µg for La^{3+}, 157 µg for Gd^{3+} and 195 µg for Pt^{4+}.

Spectrophotometric determination of Co^{2+}, Ni^{2+}, Cu^{2+}, La^{3+}, Gd^{3+} and Pt^{4+} using acenaphthenequinone-(2-methoxy-phenyl)-hydrazone as chelating agent:

The absorbances of the resulting solutions were measured at wavelengths 302 and 312 nm for various metal ions. The plot of the absorbances vs. concentrations of the metal ions in each case gives a straight lines passing through the origin. These plots are shown graphically in Fig. (47-a,b). The values of the molar extinction coefficients are depicted in Table (23), the high values permit the microspectrophotometric determination of these ions using ligand II. The linearity of the A-[M] relationship is satisfied up to 60 µg for Co^{2+} and Ni^{2+}, 63 µg for Cu^{2+}, 139 µg for La^{3+}, 157 µg for Gd^{3+} and 195 µg for Pt^{4+}.

Spectrophotometric determination of Co^{2+}, Ni^{2+}, Cu^{2+}, La^{3+}, Gd^{3+} and Pt^{4+} using acenaphthenequinone-(2-chlorophenyl)-hydrazone as chelating agent:

The relation between absorbance of each solution, measured at 302 and 314 nm, and the concentration of metal ion is shown graphically in Fig. (48-a,b). This relation gives a straight line passing through the origin. The values of the extenction coefficients are given in Table (23). These values permit the micro determination of the metal ions under investigation using ligand III. The linearity of the A-[M] relationship is satisfied up to 53 µg for Co^{2+} and Ni^{2+}, 57 µg for Cu^{2+}, 138 µg for La^{3+}, 157 µg for Gd^{3+} and 195 µg for Pt^{4+}.

Beer's Law For Chelates of Ligand I With Co^{2+}, Ni^{2+} and Cu^{2+}

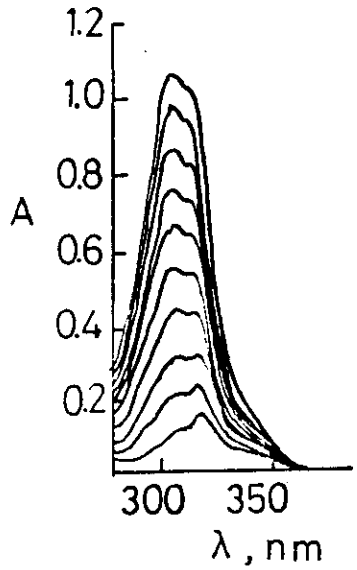

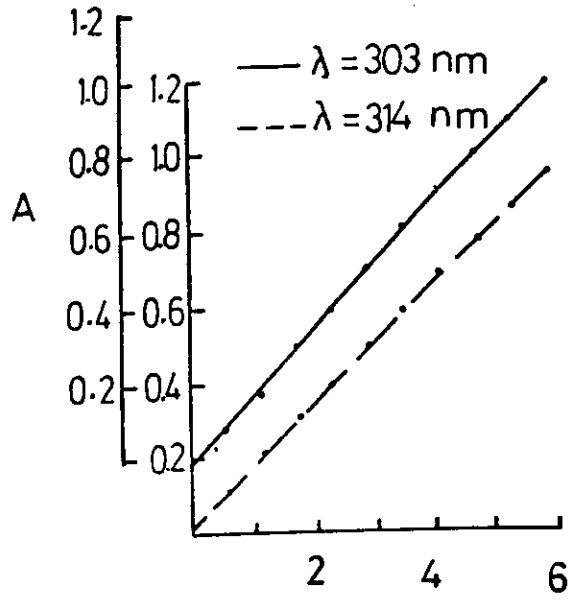

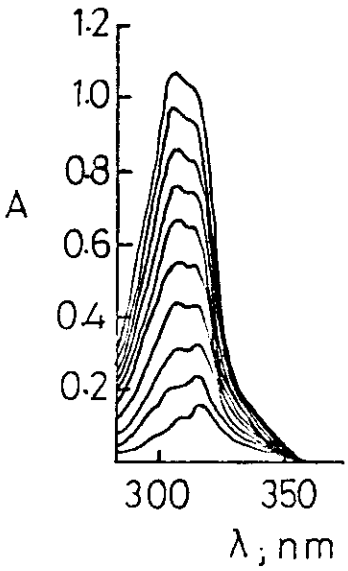

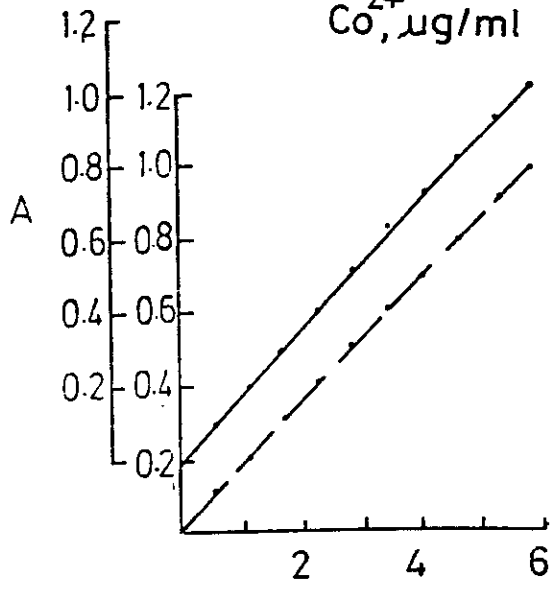

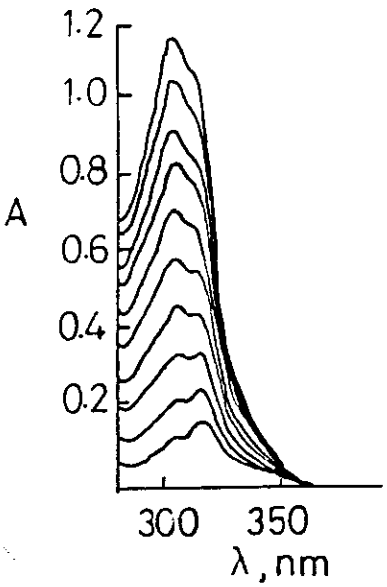

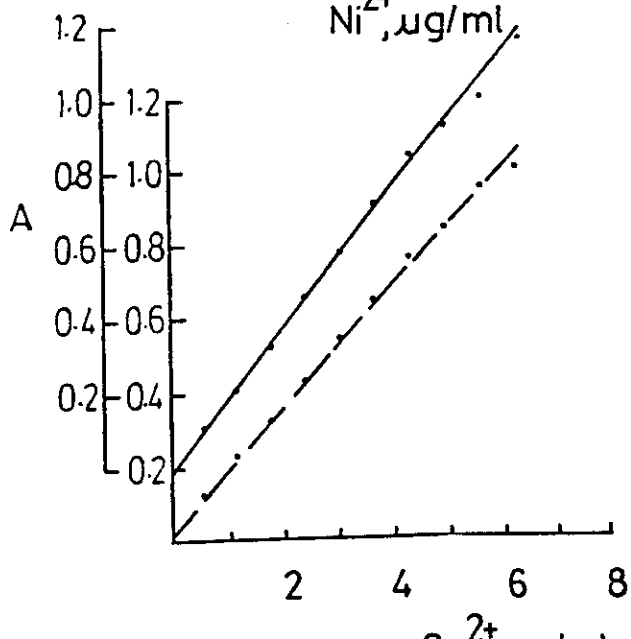

Fig (46-a)

Beer's Law For Chelates of Ligand I With La^{3+}, Gd^{3+} and Pt^{4+}

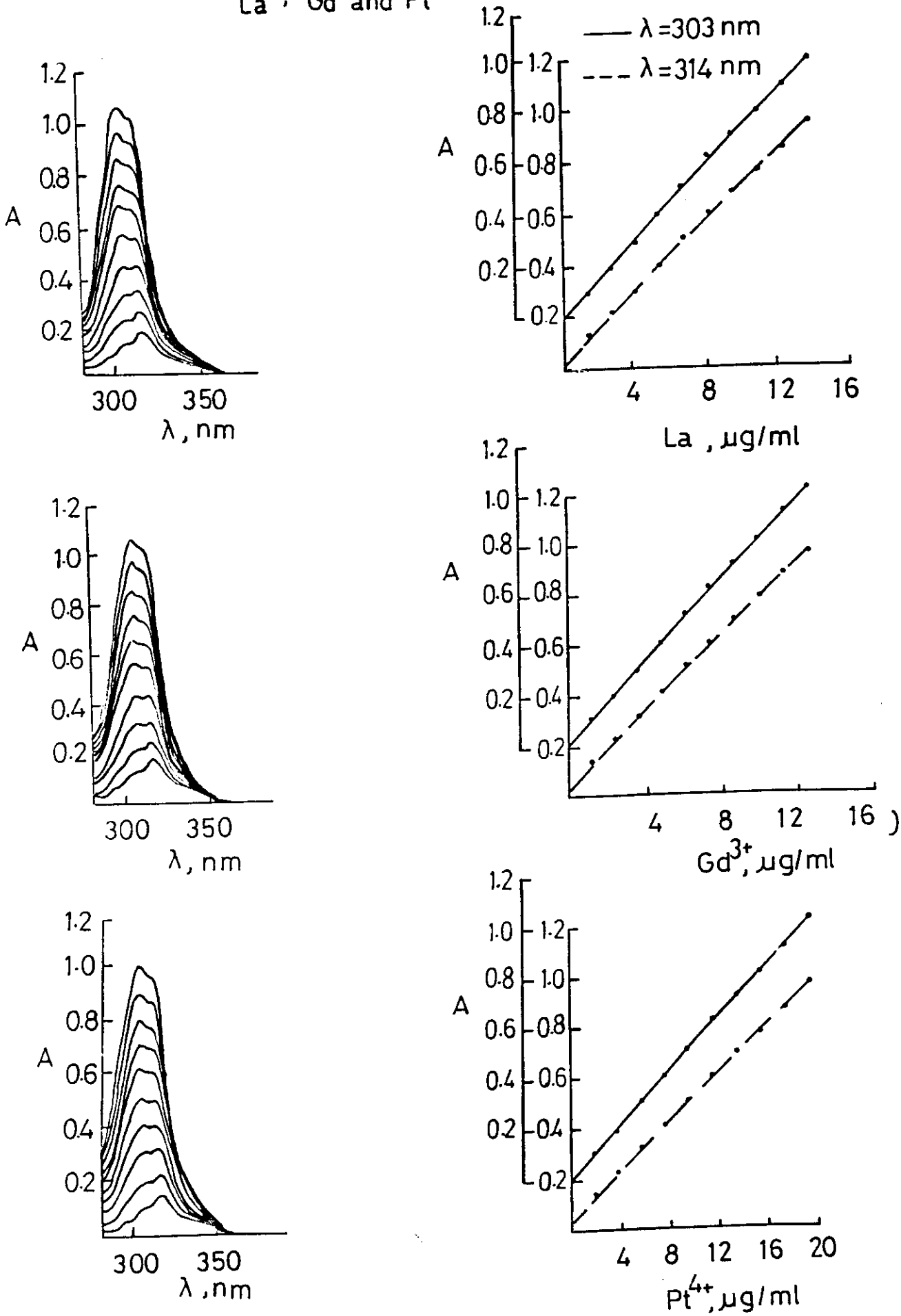

Fig (4.6 b)

Beer's Law For Chelates of Ligand II With

Co^{2+}, Ni^{2+} and Cu^{2+}

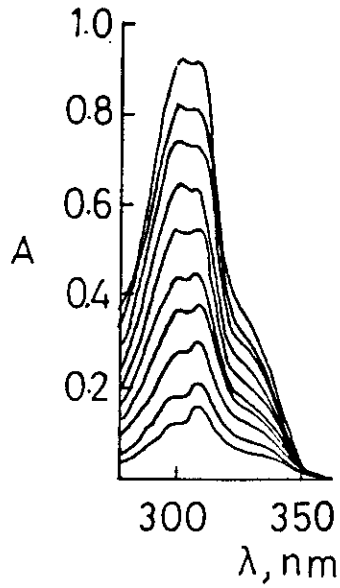

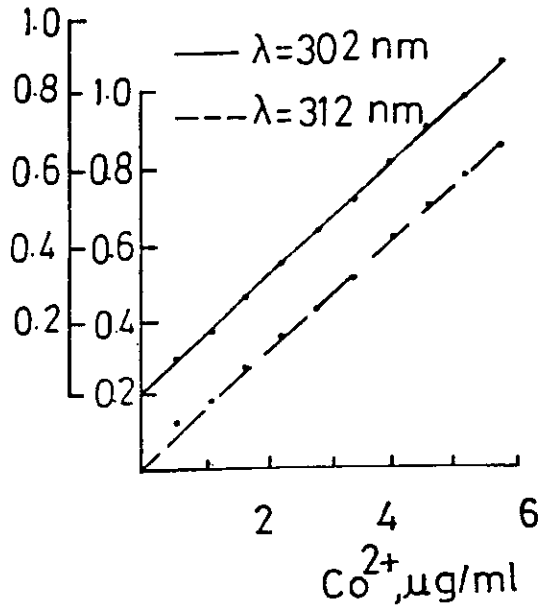

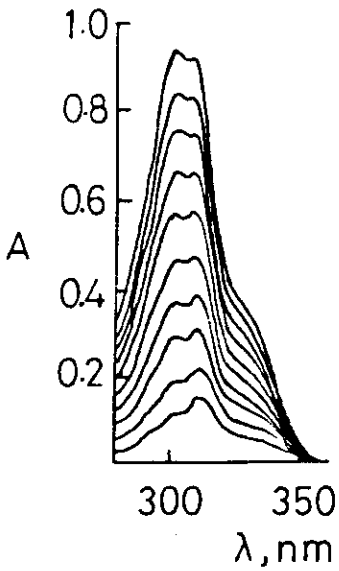

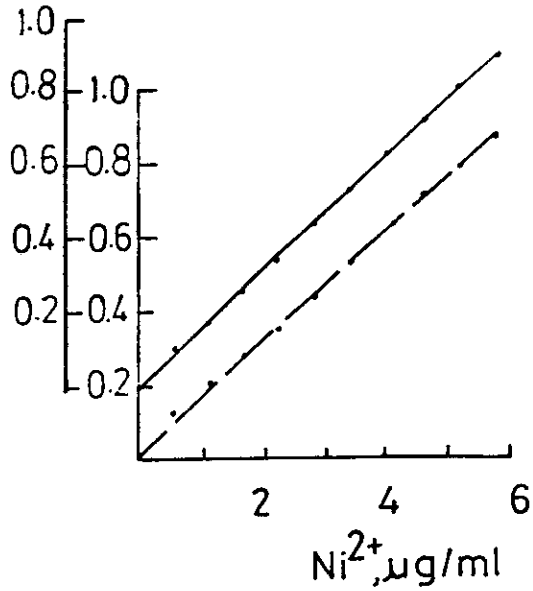

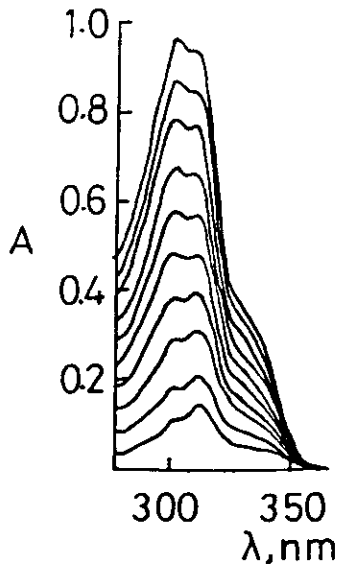

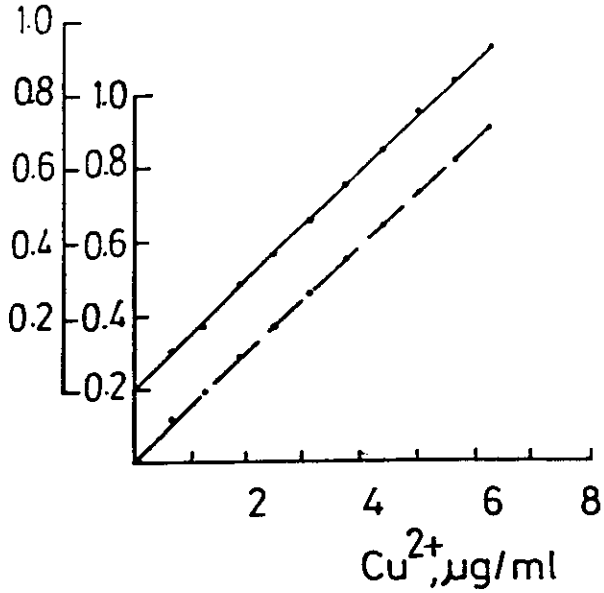

Fig (47-a)

Beer's Law For Chelates Of Ligand II With

La^{3+} Gd^{3+} and Pt^{4+}

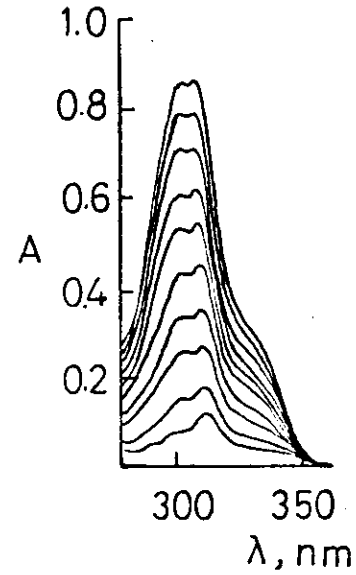

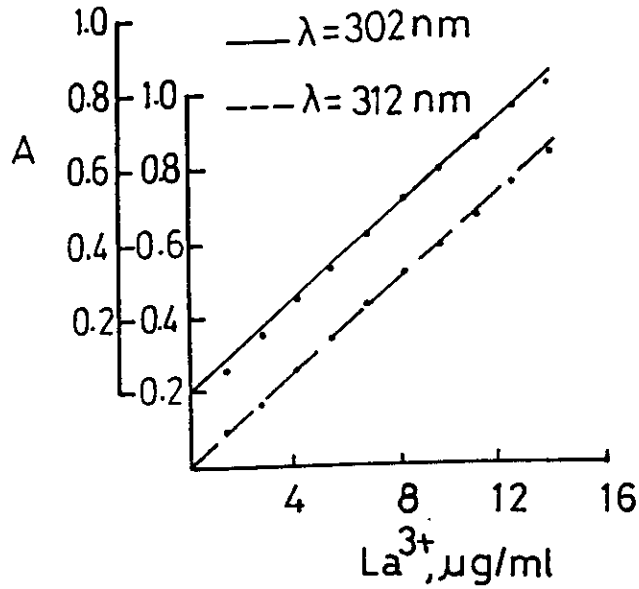

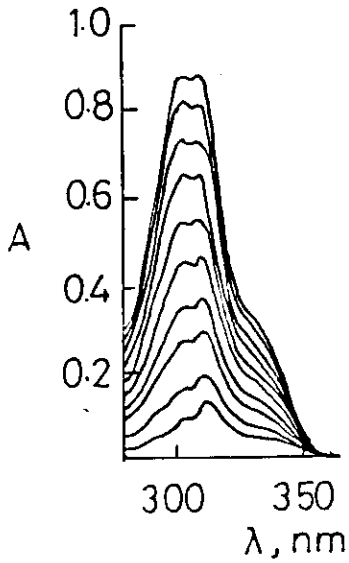

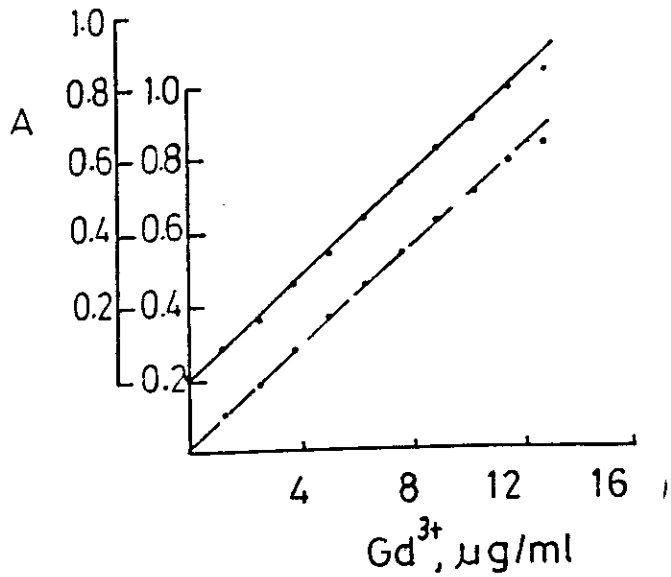

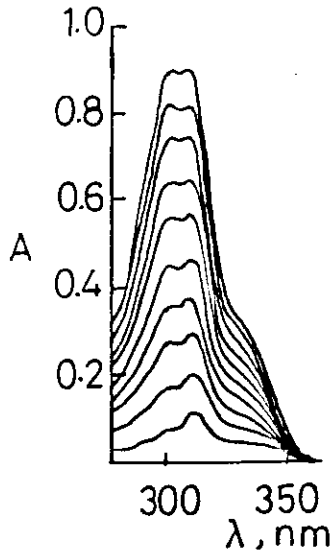

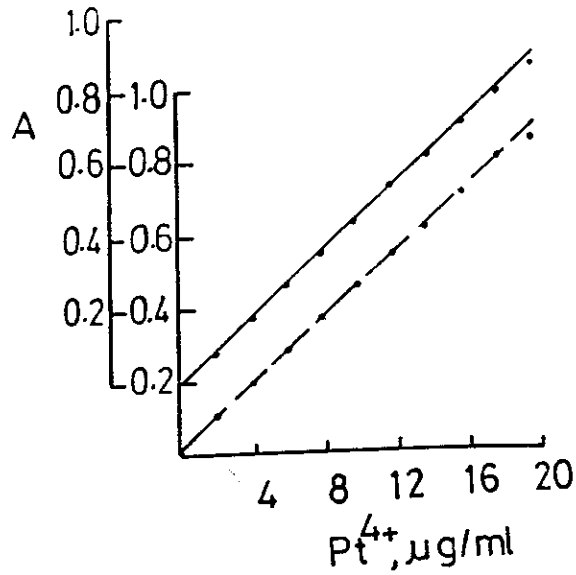

Fig (47-b)

Beer's Law For Chelates of Ligand III With Co^{2+}, Ni^{2+} and Cu^{2+}

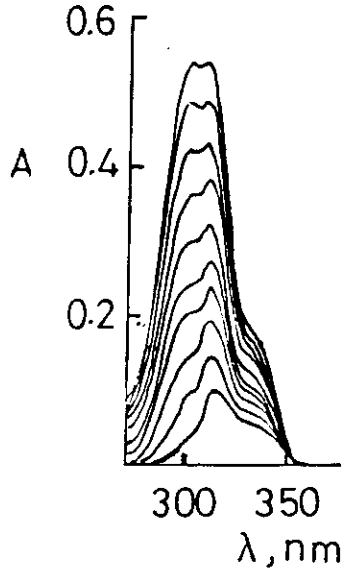

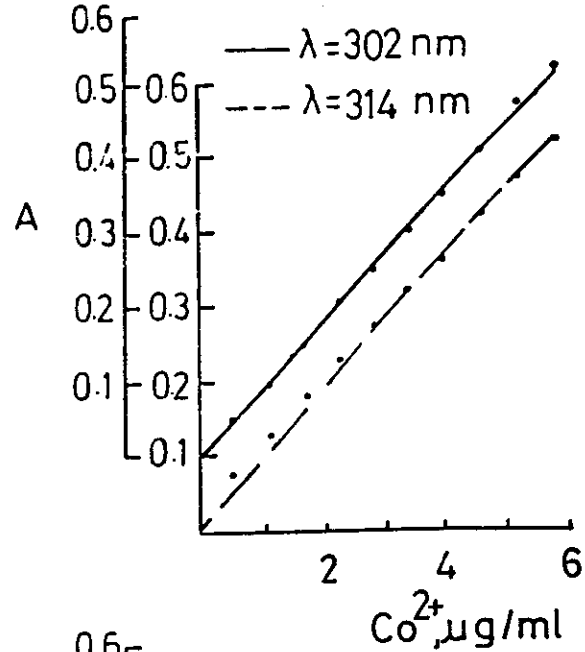

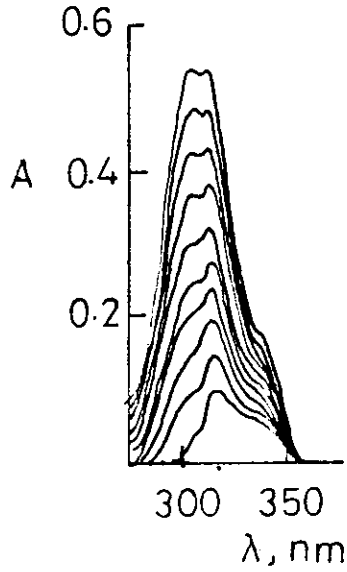

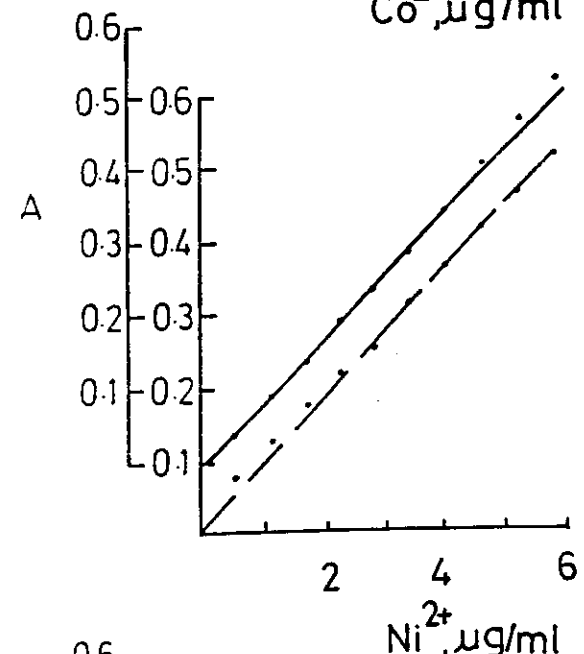

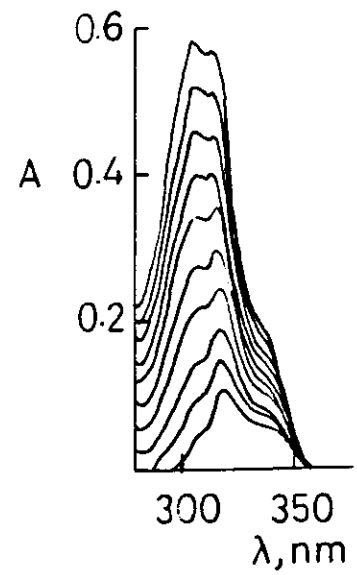

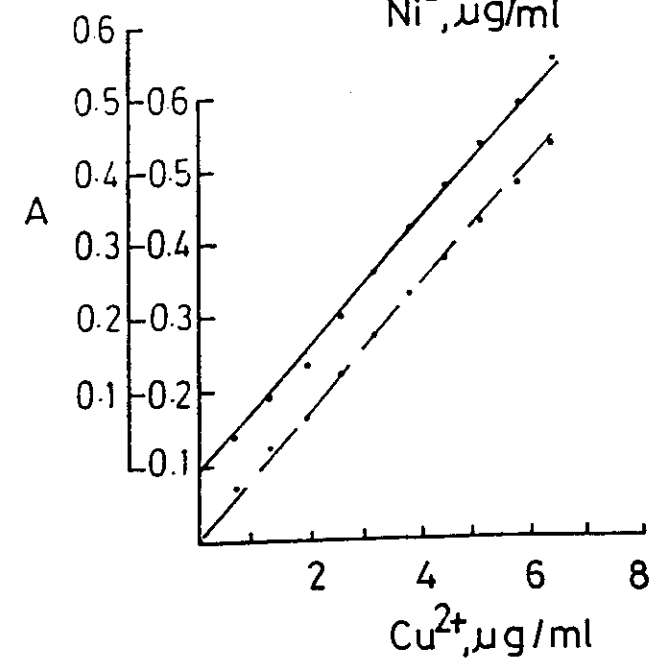

Fig (48-a)

Beer's Law For Chelates of Ligand III With La^{3+}, Gd^{3+} and Pt^{4+}

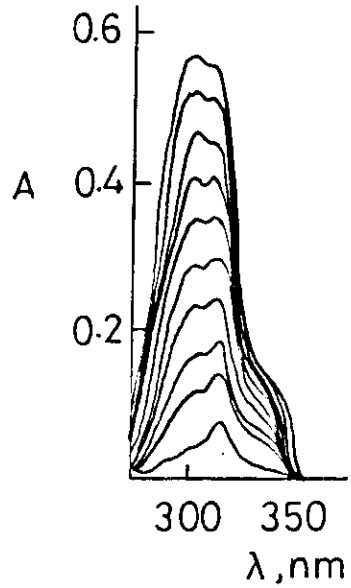

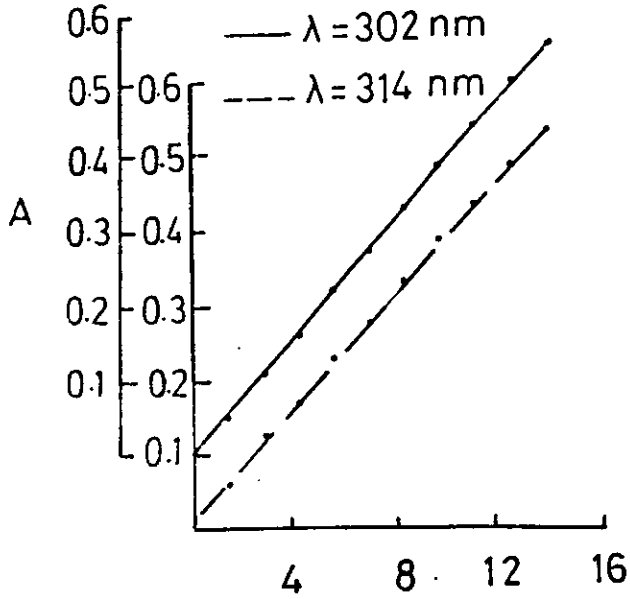

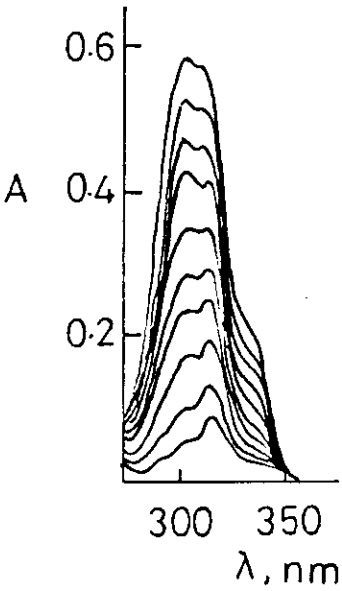

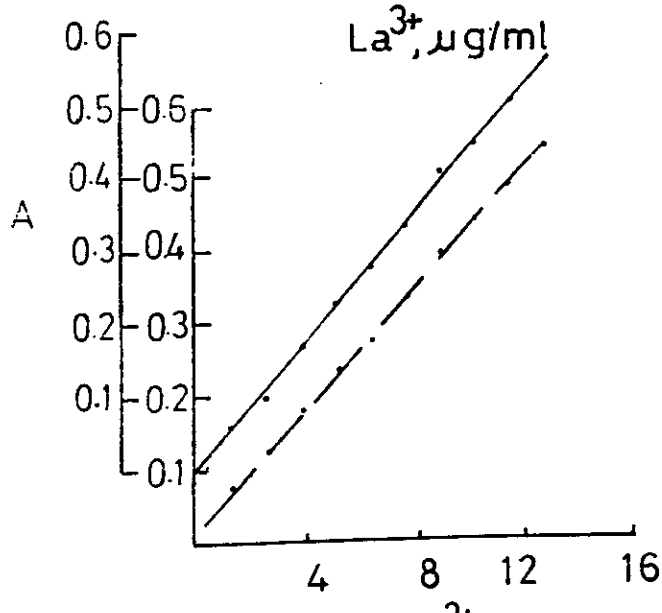

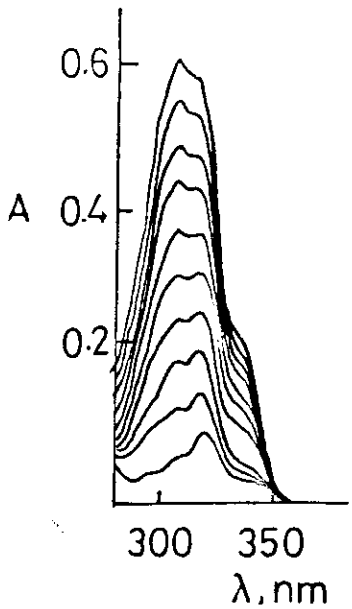

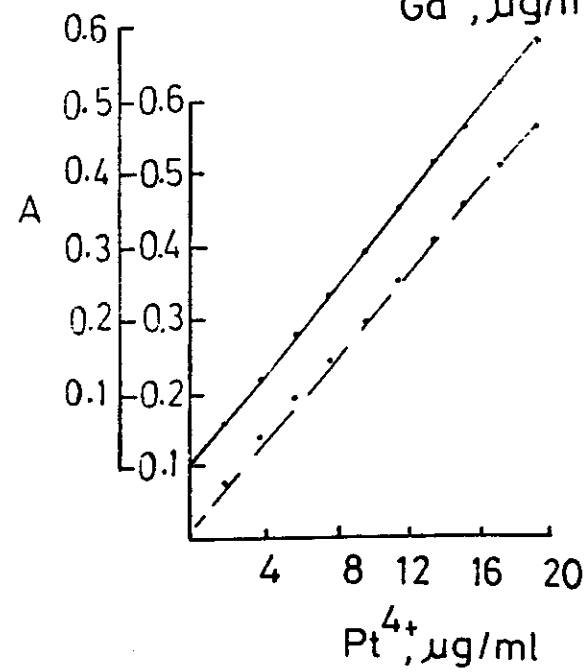

Fig (48-b)

Table (23): Analytical determination of metal ions using hydrazo compounds as chelating agents.

Metal ion	Concentration range (ppm)											
	Ligand I				Ligand II				Ligand III			
	Conc.				Conc.				Conc.			
	303	314	303	314	302	312	302	312	302	314	302	314
Co^{2+}	10300	9600	0.5-6	0.5-6	8800	8770	0.5-6	1-6	5600	5450	0.5-5.3	0.5-5.3
Ni^{2+}	10400	9600	0.5-6	0.5-6	9850	8890	1-6	1-6	4200	5150	0.5-5.3	0.5-5.3
Cu^{2+}	10400	9700	0.5-5.7	0.5-5.7	9350	9200	0.5-5.7	0.5-5.7	5870	5800	0.5-5.7	0.5-5.7
La^{3+}	10200	9600	1.2-13.9	1.2-13.9	8200	8150	1.2-13.9	12.13.9	5500	5450	1.2-13.9	1.2-13.9
Gd^{3+}	10250	9800	1.2-15.7	1.2-15.7	8888.8	8777.7	1.2-15.7	1.2-15.7	5700	5600	1.2-15.7	1.2-15.7
Pt^{4+}	10400	9900	2-19.5	2-19.5	8888.8	8888.8	2-19.5	2-19.5	5850	5750	2-19.5	2-19.5